R-1133

DAVIDSON LABORATORY

STEVENS INSTITUTE
OF TECHNOLOGY
CASTLE POINT STATION
HOBOKEN, NEW JERSEY

REPORT 1133

UNSTEADY PROPELLER LIFTING-SURFACE THEORY WITH FINITE NUMBER OF CHORDWISE MODES

by

S. Tsakonas
W. R. Jacobs
P. H. Rank, Jr.

DDC
RECEIVED
APR 7 1967
C

December 1966

Distribution of this document is unlimited.

ARCHIVE COPY

R-1133

DAVIDSON LABORATORY

Report 1133

December 1966

UNSTEADY PROPELLER LIFTING-SURFACE THEORY WITH FINITE NUMBER OF CHORDWISE MODES

by

S. Tsakonas

W. R. Jacobs

and

P. H. Rank, Jr.

Sponsored by
Naval Ship Systems Command General Hydromechanics
Research Program (S-R009-01-01)
Administered by David Taylor Model Basin
Contract Nonr 263(55)

(DL Project 2809/065)

Distribution of this document is unlimited. Application for copies may be made to the Defense Documentation Center, Cameron Station, 5010 Duke Street, Alexandria, Virginia 22314. Reproduction of the document in whole or in part is permitted for any purpose of the United States Government.

Approved
J. P. Breslin
J. P. Breslin, Director
Davidson Laboratory

viii + 63 pages
8 tables, 24 figures
6 appendices (25 pages)

ABSTRACT

A continuing investigation at Davidson Laboratory is concerned with improvement of the mathematical model developed for the evaluation of the steady and time-dependent loading distributions on the blades of marine propellers operating in spatially non-uniform flow. In the present study the surface integral equation resulting from the theory has been solved by means of the collocation method, in conjunction with the generalized lift operator, for a prescribed set of chordwise modes which reproduce the proper leading-edge singularity and fulfill the Kutta condition at the trailing edge.

General programs have been developed to accommodate any geometry of propeller operating in a specified non-uniform inflow condition for a large but finite number of chordwise modes. The calculations indicate that the spanwise loading distribution and the steady and time-dependent thrust reach stable values after three to five chordwise modes, but the chordwise distribution does not converge to its final form, particularly in the neighborhood of the leading and trailing edges.

A comparison of theoretical and experimental results for the vibratory thrust shows satisfactory agreement on the whole. It is believed that the principal cause of any existing discrepancies between measured and calculated results is lack of precise knowledge of the wake harmonics.

KEYWORDS

Hydrodynamics

Unsteady Theory for
Marine Propellers

TABLE OF CONTENTS

List of Tables vi

List of Figures vii

ABSTRACT iii

NOMENCLATURE ix

INTRODUCTION 1

THE LINEARIZED UNSTEADY LIFTING-SURFACE THEORY FOR MARINE PROPELLERS 4

THE KERNEL FUNCTION 16

- Determining the Directional Derivatives 20
- The Assumed Staircase Function Replacing the Exact Integral Path 23
- Evaluation of K_2 24
- Evaluation of K_1 for $\rho \neq r$ 26
- Evaluation of $\int_{r_i-\beta}^{r_i+\beta} K_1(r_i,\rho)\,d\rho$ 28

THE CHORDWISE LOADING DISTRIBUTION AND GENERALIZED LIFT OPERATOR 36

LOADING DUE TO BLADE CAMBER AND FLOW INCIDENCE ANGLE 43

NUMERICAL RESULTS 46

- Spanwise Loading Distribution 46
- Chordwise Loading Distribution 54

CONCLUSION 59

ACKNOWLEDGEMENT 61

REFERENCES 62

APPENDIX A. Proof of the Equivalence of Equations (28) and (29) . . . A-1
APPENDIX B. Approximation of the Infinite p-Series of K_2 . . . . . . B-1
APPENDIX C. Evaluation of f(m,q,n) C-1
APPENDIX D. Evaluation of Integrals I_1, I_2, and I_3 . . . . D-1
APPENDIX E. Evaluation of the Integrals in Equations (56a) and (56b), for the Regions Adjacent to the Singularity Strip, by the Lagrange Interpolation Method E-1
APPENDIX F. Chordwise Pressure Distribution F-1

LIST OF TABLES

1. Model Particulars 46

2. Ratio of Theoretical to DTMB - Calculated Mean Thrust 47

3. Correlation of Results of Theory and Experiments 49

4. Mean Thrust $\bar{T}$ and Double Amplitude of Vibratory Thrust in Percent of Mean Thrust $\Delta T/\bar{T}$ for 4-Blade Propeller . . . 50

5. Correlation of Theoretical and Experimental $\bar{K}_T$ Values in the Open-Water Condition for 3-Blade Propellers 51

6. Correlation of Unsteady Single Amplitude $\widetilde{K}_T$ Values for 3-Blade Propellers at First Blade Frequency 52

7. Quasi-Steady Single Amplitude $\widetilde{K}_{T_q}$ Values for 3-Blade Propellers at First Blade Frequency 52

8. Lift Ratio $R_{3/2}$ for 3-Blade Propellers 53

LIST OF FIGURES

1. Coordinate System and Notations 65

2. Spanwise Loading on 3-Bladed Propeller (EAR = 0.6) in Screen-Generated Wake 66

3. Spanwise Loading Due to Ship Wake Only on 4-Bladed Propeller 67

4. Steady Spanwise Loading Due to Wake, Camber and Flow Angle on 5-Bladed Propeller in Wake No. 1 68

5. Unsteady Spanwise Loading Due to Wake No. 1 on 5-Bladed Propeller 69

6. Steady Spanwise Loading Due to Wake, Camber, and Flow Angle on 7-Bladed Propeller in Wake No. 1 70

7. Unsteady Spanwise Loading Due to Wake No. 1 on 7-Bladed Propeller 71

8. Steady Spanwise Loading Due to Wake No. 4, Camber and Flow Angle on 5-Bladed Propeller 72

9. Unsteady Spanwise Loading Due to Wake No. 4 on 5-Bladed Propeller 73

10. Theoretical and Experimental $\bar{K}_T$ Versus J in the Open-Water Condition for 3-Bladed Propellers 74

11. Phases, β_3 and β_2, of Unsteady Blade-Frequency Loading L_W for 3-Blade Propeller No. 4118 (EAR = 0.60), by 3-Dimensional and 2-Dimensional Unsteady Theories 75

12. Phases, β_3, of Unsteady Blade-Frequency Loading L_W Measured from Those of Input Wake for 3-Blade Propellers (3 Chordwise Modes) 76

13. Phase Differences (β_3-β_2) for 3-Blade Propellers at Blade-Frequency 77

14a. Unsteady Chordwise Loading Distribution at 0.75r_o for Propeller 4118 (EAR = 0.6) at Design J = 0.831 (Cesãro-Summability of Sine Terms) 78

14b. Unsteady Chordwise Loading Distribution at 0.75r_o for Propeller 4118 (EAR = 0.6) at Design J = 0.831 (Cesãro-Summability of Sine Terms) 79

15a. Unsteady Chordwise Loading Distribution at 0.75r_o for Propeller 4118 (EAR = 0.6) at Design J = 0.831 (Cesãro-Summability of Sine Terms) 80

[Cont'd]

List of Figures (Cont'd)

15b. Unsteady Chordwise Loading Distribution at 0.75 r_o for Propeller 4118 (EAR = 0.6) at Design J = 0.831 (Cesãro-Summability of Sine Terms) 81

16a. Unsteady Chordwise Loading Distribution at 0.75 r_o for Propeller 4118 (EAR = 0.6) at Design J = 0.831 (Cesãro-Summability of Sine Terms) 82

16b. Unsteady Chordwise Loading Distribution at 0.75 r_o for Propeller 4118 (EAR = 0.6) at Design J = 0.831 (Cesãro-Summability of Sine Terms) 83

17a. Steady Chordwise Loading Distribution at 0.75 r_o for Propeller 4118 (EAR = 0.6) at Design J = 0.831 (Normal Sum) 84

17b. Steady Chordwise Loading Distribution at 0.75 r_o for Propeller 4118 (EAR = 0.6) at Design J = 0.831 (Cesãro-Summability of Sine Terms) 85

18a. Steady Chordwise Loading Distribution at 0.75 r_o for Propeller 4118 (EAR = 0.6) at J = 0.7 (Normal Sum) 86

18b. Steady Chordwise Loading Distribution at 0.75 r_o for Propeller 4118 (EAR = 0.6) at J = 0.7 (Cesãro-Summability of Sine Terms) 87

19a. Steady Chordwise Loading Distribution at 0.75 r_o Due to Wake No. 1, Camber and Flow Angle for 5-Blade Propeller at J = 0.762 (Normal Sum) 88

19b. Steady Chordwise Loading Distribution at 0.75 r_o Due to Wake No. 1, Camber and Flow Angle for 5-Blade Propeller at J = 0.762 (Cesãro-Summability of Sine Terms) 89

20. Steady Chordwise Loading Distribution at 0.75 r_o Due to Wake No. 1 for 5-Blade Propeller at J = 0.762 (Cesãro-Summability of Sine Terms) 90

21. Steady Chordwise Loading Distribution at 0.75 r_o Due to Camber and Flow Angle Effects for 5-Blade Propeller at J = 0.762 (Cesãro-Summability of Sine Terms) 91

B-1 Approximations of the Infinite p-Series B-5

NOMENCLATURE

a	Ω/U
a_{ms} b_{ms}	coefficients defined in Equation (52)
b	semichord length
D	propeller diameter
EAR	expanded area ratio
$F(\ )$	function
$f(r,s)$	camber line
$f(\ )$	function
$g(\ )$	function
$I^{\bar{m}}(x)$	defined in Equation (61)
$I_m(\ )$, $K_m(\ )$	modified Bessel functions of order m
i	index of radial strip
J	U/nD , advance ratio (n = rps)
J	number of radial strips
$J_m(\ )$	Bessel function of order m
j	index of radial strip
$K(\ )$	kernel of integral equation

$\bar{K}(\ )$	kernel after θ_α-integration and φ_α-integration
K_T	$T/\rho n^2 D^4$, thrust coefficient (n = rps)
k	variable of integration
$\bar{k}(\ )$	ρ-integral of $\bar{K}(\ )$
k	$q\theta_b^r$, reduced frequency
$L(r)$	spanwise loading distribution
$L^{(\bar{n})}(\rho)$	spanwise loading components (coefficients of Birnbaum distribution)
$L_o(r,q)$	loading by two-dimensional theory
$\bar{m}$	order of lift-operator
m	index of summation
N	number of blades
$\bar{n}$	order of chordwise mode
n	blade index
$\vec{n}$	normal to helicoidal surface at loading point
$\vec{n}'$	normal to helicoidal surface at control point
P	propeller pitch
p	perturbation pressure
p	index of summation
$Q_{m-\frac{1}{2}}(\ )$	Legendre spherical function of half odd-integer order
$\bar{q}$	perturbation velocity
q	ω/Ω , order of blade harmonic

R	Descartes distance
R'	Descartes distance
r	radial coordinate of control point
r_o	$D/2$, propeller radius
S	lifting surface
$S(\rho,\theta_o)$	blade loading distribution
$S(k)$	Sears function
s	$b(1 - \cos \varphi_{\alpha})$, ordinate along chord
s'	$s/2b$
T	thrust
$\bar{T}$	mean thrust
ΔT	double amplitude of vibratory thrust
t	time
U	uniform velocity in x-direction
$V(r)$	Fourier coefficients of wake velocity normal to the blade
V_c	velocity normal to blade due to camber effect
V_f	velocity normal to blade due to incident flow angle
$W(x,r,\varphi_o;t)$	self-induced velocity at the control point
X	$y/a - (x-\xi)$ Equation (29)
x	longitudinal ordinate
x,r,φ	cylindrical coordinate system of control points

y	$-\ a(\tau - x + \xi)$
z	defined in Equation (32) and others
β	small radial length
β_3	phase angle by three-dimensional theory
β_2	phase angle by two-dimensional theory
δ	small length
$\delta(\ )$	Dirac delta function
Θ	defined in Equation (29)
θ	angular coordinate of loading point
θ_o	initial angular position of loading point in propeller plane
θ_α	angular chordwise location of loading point
θ_b	projected propeller semichord length, in radians
$\bar{\theta}_n$	$\frac{2\pi}{N}(n-1)$, $n = 1 \ldots N$,
$\bar{\theta}_o$	$\frac{2\pi}{N}$
$\theta_p(r)$	$\tan^{-1} \frac{P(r)}{2\pi r}$, geometric pitch angle
$\Lambda^{\bar{n}}(\ )$	defined in Equation (60)
λ	positive integer multiple
ξ, ρ, θ	cylindrical coordinate system of loading points
ρ	radial coordinate of loading point
ρ_f	mass density of fluid
σ	angular measure of skewness

τ, τ'	variables of integration
Φ	velocity potential
φ	angular coordinate of control point
φ_o	initial angular position of control point in propeller plane
φ_α	angular chordwise location of control point
Ψ	acceleration potential
Ω	angular velocity of propeller
ω	angular frequency of the loading

BLANK PAGE

INTRODUCTION

In the past few years, Davidson Laboratory has undertaken a series of investigations[1,2,3,4,5] concerned with the unsteady propeller lifting-surface theory. The primary purpose is the evaluation of the loading distribution on propeller blades and of the vibratory thrust and torque generated by the propeller when it operates in a non-uniform inflow condition.

This problem has lately attracted considerable attention, since it is intimately related to the problems of ship vibration, underwater noise generation and transmission, cavitation inception, and dynamic stability and control of water-borne vehicles. The need of an accurate and detailed description of the loading distribution of the lifting surface (i.e. propeller blade) is especially important with today's tendency toward high-speed vehicles.

Investigations both theoretical and experimental have been conducted in other laboratories in the United States and abroad. Among the analytical approaches are the studies of Sparenberg,[6] Hanaoka,[7] Yamazaki,[8] Brown,[9] and Greenberg.[10] Sparenberg derived the three-dimensional integral equation for the screw propeller in steady flow, and Hanaoka the corresponding equation for the case of unsteady flow. The other investigators cited were concerned with the solution of the integral equations under a variety of assumptions, some valid in the range of practical interest, others valid for values of parameters at the limits of practical interest. Yamazaki derived the linearized lifting-surface integral equation on the basis of vortex theory and solved it on the assumption of flat-plate chordwise loading, making use of the lift operator. Brown and Greenberg each developed the lifting-surface integral equation through vortex theory; but Brown used Reissner's high-aspect-ratio wing theory in attempting to solve the equation, while Greenberg assumed that the induced downwash is that due to a flat wing of finite aspect ratio, with a "helicoidal deviation" which was accounted for approximately.

The problem of determining the loading distribution on propeller blades of known geometry operating under known flow conditions leads to a surface integral equation difficult to solve even by numerical methods. Due to the mathematical complexity of the problem, the investigations at Davidson Laboratory have followed in order an ascending degree of difficulty.

A series of concessions has been made regarding the propeller geometry and the shape of the chordwise loading distributions, for the sake of simplicity; and certain other mathematical simplifications have been introduced. In References 1, 2, and 3 the solution of the surface integral equation was obtained for two loading conditions: (a) loading concentrated at the 1/4-chord line (Weissinger model), and (b) flat-plate chordwise loading (first term of the Birnbaum distribution). In both cases the solution was for a sector-form blade with low pitch and the helicoidal wake approximated in a staircase fashion. In Reference 4, the theory was further developed to accommodate skewness and arbitrary blade form.

Recently, an investigation[5] was completed for a sector-form blade of arbitrary pitch, with flat-plate chordwise loading distribution, where the helicoidal wake of the blade is treated accurately, to supersede the earlier approximation. This investigation has shown the complexity involved in the rigorous treatment of even this simple blade form. The values obtained for vibratory thrust and torque are in satisfactory agreement with those obtained with the staircase approximation of the helicoidal wake. The vibratory thrust obtained by the exact treatment of the wake is shown to be about 15-percent larger than that obtained by the approximate treatment, and the mean thrust about 2-percent higher. It is believed that a further improvement of the numerical procedure in the exact treatment will reduce the discrepancy. Hence, the mathematical model with staircase approximation of the helicoidal wake is an acceptable model. Through its use, all complications arising from the exact treatment can be avoided, particularly when arbitrary blade form and sweep angle are incorporated into the problem.

The present investigation is concerned with the improvement of this mathematical model with respect to its chordwise modes. A large number of modes given by the Birnbaum distribution is assumed, and then the integral equation is solved for the unknown spanwise distribution by the collocation method. In this way the proper loading distribution and the vibratory thrust and torque generated by a propeller operating in a three-dimensional non-uniform flow are determined.

The study was sponsored by the Naval Ship Systems Command, General Hydromechanics Research Program S-R009-01-01, Contract Nonr 263(55), administered by the David Taylor Model Basin.

THE LINEARIZED UNSTEADY LIFTING-SURFACE THEORY FOR MARINE PROPELLERS

The linearized formulation for a propeller with its N-blades lying on a helicoidal surface and operating in the non-uniform flow of an incompressible, ideal fluid was derived by means of the acceleration-potential method in the earlier papers.[1-5] A brief recapitulation is presented as background for subsequent discussion.

The blades rotate at constant angular velocity Ω in flow of velocity $U + \bar{q}$, where U is uniform velocity in the x-direction and $\bar{q}$ is the perturbation velocity. The linearized equation of motion and the equation of continuity for the perturbed field are

$$\frac{\partial \bar{q}}{\partial t} + U \frac{\partial \bar{q}}{\partial x} = - \nabla \frac{p}{\rho_f} \tag{1}$$

$$\nabla \cdot \bar{q} = 0 \tag{2}$$

where ρ_f = fluid density, p = perturbation pressure, t = time.

The quantity

$$\frac{p}{\rho_f} = \Psi \tag{3}$$

is known as the acceleration potential. With the velocity potential Φ from

$$\bar{q} = \nabla \Phi \tag{4}$$

the first two equations yield

$$-\Psi = \frac{\partial\Phi}{\partial t} + U\frac{\partial\Phi}{\partial x} \tag{5}$$

$$\nabla^2 \Psi = 0 \tag{6}$$

The solution of Equation (5) satisfying the condition $\Phi = 0$ at $x = -\infty$ is given by

$$\Phi(x,r,\varphi;t) = -\frac{1}{U}\int_{-\infty}^{x} \Psi\left(\tau', r, \varphi; t - \frac{x-\tau'}{U}\right) d\tau' \tag{7}$$

where x,r,φ represent a cylindrical coordinate system fixed in the propeller (Fig. 1). It has been shown[1,3] that the pressure field generated by a lifting surface S is given by distributed doublets with axis parallel to the local normal, and with strength equal to the pressure jump across the surface S. Thus the pressure at a point (x,r,φ) at time t will be given by

$$\Psi(x,r,\varphi;t) = \frac{1}{4\pi\rho_f}\iint_S \Delta p(\xi,\rho,\theta;t)\,\frac{\partial}{\partial n}\,\frac{1}{R'(x,r,\varphi;\xi,\rho,\theta)}\,dS \tag{8}$$

where $\frac{\partial}{\partial n}$ = normal derivative on the surface S at the loading point (ξ,ρ,θ)

$\vec{n}$ = unit normal vector having positive axial component

$\Delta p(\xi,\rho,\theta,t)$ = pressure jump across the lifting surface, i.e. $\Delta p = p_+ - p_-$

$R'(x,r,\varphi;\xi,\rho,\theta) = \sqrt{(x-\xi)^2 + r^2 + \rho^2 - 2r\rho\cos(\theta-\varphi)}$

= Descartes distance between the given control point and loading point

For doublets with pulsating strength $\Delta p(\xi,\rho,\theta)\ e^{i\omega t}$ at point (ξ,ρ,θ), which rotates with angular velocity $-\Omega$, Equation (8) yields

$$\Psi(x,r,\varphi;t) = \frac{1}{4\pi\rho_f} \iint\limits_S \Delta p(\xi,\rho,\theta_o)\ e^{i\omega t} \frac{\partial}{\partial n} \frac{1}{R'(x,r,\varphi;\xi,\rho,\theta_o-\Omega t)}\ dS \tag{9}$$

where ω = frequency

θ_o = initial angular position

The corresponding expression for the velocity potential at (x,r,φ) is obtained by substituting Equation (9) in Equation (7).

When the lifting surface is identified as the helicoidal surface of an N-bladed propeller, where both control and loading points rotate with angular velocity $-\Omega$, the expression for the velocity potential is given by

$$\Phi(x,r,\varphi_o;t) = -\sum_{n=1}^{N} \frac{e^{iq\Omega t}}{4\pi\rho_f U} \iint\limits_S \Delta p(\xi,\rho,\theta_o) \int_{-\infty}^{x} e^{iq[a(\tau'-x)-\bar{\theta}_n]} \frac{\partial}{\partial n}\left(\frac{1}{R}\right) d\tau'\ dS \tag{10}$$

where $a = \Omega/U$

$q = \omega/\Omega$ is order of blade harmonic

$\bar{\theta}_n = \frac{2\pi}{N}(n-1)$, $n = 1, 2 \ldots N$

$R = \sqrt{(\tau'-\xi)^2 + r^2 + \rho^2 - 2r\rho\cos[\theta_o - \varphi_o + \bar{\theta}_n - a(\tau'-x)]}$

φ_o = initial angular position of control point

The self-induced velocity at $(x,r,\varphi_o;t)$ will be given by

$$W(x,r,\varphi_o;t) = -\sum_{n=1}^{N} \frac{e^{iq\Omega t}}{4\pi\rho_f U} \iint_S \Delta p(\xi,\rho,\theta_o)$$

$$\cdot \frac{\partial}{\partial n'} \int_{-\infty}^{x} e^{iq[a(\tau'-x)-\bar{\theta}_n]} \frac{\partial}{\partial n} \left(\frac{1}{R}\right) d\tau' \, dS \tag{11}$$

where $\frac{\partial}{\partial n'}$ is the normal derivative on the helicoidal surface at (x,r,φ), the control point.

The directional derivatives normal to the helicoidal surface, which is given by $x = \varphi_o/a$ or $\xi = \theta_o/a$, are:

At the control point,

$$\frac{\partial}{\partial n'} = \frac{r}{\sqrt{1+a^2 r^2}} \left(a \frac{\partial}{\partial x} - \frac{1}{r^2} \frac{\partial}{\partial \varphi_o}\right) \tag{12}$$

At the loading (doublet) point,

$$\frac{\partial}{\partial n} = \frac{\rho}{\sqrt{1+a^2 \rho^2}} \left(a \frac{\partial}{\partial \xi} - \frac{1}{\rho^2} \frac{\partial}{\partial \theta_o}\right) \tag{13}$$

If the self-induced velocity is equated with the known (measured) velocity distribution (downwash velocity) normal to the propeller blades, Equation (11) becomes

$$V(r)\, e^{iq(\Omega t-\varphi_o)} = \frac{e^{iq\Omega t}}{4\pi\rho_f U} \int_{-\theta_b^\rho}^{\theta_b^\rho} \int_\rho \Delta p(\rho,\theta_o)\, K(r,\varphi_o;\rho,\theta_o;q)\, \rho \, d\rho \, d\theta_o \tag{14}$$

where $\theta_b{}^{\rho}$ is the projected semichord length of the propeller blade at the loading point, in radians, and the singular kernel K is

$$K(r,\varphi_o;\rho,\theta_o;q) = -\frac{\sqrt{1+a^2\rho^2}}{a\rho} \lim_{\delta\to o} \sum_{n=1}^{N} e^{-iq\bar{\theta}_n} \frac{\partial}{\partial n'} \int_{-\infty}^{x} e^{iqa(\tau'-x)} \frac{\partial}{\partial n} \left(\frac{1}{R}\right) d\tau' \tag{15}$$

Here the factor $\sqrt{1+a^2\rho^2}/a\rho$ is the result of changing the integration over the actual propeller blade to integration over the projection in the propeller plane and $\delta = (\varphi_o-\theta_o)/a - (x-\xi) \rightarrow 0$ means that $x \rightarrow \varphi_o/a$ and $\xi \rightarrow \theta_o/a$. The limiting process is introduced to avoid the mathematical difficulty due to the presence of a high-order singularity. The mathematical manipulations are performed at control points on a surface slightly shifted from the lifting surface, and finally the former surface is bought into coincidence with the latter.

If use is made of the transformation $\theta_o = -\theta_b{}^{\rho} \cos\theta_\alpha$, Equation (14) becomes

$$\frac{V(r)}{U} e^{iq(\Omega t-\varphi_o)} = \frac{e^{iq\Omega t}}{4\pi\rho_f U^2} \int_o^{\pi} \int_{\rho} S(\rho,\theta_o)\, K(r,\varphi_o;\rho,\theta_o;q) \sin\theta_\alpha \, d\theta_\alpha \, d\rho \tag{16}$$

where $S(\rho,\theta_o) = [\Delta p(\rho,\theta_o) \cdot \rho\theta_b{}^{\rho}]$ is the unknown blade-loading function which depends on radial position ρ and angular position θ_o.

The kernel function appears to be one of the most complicated kernel functions in boundary-value problems of lifting surfaces. It has, in addition to the complications arising from the helicoidal surface and from the interference of the other blades, the additional drawback of a high-order singularity with finite Hadamard part. There is little hope of a direct solution of the integral equation, and a numerical solution suitable to high-speed digital computers is therefore advisable. The analysis must be pursued to the point at which laborious computations can be efficiently performed by numerical schemes, and the correct finite part of the high-order singularity obtained. The numerical solution of this integral equation, very difficult and challenging, is obtained along the lines suggested by Watkins, et al.[11]

The unknown loading function $S(\rho,\theta_o)$ is approximated in the chordwise direction by a set of functions which reproduce the proper leading-edge singularity and fulfill the Kutta condition along the trailing edge. Such a loading distribution is given by the Birnbaum distribution, and then the unknown loading function reads as

$$S(\rho,\theta_o) = \frac{1}{\pi}\left\{ L^{(1)}(\rho)\cot\frac{\theta_\alpha}{2} + \sum_{\bar{n}=2}^{\infty} L^{(\bar{n})}(\rho)\,\frac{\sin(\bar{n}-1)\theta_\alpha}{\bar{n}-1} \right\} \tag{17}$$

where $L^{(\bar{n})}(\rho)$ are the spanwise loading components. It is judged safer not to specify the spanwise loading distribution, as is usually done, since conditions at the location of the hub remain unknown; the unknown spanwise distribution is left to be determined by the integral equation.

After the chordwise integration is performed, the surface integral equation is reduced to a line integral equation, viz., to

$$\frac{V(r)}{U}\, e^{iq(\Omega t-\varphi_o)} = \frac{e^{iq\Omega t}}{4\pi\rho_f U^2}\left\{ \mathop{\int\!\!\!\!\!\!\times}_{\rho} L^{(1)}(\rho)\,\bar{K}^{(1)}(r,\rho,\varphi_o;q)\,d\rho + \mathop{\int\!\!\!\!\!\!\times}_{\rho} \sum_{\bar{n}=2}^{\infty} L^{(\bar{n})}(\rho)\,\bar{K}^{(\bar{n})}(r,\rho,\varphi_o;q)\,d\rho \right\} \tag{18}$$

where the cross on the integral sign signifies the singular behavior of the integrand when $\rho \to r$ as $\delta \to 0$. The new kernels of the line integral equation, $\bar{K}^{(\bar{n})}$, are the results after the θ_α-integrations.

At this stage the notion of the lift operator was considered, as an extension of its application in the field of two-dimensional steady and unsteady aerodynamic theory. It had been thought that its use in the three-dimensional flow condition was the best expedient in the present state of the art, and that, as stated in Reference 12, the chordwise boundary condition would then be approximated by a weighted average. It was realized recently* that the function labeled lift operator is dictated by the integral equation itself and that its success rests in the main on the special structure of the kernel. Actually, the separable form of the kernel function (or, in the language of the theory of integral equations, the "degenerate" form of the kernel) dictates the structure and application of the lift operator. Indeed, a method of solving integral equations is in hand when the kernel function is of the degenerate form.[13]

Therefore, there is no approximation involved in applying the generalized lift operator

$$\frac{1}{\pi}\int_0^{\pi} \cos \bar{m}\, \varphi_\alpha \left\{\ \right\} d\varphi_\alpha \ , \quad \bar{m} = 0, 1, \ldots \tag{19a}$$

or that selected in the present case,

$$\begin{aligned} \bar{m} &= 1 \ , & \frac{1}{\pi}\int_0^{\pi} (1 - \cos \varphi_\alpha) \left\{\ \right\} d\varphi_\alpha & \ \text{(the Glauert lift operator)} \\ \bar{m} &= 2 \ , & \frac{1}{\pi}\int_0^{\pi} (1 + 2 \cos \varphi_\alpha) \left\{\ \right\} d\varphi_\alpha & \\ \bar{m} &> 2 \ , & \frac{1}{\pi}\int_0^{\pi} \frac{\cos (\bar{m}-1)\, \varphi_\alpha}{(\bar{m}-1)} \left\{\ \right\} d\varphi_\alpha & \end{aligned} \tag{19b}$$

---

*Re-examination of the function was spurred by a discussion with Dr. Pien, Dr. Morgan, and Mr. Chen of DTMB, who pointed out that effects of angle of attack and high-order camber oscillations can be obtained by means of the lift operator.

where $\varphi_o = - \theta_b{}^r \cos \varphi_\alpha$

$\theta_b{}^r$ = projected semichord length of the propeller blade at the control point, in radians

It is an indispensable part of the solution and is recommended for use for all lifting-surface integral equations, once the kernel is expressed in the corresponding separable form.

It will be seen in the next section that, by means of a series expansion of the inverse Descartes distance 1/R, the kernel function can be expressed in such manner that the φ_o and θ_o dependences occur as exponential factors separate from each other and from the other spatial coordinates. With

$$\theta_o = - \theta_b{}^\rho \cos \theta_\alpha$$

the θ_α-integration indicated in Equations (16) and (17) is easily performed. Then, with

$$\varphi_o = - \theta_b{}^r \cos \varphi_\alpha$$

the form of Equation (18) becomes

$$\frac{V(r)}{U} e^{iq\theta_b{}^r \cos \varphi_\alpha} = \frac{1}{4\pi\rho_f U^2} \oint_\rho \sum L^{(\bar{n})}(\rho) \sum_{m=-\infty}^{\infty} f_m(q,\varphi_\alpha) \bar{K}_m{}^{(\bar{n})}(r,\rho,q)\, d\rho$$

where the φ_α or φ_o dependence on the right-hand side appears in $f_m(q,\varphi_\alpha)$ in exponential form. The exponential form

$$e^{\pm ix \cos \varphi_\alpha}$$

which is present on both sides of the equation, can be expanded in terms of the orthogonal and complete set

$$1\ ,\ \cos\varphi_\alpha\ ,\ \cos 2\varphi_\alpha\ ,\ldots,\ \cos\bar{m}\,\varphi_\alpha,\ldots\ ,\qquad 0\le\varphi_\alpha\le\pi$$

in the form

$$e^{\pm ix\cos\varphi_\alpha} = J_0(x) + 2\sum_{\lambda=1}^{\infty}(-1)^{\lambda}J_{2\lambda}(x)\cos 2\lambda\varphi_\alpha \mp 2i\sum_{\lambda=1}^{\infty}(-1)^{\lambda}J_{2\lambda-1}(x)\cos(2\lambda-1)\varphi_\alpha$$

The orthogonality property dictates operation on both sides of the integral equation by the operators given in (19a), which are derived from the complete set mentioned above; or by the operators given in (19b), which are derived from the complete orthogonal set

$$1-\cos\varphi_\alpha\ ,\quad 1+2\cos\varphi_\alpha\ ,\quad \cos 2\varphi_\alpha\ ,\ \ldots\frac{\cos(\bar{m}-1)\varphi_\alpha}{(\bar{m}-1)},\ldots\ ,\quad 0\le\varphi_\alpha\le\pi$$

The latter set was chosen in order to utilize (as first mode) the "lift operator" defined in steady and unsteady airfoil theory. The set is orthogonal without the second term, but incomplete. Inclusion of the second term

$$1+2\cos\varphi_\alpha$$

assures that the formal expansion of any function (like $e^{\pm ix\cos\varphi_\alpha}$) in terms of the set is a valid representation of the function and not an approximation.

By applying the lift operators to both sides of Equation (18), a set of integral equations is obtained which can be expressed as

$$\frac{V(r)}{U}\, I^{(\bar{m})}(q\theta_b{}^{r}) = \frac{1}{4\pi\rho_f U^2}\left\{ \underset{\rho}{\not\int} L^{(1)}(\rho)\, \bar{K}^{(\bar{m},1)}(r,\rho,q)\, d\rho + \sum_{\bar{n}=2}^{\infty} \underset{\rho}{\not\int} L^{(\bar{n})}(\rho)\, \bar{K}^{(\bar{m},\bar{n})}(r,\rho,q)\, d\rho \right\} \tag{20}$$

where

$$\bar{m} = 1\,,\quad I^{(1)}(q\theta_b{}^{r}) = \frac{1}{\pi}\int_0^{\pi} (1 - \cos\varphi_\alpha)\, e^{iq\theta_b{}^{r}\cos\varphi_\alpha}\, d\varphi_\alpha$$

$$\bar{m} = 2\,,\quad I^{(2)}(q\theta_b{}^{r}) = \frac{1}{\pi}\int_0^{\pi} (1 + 2\cos\varphi_\alpha)\, e^{iq\theta_b{}^{r}\cos\varphi_\alpha}\, d\varphi_\alpha$$

$$\bar{m} > 2\,,\quad I^{(\bar{m})}(q\theta_b{}^{r}) = \frac{1}{\pi}\int_0^{\pi} \frac{\cos(\bar{m}-1)\,\varphi_\alpha}{(\bar{m}-1)}\, e^{iq\theta_b{}^{r}\cos\varphi_\alpha}\, d\varphi_\alpha$$

and $\bar{K}^{(\bar{m},\bar{n})}$ are the kernels after both θ_α and φ_α integrations. The number $\bar{m}$ of integral equations is equal to the number $\bar{n}$ of unknown chordwise modes.

The solution of $\bar{m} = \bar{n}$ integral equations is obtained by the collocation method. Subdividing the blade into i-strips along the span, of length 2β, reduces the $\bar{m}$ integral equations to a set of algebraic equations:

$$\frac{V(r_i)}{U}\, I^{(\bar{m})}(q\theta_b{}^{r_i}) = \frac{1}{4\pi\rho_f U^2}\left\{ \sum_{\bar{n}=1}^{\bar{n}_{max}} \sum_{j=1}^{J} L^{(\bar{n})}(\rho_j)\, k_{ij}{}^{(\bar{m},\bar{n})}(r_i,\rho_j) \right\} \tag{21}$$

where $\bar{m} = 1, 2, \ldots \bar{n}$, $j = 1, 2, \ldots J$ (number of strips)

$i = 1, 2, \ldots J$

and $$k_{i,j}^{(\bar{m},\bar{n})}(r_i,\rho_j) = \int_{\rho_j-\beta}^{\rho_j+\beta} \bar{K}^{(\bar{m},\bar{n})}(r_i,\rho)\, d\rho$$

In this way the unknown spanwise loading components $L^{(\bar{n})}(\rho_j)$ are determined, and the resultant spanwise loading distribution then follows from Equation (17).

$$L(r) = \int_0^{\pi} S(\rho,\theta_0) \sin\theta_\alpha \, d\theta_\alpha = \frac{1}{\pi}\int_0^{\pi} L^{(1)}(\rho_j)\,(1+\cos\theta_\alpha)\, d\theta_\alpha$$

$$+ \frac{1}{\pi}\sum_{\bar{n}=2}^{\infty}\int_0^{\pi} L^{(\bar{n})}(\rho_j)\,\frac{\sin(\bar{n}-1)\theta_\alpha}{(\bar{n}-1)} \sin\theta_\alpha \, d\theta_\alpha$$

$$= L^{(1)}(\rho_j) + \frac{1}{2} L^{(2)}(\rho_j) \tag{22}$$

In accordance with the linearized theory which assumes the loading is distributed on a helicoidal surface with pitch angle equal to the hydrodynamic angle $\lambda = \tan^{-1}(1/ar)$, the formula for total thrust at each blade frequency q should be

$$T(q) = -\,\mathrm{Re}\left[N e^{iq\Omega t}\int_0^{r_0} L(r)\,\frac{ar}{\sqrt{1+a^2 r^2}}\, dr\right] \tag{23}$$

However, since the effects of angle of attack (the difference between geometric and hydrodynamic pitch) and camber are also taken into account, as will be shown later, it can be argued that the loading is distributed on the actual blades which lie on a helicoidal surface of given (geometric) pitch angle $\theta_p(r)$.

On this basis the expression for total thrust will be given by

$$T(q) = - \text{Re}\left[N e^{iq\Omega t} \int_o^{r_o} L(r) \cos \theta_p(r)\, dr \right] \qquad (24)$$

In order to simplify the mathematics, utilization has been made of the approximation of the helicoidal wake of the blades which deforms the helicoid into a staircase function, since the result of this approximation is in satisfactory agreement with that of the exact treatment.[5] Furthermore, the complications arising from the exact treatment bar the possibility of accommodating important variations like blade shape and skewness.

Blade shape variation is taken into account through the parameters $\theta_b{}^\rho$ and $\theta_b{}^r$, which are the projected semichord lengths in angular measure at each radial position of loading point (ρ) and control point (r). Skewness is defined as the angular position σ of the midchord line of the projected blade at each radial position from the vertical through the hub, so that now

$$\begin{aligned} \varphi_o &= \sigma^r - \theta_b{}^r \cos \varphi_\alpha \\ \theta_o &= \sigma^\rho - \theta_b{}^\rho \cos \theta_\alpha \end{aligned} \qquad (25)$$

THE KERNEL FUNCTION

If $\tau' = \tau + \xi$ is substituted in Equation (15), the kernel becomes

$$K(r,\varphi_o,\rho,\theta_o;q) = - \frac{\sqrt{1+a^2\rho^2}}{a\rho} \sum_{n=1}^{N} \lim_{\delta \to o} \frac{\partial}{\partial n'} \cdot \frac{\partial}{\partial n}$$

$$\cdot \int_{-\infty}^{x-\xi} \frac{e^{iq[a(\tau-x+\xi)-\bar{\theta}_n]}\, d\tau}{\sqrt{\tau^2+r^2+\rho^2-2r\rho \cos\,[\theta_o-\varphi_o+\bar{\theta}_n-a(\tau-x+\xi)]}} \tag{26}$$

The integral has been evaluated by means of the expansion of the inverse Descartes distance in Reference 5, which treats the helicoidal wake exactly. If the expansion scheme

$$\frac{1}{R} = \frac{1}{\sqrt{\tau^2+r^2+\rho^2-2r\rho\cos\beta}} = \begin{cases} \dfrac{1}{\pi} \displaystyle\sum_{m=-\infty}^{\infty} e^{im\beta} \int_{-\infty}^{\infty} I_m(k\rho)\, K_m(kr)\, e^{i\tau k}\, dk & \text{for } \rho < r \\ \dfrac{1}{\pi} \displaystyle\sum_{m=-\infty}^{\infty} e^{im\beta} \int_{-\infty}^{\infty} I_m(kr)\, K_m(k\rho)\, e^{i\tau k}\, dk & \text{for } \rho > r \end{cases} \tag{27}$$

is utilized, where $I_m(\;)$, $K_m(\;)$ are modified Bessel functions of order m, then, as shown in the reference cited, the kernel is (for $\rho < r$)

$$K(r,\varphi_o,\rho,\theta_o;q) = -\frac{N}{\pi}\,\frac{r}{a\sqrt{1+a^2r^2}}$$

$$\cdot \sum_{\substack{m=-\infty \\ m=q+\lambda N}}^{\infty} \left\{ \pi e^{-iq(\varphi_o-\theta_o)} \left[a^2(m-q)+\frac{m}{r^2}\right]\left[a^2(m-q)+\frac{m}{\rho^2}\right] I_m(a|m-q|\rho)\,K_m(a|m-q|r)\right.$$

$$- ia^2\, e^{-im(\varphi_o-\theta_o)} \int_{-\infty}^{\infty} \frac{k^2 I_m(k\rho)\,K_m(kr)\,e^{i\frac{k}{a}(\varphi_o-\theta_o)}}{k-a\,(m-q)}\,dk$$

$$-iam\left(\frac{1}{r^2}+\frac{1}{\rho^2}\right) e^{-im(\varphi_o-\theta_o)} \int_{-\infty}^{\infty} \frac{k I_m(k\rho)\,K_m(kr)\,e^{i\frac{k}{a}(\varphi_o-\theta_o)}}{k-a\,(m-q)}\,dk$$

$$\left. -i\,\frac{m^2}{r^2\rho^2}\, e^{-im(\varphi_o-\theta_o)} \int_{-\infty}^{\infty} \frac{I_m(k\rho)\,K_m(kr)\,e^{i\frac{k}{a}(\varphi_o-\theta_o)}}{k-a\,(m-q)}\,dk \right\} \tag{28}$$

For $\rho > r$, ρ and r are interchanged in the modified Bessel functions.

In Reference 1, Shioiri and Tsakonas simplified the computations by substituting a staircase function for the true helicoidal path. The various steps of their method are given below.

Let $y = -a(\tau-x+\xi)$ in Equation (26). Then the interchanging of the integral sign and the differential operation becomes possible:

$$K = -\frac{1}{a}\,\frac{\sqrt{1+a^2\rho^2}}{a\rho}\sum_{n=1}^{N}\lim_{\delta\to 0}\int_0^{\infty} e^{-iq(\bar{\theta}_n+y)}$$

$$\cdot\ \frac{\partial}{\partial n'}\,\frac{\partial}{\partial n}\left\{\frac{dy}{\left\{\left[(x-\xi)-\frac{y}{a}\right]^2+r^2+\rho^2-2r\rho\cos\left(\theta_0-\varphi_0+\bar{\theta}_n+y\right)\right\}^{1/2}}\right\}$$

Now, if $X = \frac{y}{a} - (x-\xi)$

and

$$\Theta = \bar{\theta}_n + \theta_0 - \varphi_0 + y$$

the kernel can be expressed as

$$K = -\frac{1}{a}\sum_{n=1}^{N}\lim_{\delta\to 0}\int_{\bar{\theta}_n+\theta_0-\varphi_0}^{\infty} e^{-iq(\Theta+\varphi_0-\theta_0)}\cdot\left(\frac{-r}{a\sqrt{1+a^2r^2}}\right)$$

$$\cdot\left[\left(a\frac{\partial}{\partial X}-\frac{1}{r^2}\frac{\partial}{\partial\Theta}\right)\left(a\frac{\partial}{\partial X}-\frac{1}{\rho^2}\frac{\partial}{\partial\Theta}\right)\frac{d\Theta}{\sqrt{X^2+r^2+\rho^2-2r\rho\cos\Theta}}\right]_{X=\frac{\Theta-\bar{\theta}_n}{a}+\delta} \qquad (29)$$

where the derivatives with respect to X and Θ are performed as if X and Θ were not related functions, and then the substitution

$$X = \frac{\Theta - \bar{\theta}_n + \varphi_0 - \theta_0}{a} - (x-\xi) \qquad (29a)$$

is made. This device will give the same results as before (Equation [28]), if the expansion

$$\frac{1}{R} = \frac{1}{\sqrt{X^2+r^2+\rho^2-2r\rho\cos\Theta}} = \frac{1}{\pi}\sum_{m=-\infty}^{\infty} e^{im\Theta}\int_{-\infty}^{\infty} I_m(k\rho)\,K_m(kr)\,e^{-iXk}\,dk \qquad (\text{for } \rho < r) \tag{29b}$$

is used (see Appendix A).

In References 1-4, the assumption was made that the propeller pitch is low, i.e., a = Ω/U is large since a can be considered as inverse advance ratio or as being inversely proportional to the pitch. Then

$$\begin{aligned} -\frac{r}{\sqrt{1+a^2r^2}}\left(a\frac{\partial}{\partial X}-\frac{1}{r^2}\frac{\partial}{\partial\Theta}\right) &\to -\frac{\partial}{\partial X} \\ \frac{\rho}{\sqrt{1+a^2\rho^2}}\left(a\frac{\partial}{\partial X}-\frac{1}{\rho^2}\frac{\partial}{\partial\Theta}\right) &\to \frac{\partial}{\partial X} \end{aligned} \tag{30}$$

In other words, the directional derivatives are in the axial direction normal to the staircase path, which makes the mathematical model consistent.

Although it appears that approximation (30) is valid only for the low-pitch case, a closer study of the line integral in Equation (29), before and after the deformation into staircase form which is described in a subsequent section on "The Assumed Staircase Function Replacing the Exact Integral Path," indicates that a change in the path of integration should be accompanied by a change in the directional derivatives. The results of the line integration are identical for both consistent models, the one with helical path and directional derivatives normal to that path (Equations [12] and [13]) and the other with path of integration along the projections of the helical (staircase) and directional derivatives normal to the new path (Equation [30]). Indeed, it has been shown in Reference 5, where the exact helical path is treated, that the use of assumption (30) with that model leads to results far different from the results obtained when either of the consistent models is used, and that the consistent models yielded values of thrust which were in good agreement. For comparison with the results of Reference 5, the present report will also consider the case where the wake is approximated by the staircase function but the derivatives are taken normal to the helicoid.

It should be noted that the basic assumption in the staircase path approximation comes when the decoupling of X and Θ is introduced, as will be seen in the section on page 23.

DETERMINING THE DIRECTIONAL DERIVATIVES

Here, as in References 3 and 4, the Descartes distance $R = \sqrt{X^2+r^2+\rho^2-2r\rho\cos\Theta}$ will be expressed in terms of Legendre functions of the second kind:*

$$\frac{1}{R} = \sum_{m=0}^{\infty} \epsilon_m \cos m\Theta \, \frac{1}{\pi\sqrt{r\rho}} \, Q_{m-\frac{1}{2}}\left(\frac{X^2+r^2+\rho^2}{2r\rho}\right)$$

$$\text{where } \epsilon_m = \begin{cases} 1\ , & m = 0 \\ 2\ , & m \neq 0 \end{cases} \tag{31}$$

---

*It can also be expressed in terms of Bessel functions of the first kind:

$$\frac{1}{R} = \sum_{m=0}^{\infty} \epsilon_m \cos m\Theta \int_0^{\infty} J_m(kr)\, J_m(k\rho)\, e^{-|X|k}\, dk$$

Taking the derivatives of $\frac{1}{R}$ with respect to X and Θ results in

$$(1) \qquad \frac{\partial}{\partial X}\left(\frac{1}{R}\right) = \frac{X}{\pi(r\rho)^{3/2}} \sum_{m=0}^{\infty} \epsilon_m \cos m\Theta \; Q'_{m-\frac{1}{2}}(z)$$

where $z = \frac{X^2+r^2+\rho^2}{2r\rho}$

$$Q'_{m-\frac{1}{2}}(z) = \frac{\partial}{\partial z} Q_{m-\frac{1}{2}}(z)$$

$$(2) \qquad \frac{\partial^2}{\partial X^2}\left(\frac{1}{R}\right) = \frac{1}{\pi(r\rho)^{3/2}} \sum_{m=0}^{\infty} \epsilon_m \cos m\Theta \left[Q'_{m-\frac{1}{2}}(z) + \frac{X^2}{r\rho} Q''_{m-\frac{1}{2}}(z)\right]$$

where $Q''_{m-\frac{1}{2}}(z) = \frac{\partial^2}{\partial z^2} Q_{m-\frac{1}{2}}(z)$

$$(3) \qquad \frac{\partial^2}{\partial \Theta^2}\left(\frac{1}{R}\right) = -\frac{1}{\pi\sqrt{r\rho}} \sum_{m=0}^{\infty} \epsilon_m \, m^2 \cos m\Theta \; Q_{m-\frac{1}{2}}(z)$$

$$(4) \qquad \frac{\partial^2}{\partial \Theta \partial X}\left(\frac{1}{R}\right) = -\frac{X}{\pi(r\rho)^{3/2}} \sum_{m=0}^{\infty} \epsilon_m \, m \sin m\theta \; Q'_{m-\frac{1}{2}}(z) \qquad (32)$$

These values are substituted in Equation (29) so that taking the derivatives normal to the helicoidal, as shown in that equation, yields

$$K(r,\varphi_o,\rho,\theta_o;q) = -\frac{1}{a}\left(\frac{1}{\pi a\rho\sqrt{1+a^2r^2}}\right)e^{-iq(\varphi_o-\theta_o)}$$

$$\cdot\sum_{n=1}^{N}\sum_{m=o}^{\infty}\epsilon_m\lim_{\delta\to o}\int_{\bar{\theta}_n-(\varphi_o-\theta_o)}^{\infty}e^{-iq\Theta}\left\{-\frac{a^2}{\sqrt{r\rho}}\cos m\Theta\left[Q'_{m-\frac{1}{2}}(z)+\frac{X^2}{r\rho}Q''_{m-\frac{1}{2}}(z)\right]\right.$$

$$-\frac{a(r^2+\rho^2)}{(r\rho)^{5/2}}\,m\sin m\Theta\,XQ'_{m-\frac{1}{2}}(z)$$

$$\left.+\frac{m^2}{(r\rho)^{3/2}}\cos m\Theta\,Q_{m-\frac{1}{2}}(z)\right\}\Bigg|_{X=\frac{\Theta-\bar{\theta}_n}{a}+\delta}d\theta \qquad (33a)$$

If the directional derivatives normal to the staircase path are used (Equation [30]),

$$K(r,\varphi_o,\rho,\theta_o;q) = -\frac{1}{a}\,e^{-iq(\varphi_o-\theta_o)}\sum_{n=1}^{N}\sum_{m=o}^{\infty}\epsilon_m\lim_{\delta\to o}$$

$$\cdot\left(-\frac{1}{\pi(r\rho)^{3/2}}\right)\int_{\bar{\theta}_n-(\varphi_o-\theta_o)}^{\infty}e^{-iq\Theta}\cos m\Theta\left[Q'_{m-\frac{1}{2}}(z)+\frac{X^2}{r\rho}Q''_{m-\frac{1}{2}}(z)\right]\Bigg|_{X=\frac{\Theta-\bar{\theta}_n}{a}+\delta}d\Theta \qquad (33b)$$

THE ASSUMED STAIRCASE FUNCTION REPLACING THE EXACT INTEGRAL PATH

The functional relationship between X and Θ (see Equation [29a]) is approximated by a staircase function,

$$X = \frac{p\bar{\theta}_o}{a} + \delta$$

where $\bar{\theta}_o = 2\pi/N$. Then Equation (29) can be reduced to the following form (with r, ρ, X and a non-dimensionalized with respect to propeller radius r_o):

$$K = -\frac{1}{a r_o^2}(K_1 + K_2) \tag{34}$$

where

$$K_1 = \sum_{n=1}^{N} \lim_{\delta \to o} \int_{\bar{\theta}_n - (\varphi_o - \theta_o)}^{\bar{\theta}_n + \bar{\theta}_o/2} e^{-iq(\Theta + \varphi_o - \theta_o)} \left[-\frac{r}{a\sqrt{1+a^2 r^2}} \left(\frac{a\partial}{\partial X} - \frac{1}{r^2}\frac{\partial}{\partial \Theta} \right) \left(\frac{a\partial}{\partial X} - \frac{1}{\rho^2}\frac{\partial}{\partial \Theta} \right) \frac{1}{R} \right]_{\substack{X = \delta \\ p = o}} d\Theta \tag{35}$$

$$K_2 = \lim_{\delta \to o} \sum_{p=1}^{\infty} \int_{o}^{2\pi} e^{-iq(\Theta + \varphi_o - \theta_o)} \left[-\frac{r}{a\sqrt{1+a^2 r^2}} \left(\frac{a\partial}{\partial X} - \frac{1}{r^2}\frac{\partial}{\partial \Theta} \right) \left(\frac{a\partial}{\partial X} - \frac{1}{\rho^2}\frac{\partial}{\partial \Theta} \right) \frac{1}{R} \right]_{X = p\frac{\bar{\theta}_o}{a} + \delta} d\Theta \tag{36}$$

and now r, ρ, and X are fractions of r_o and $a = \frac{\Omega r_o}{U}$.

EVALUATION OF K_2

On substituting Equation (32) in Equation (36) it is seen that there are no singularities, and therefore the limit $\delta \to 0$ may be taken before integration. The Θ-integration involves

$$\int_0^{2\pi} \epsilon_m \cos m\Theta \; e^{-iq\Theta} \, d\Theta = \begin{cases} 0 \, , & m \neq q \\ 2\pi \, , & m = q \end{cases}$$

and

$$\int_0^{2\pi} \epsilon_m \sin m\Theta \, e^{-iq\Theta} \, d\Theta = \begin{cases} 0 \, , & m \neq q \text{ and } m = q = 0 \\ -i2\pi \, , & m = q \neq 0 \end{cases}$$

When $m \neq q$, $K_2 = 0$; and when $m = q$,

$$K_2 = \sum_{p=1}^{\infty} \frac{2e^{-iq(\varphi_0 - \theta_0)}}{\sqrt{1+a^2 r^2} \; a\rho} \left\{ -\frac{a^2}{\sqrt{r\rho}} \left[Q'_{q-\frac{1}{2}}(z) + \frac{X^2}{r\rho} Q''_{q-\frac{1}{2}}(z) \right] \right.$$

$$+ \frac{q^2}{(r\rho)^{3/2}} \; Q_{q-\frac{1}{2}}(z)$$

$$\left. + \frac{ia(r^2+\rho^2)}{(r\rho)^{5/2}} \, q \, X \, Q'_{q-\frac{1}{2}}(z) \right\} \tag{37a}$$

where $X = p \, \bar{\theta}_0 / a$.

If the directional derivatives (Equation 30) normal to the staircase path are used,

$$K_2 = \sum_{p=1}^{\infty} - \frac{2e^{-iq(\varphi_o-\theta_o)}}{(r\rho)^{3/2}} \left[Q'_{q-\frac{1}{2}}(z) + \frac{X^2}{r\rho} Q''_{q-\frac{1}{2}}(z)\right] \tag{37b}$$

In Appendix B it is shown that Equation (37a) can be approximated by

$$\begin{aligned} K_2 \approx \frac{2e^{-iq(\varphi_o-\theta_o)}}{\sqrt{1+a^2r^2}\; a\rho} \Bigg\{ & - \frac{a^4\sqrt{r\rho}}{\bar{\theta}_o^{\,2}} \left[5.94\, Q_{q-\frac{1}{2}}(z_1) - 19.53\, Q_{q-\frac{1}{2}}(z_2) + 13.59\, Q_{q-\frac{1}{2}}(z_3)\right] \\ & - \frac{ia^2(r^2+\rho^2)q}{\bar{\theta}_o (r\rho)^{3/2}} \left[Q_{q-\frac{1}{2}}(z_4) + Q_{q-\frac{1}{2}}(z_5) - Q_{q-\frac{1}{2}}(z_6)\right] \\ & + \frac{q^2}{(r\rho)^{3/2}} \left[Q_{q-\frac{1}{2}}(z_7) + Q_{q-\frac{1}{2}}(z_8) + Q_{q-\frac{1}{2}}(z_9) + 6.7\, Q_{q-\frac{1}{2}}(z_{10})\right] \Bigg\} \end{aligned} \tag{38a}$$

and Equation (37b) by

$$K_2 \approx - \frac{2e^{-iq(\varphi_o-\theta_o)}}{(r\rho)^{1/2}} \frac{a^2}{\bar{\theta}_o^{\,2}} \left[5.94\, Q_{q-\frac{1}{2}}(z_1) - 19.53\, Q_{q-\frac{1}{2}}(z_2) + 13.59\, Q_{q-\frac{1}{2}}(z_3)\right] \tag{38b}$$

where z_i is given in Appendix B, Equation (B-11).

Since the kernel is in the separable form, the ρ-integration and the φ_α- and θ_α-integrations are independent. Calculations have shown that in the case of K_2 the ρ-integration can be performed by the tangential rule,

$$\int_{\rho_j-\beta}^{\rho_j+\beta} K_2(r_i,\rho)\, d\rho = 2\beta\, K_2(r_i,\rho_j)$$

or

$$\int_{\rho_j-\beta}^{\rho_j+\beta} \bar{K}_2^{(\bar{m},\bar{n})}(r_i,\rho)\,d\rho = 2\beta\,\bar{K}_2^{(\bar{m},\bar{n})}(r_i,\rho_j) \tag{39}$$

where the kernels are evaluated at median ρ of the j-strip of length 2β. A value of $\beta = 0.05$ (in terms of r_o) is satisfactory.

EVALUATION OF K_1 FOR $\rho \neq r$

Since there is no singularity in K_1 when $\rho \neq r$, the limit value $X = \delta = 0$ can be substituted before integration. From Equations (35) and (32),

$$K_1 = \frac{e^{-iq(\varphi_o-\theta_o)}}{\pi(r\rho)^{3/2}\sqrt{1+a^2r^2}\;a\rho} \cdot \sum_{n=1}^{N} \int_{\bar{\theta}_n-(\varphi_o-\theta_o)}^{\bar{\theta}_n+\bar{\theta}_o/2} e^{-iq\Theta}$$

$$\cdot \sum_{m=o}^{\infty} \epsilon_m \left\{ -a^2r\rho\cos m\Theta\; Q'_{m-\frac{1}{2}}(z) + m^2\cos m\Theta\, Q_{m-\frac{1}{2}}(z) \right\} d\Theta \tag{40}$$

where now $z = (r^2+\rho^2)/2r\rho$.

Let

$$f(m,q,n) = e^{-iq(\varphi_o-\theta_o)} \int_{\bar{\theta}_n-(\varphi_o-\theta_o)}^{\bar{\theta}_n+\bar{\theta}_o/2} e^{-iq\Theta}\cos m\Theta\, d\Theta \tag{41}$$

Then, for $\rho \neq r$, with derivatives normal to the helicoid,

$$K_1 = \frac{1}{\pi(r\rho)^{3/2}\sqrt{1+a^2r^2}\;a\rho} \sum_{\substack{m=\lambda N \\ \lambda=0,1,\dots}}^{\infty} \epsilon_m \sum_{n=1}^{N} f(m,q,n) \left[m^2 Q_{m-\frac{1}{2}}(z) - a^2 r\rho\, Q'_{m-\frac{1}{2}}(z)\right] \tag{42a}$$

and with derivatives normal to the staircase path,

$$K_1 = -\frac{1}{\pi(r\rho)^{3/2}} \sum_{m=0,N}^{\infty} \epsilon_m \sum_{n=1}^{N} f(m,q,n)\, Q'_{m-\frac{1}{2}}(z) \tag{42b}$$

Appendix C gives the proof that m is an integer multiple of N and evaluates $f(m,q,n)$.

For $m \neq q$,

$$\sum_{n=1}^{N} f(m,q,n) = i\,\frac{N}{2} \left\{ e^{-iq(\varphi_0-\theta_0)} \left[\frac{e^{-i(m+q)\bar{\theta}_0/2}}{m+q} - \frac{e^{+i(m-q)\bar{\theta}_0/2}}{m-q}\right] + \frac{e^{-im(\varphi_0-\theta_0)}}{m-q} - \frac{e^{im(\varphi_0-\theta_0)}}{m+q} \right\} \tag{43}$$

for $m = q \neq 0$,

$$\sum_{n=1}^{N} f(m,q,n) = \frac{N}{2} \left\{ e^{-iq(\varphi_0-\theta_0)} \left[\frac{\bar{\theta}_0}{2} + \varphi_0 - \theta_0 + \frac{ie^{-iq\bar{\theta}_0}}{2q}\right] - \frac{ie^{iq(\varphi_0-\theta_0)}}{2q} \right\}$$

and for $m = q = 0$,

$$\sum_{n=1}^{N} f(m,q,n) = N\left[\frac{\bar{\theta}_o}{2} + \varphi_o - \theta_o\right]$$

where $\varphi_o = \sigma^r - \theta_b{}^r \cos \varphi_\alpha$

$$\theta_o = \sigma^\rho - \theta_b{}^\rho \cos \theta_\alpha$$

The integration

$$\int_{\rho_j-\beta}^{\rho_j+\beta} K_1(r_i,\rho)\, d\rho \quad \text{or} \quad \int_{\rho_j-\beta}^{\rho_j+\beta} \bar{K}_1{}^{(\bar{m},\bar{n})}(r_i,\rho)\, d\rho$$

is done by Gaussian quadrature for the strips $\rho_j = r_i \pm 2\beta$; i.e., for the elements of the kernel matrix next to the main diagonal and thus closest to the singularity. For all other off-diagonal elements,

$$\int_{\rho_j-\beta}^{\rho_j+\beta} \left\{ \begin{matrix} K_1(r_i,\rho) \\ \bar{K}_1{}^{(\bar{m},\bar{n})}(r_i,\rho) \end{matrix} \right\} d\rho = 2\beta \left\{ \begin{matrix} K_1(r_i,\rho_j) \\ \bar{K}_1{}^{(\bar{m},\bar{n})}(r_i,\rho_j) \end{matrix} \right\} \qquad (44)$$

where the kernel is evaluated at median ρ_j . A value of $\beta = 0.05$ for the half-strip is satisfactory.

EVALUATION OF $\int_{r_i-\beta}^{r_i+\beta} K_1(r_i,\rho)\, d\rho$

After the substitution of Equation (32) in (35), it is seen that, when ρ approaches r_i as X approaches 0 , $z = (X^2 + r^2 + \rho^2)/2r\rho$ approaches unity and $Q_{m-\frac{1}{2}}(z)$ becomes infinite. The integral

$$\int_{r_i-\beta}^{r_i+\beta} K_1(r_i,\rho)\, d\rho$$

has a high-order singularity with Hadamard finite contribution.

Let

$$g(m,q,n) = e^{-iq(\varphi_o-\theta_o)} \int_{\bar{\theta}_n-\varphi_o+\theta_o}^{\bar{\theta}_n+\bar{\theta}_o/2} e^{-iq\Theta} \sin m\Theta \, d\Theta \tag{45}$$

and $f(m,q,n)$ be defined by Equation (41). The K_1 kernel for ρ close to r, with derivatives normal to the helicoid, is expressed as

$$K_1 = \frac{1}{\pi(r\rho)^{3/2}\sqrt{1+a^2r^2}\ a\rho} \lim_{X\to o} \sum_{m=o,N}^{\infty} \epsilon_m$$

$$\cdot \left\{ \sum_{n=1}^{N} f(m,q,n) \left[- a^2 r\rho Q'_{m-\frac{1}{2}}(z) - a^2X^2Q''_{m-\frac{1}{2}}(z) + m^2Q_{m-\frac{1}{2}}(z)\right]\right.$$

$$\left. - \sum_{n=1}^{N} g(m,q,n) \left[\frac{a(r^2+\rho^2)m}{r\rho} X\ Q'_{m-\frac{1}{2}}(z)\right]\right\} \tag{46a}$$

with $z = (X^2 + r^2 + \rho^2)/2r\rho$.

With derivatives normal to the staircase path,

$$K_1 = \frac{1}{\pi (r\rho)^{5/2}} \lim_{X \to 0} \sum_{m=0,N}^{\infty} \epsilon_m \sum_{n=1}^{N} f(m,q,n) \left[- r\rho Q'_{m-\frac{1}{2}}(z) - X^2 Q''_{m-\frac{1}{2}}(z) \right] \quad (46b)$$

The integration over ρ becomes, from (46a),

$$\int_{r_1-\beta}^{r_1+\beta} K_1(r_1,\rho)\, d\rho = \frac{1}{\pi \sqrt{1+a^2 r^2}} \lim_{X \to 0} \sum_{m=0,N}^{\infty} \epsilon_m$$

$$\cdot \left\{ \sum_{n=1}^{N} f(m,q,n) \int_{r_1-\beta}^{r_1+\beta} \frac{\left[- a^2 r\rho Q'_{m-\frac{1}{2}}(z) - a^2 X^2 Q''_{m-\frac{1}{2}}(z) + m^2 Q_{m-\frac{1}{2}}(z) \right]}{(r\rho)^{3/2}\, a\rho}\, d\rho \right.$$

$$\left. - m \sum_{n=1}^{N} g(m,q,n) \int_{r_1-\beta}^{r_1+\beta} \frac{(r^2+\rho^2)\, X\, Q'_{m-\frac{1}{2}}(z)}{(r\rho)^{5/2}\, \rho}\, d\rho \right\} \quad (47a)$$

and from (46b),

$$\int_{r_1-\beta}^{r_1+\beta} K_1(r_1,\rho)\, d\rho = \frac{1}{\pi} \lim_{X \to 0} \sum_{m=0,N}^{\infty} \epsilon_m \sum_{n=1}^{N} f(m,q,n) \int_{r_1-\beta}^{r_1+\beta} \frac{\left[- r\rho Q'_{m-\frac{1}{2}}(z) - X^2 Q''_{m-\frac{1}{2}}(z) \right]}{(r\rho)^{5/2}}\, d\rho \quad (47b)$$

As $X \to 0$ and $\rho \to r$, $z \to 1$. The Legendre functions can be expanded in series valid near $z = 1$, provided β is chosen small enough.

In Reference 14 a series representation of $Q_{m-\frac{1}{2}}(z)$ valid near $z = 1$ is obtained by assuming a solution to the appropriate Legendre differential equation

$$(1 - z^2)\, Q''_{m-\frac{1}{2}}(z) - 2z\, Q'_{m-\frac{1}{2}}(z) + (m^2 - 1/4)\, Q_{m-\frac{1}{2}}(z) = 0 \quad (48)$$

of the form

$$Q_{m-\frac{1}{2}}(z) = \sum_{s=0}^{\infty} a_{ms}(z-1)^s + \ln(z-1)\sum_{s=0}^{\infty} b_{ms}(z-1)^s \qquad (49)$$

Then

$$Q'_{m-\frac{1}{2}}(z) = \sum_{s=0}^{\infty} a_{ms}s(z-1)^{s-1} + \sum_{s=0}^{\infty} b_{ms}(z-1)^{s-1} + \ln(z-1)\sum_{s=0}^{\infty} b_{ms}s(z-1)^{s-1} \qquad (50)$$

and

$$Q''_{m-\frac{1}{2}}(z) = \sum_{s=0}^{\infty} a_{ms}s(s-1)(z-1)^{s-2} + \sum_{s=0}^{\infty} b_{ms}(s-1)(z-1)^{s-2}$$

$$+ \sum_{s=0}^{\infty} b_{ms}s(z-1)^{s-2} + \ln(z-1)\sum_{s=0}^{\infty} b_{ms}s(s-1)(z-1)^{s-2} \qquad (51)$$

where

$$(z-1) = \frac{X^2 + (r-\rho)^2}{2r\rho}$$

and the coefficients are given by Sluyter[14] as:

$$a_{mo} = \frac{5}{2}\ln 2 - 2\sum_{j=1}^{m} \frac{1}{2j-1}(1-\delta_{mo})$$

$$\delta_{mo} = \begin{cases} 1 & \text{for } m = 0 \\ 0 & \text{for } m \neq 0 \end{cases}$$

$$b_{mo} = -1/2$$

[Cont'd]

$$b_{m,p+1} = b_{mp} \frac{m^2 - \frac{1}{4} - p(p+1)}{2(p+1)^2}$$

$$a_{m,p+1} = a_{mp} \frac{m^2 - \frac{1}{4} - p(p+1)}{2(p+1)^2} - b_{mp} \frac{2(m^2 - \frac{1}{4}) + p + 1}{2(p+1)^3} \tag{52}$$

By using these series representations it is shown in Appendix D that

$$I_3 = \lim_{X \to 0} \int_{r_i - \beta}^{r_i + \beta} \frac{(r^2 + \rho^2) \ X \ Q'_{m-\frac{1}{2}}(z) \ d\rho}{(r\rho)^{5/2} \ \rho} \to 0$$

Since β is small, in the region $r_i - \beta < \rho < r_i + \beta$ it will be assumed that the mean value of $\rho (= r_i)$ can be substituted in the denominators of the remaining integrals of Equations (47a) and (47b). It is necessary then to evaluate the following integrals:

$$I_1 = \lim_{X \to 0} \int_{r-\beta}^{r+\beta} Q_{m-\frac{1}{2}}(z) \ d\rho$$

$$I_2 = \lim_{X \to 0} \int_{r-\beta}^{r+\beta} [r\rho Q'_{m-\frac{1}{2}}(z) + X^2 Q''_{m-\frac{1}{2}}(z)] \ d\rho$$

These integrals are evaluated in Appendix D. Equation (47a) becomes

$$\int_{r_i - \beta}^{r_i + \beta} K_1(r_i, \rho) \ d\rho \approx \left[\frac{1}{\pi a r^4 \sqrt{1 + a^2 r^2}} \right] \sum_{m=o,N}^{\infty} \epsilon_m \sum_{n=1}^{N} f(m,q,n) \left[m^2 I_1 - a^2 I_2 \right] \tag{53a}$$

and Equation (47b) becomes, for the case of derivatives in the axial direction,

$$\int_{r_i-\beta}^{r_i+\beta} K_1(r_i,\rho)\, d\rho \approx \frac{1}{\pi r^5} \sum_{m=0,N}^{\infty} \epsilon_m \sum_{n=1}^{N} f(m,q,n) \left[- I_2\right] \qquad (53b)$$

where I_1 and I_2 are given in Appendix D as

$$I_1 \approx 2\beta \sum_{s=0}^{\infty} \left(\frac{\beta^2}{2r^2}\right)^s \left\{\left(\frac{1}{2s+1}\right)\left[a_{ms} + b_{ms} \ln\left(\frac{\beta^2}{2r^2}\right)\right] - 2b_{ms} \frac{1}{(2s+1)^2}\right\} \qquad (54)$$

$$I_2 \approx -\frac{4r^4 b_{mo}}{\beta} + 2\beta r^2 \sum_{s=1}^{\infty} \left(\frac{\beta^2}{2r^2}\right)^{s-1} \left\{\left(\frac{s}{2s-1}\right)\left[a_{ms} + b_{ms} \ln\left(\frac{\beta^2}{2r^2}\right)\right] - b_{ms} \frac{1}{(2s-1)^2}\right\} \qquad (55)$$

It is interesting to note that, since $I_3=0$ and $I_1 < < I_2$, there is very little difference between Equations (47a) and (47b), or between Equations (53a) and (53b). This is reasonable since in the small region around the singular point there should be only small differences between the normals to helicoidal and staircase paths.

For the ρ-integration of K_2, and K_1 when $\rho \neq r$, a value $\beta = 0.05$ for the half-strip is satisfactory. However, calculations have shown that the integration around the singularity $\rho = r$ can be safely performed only for β no larger than 0.01.

The integration of K_1 in the regions adjacent to the singularity strip, $r_i - 0.05 \le \rho \le r_i - 0.01$ and $r_i + 0.01 \le \rho \le r_i + 0.05$, is done by means of the Lagrange interpolation method described in Appendix E, where the values of $K_1(r_i,\rho)$ are taken from Equation (42a) or (42b). For the case with derivatives normal to the helicoidal path,

$$\left[\int_{r-.05}^{r-.01} + \int_{r+.01}^{r+.05}\right] K_1(r,\rho)\, d\rho = \frac{1}{\pi r^{3/2}\sqrt{1+a^2 r^2}} \sum_{m=o,N}^{\infty} \epsilon_m \sum_{n=1}^{N} f(m,q,n)$$

$$\cdot \left[\int_{r-.05}^{r-.01} + \int_{r+.01}^{r+.05}\right] \left[\frac{m^2 Q_{m-\frac{1}{2}}(z)}{a\rho^{5/2}} - \frac{arQ'_{m-\frac{1}{2}}(z)}{\rho^{3/2}}\right] d\rho \tag{56a}$$

and, when the derivatives are in the axial direction,

$$\left[\int_{r-.05}^{r-.01} + \int_{r+.01}^{r+.05}\right] K_1(r,\rho)\, d\rho = -\frac{1}{\pi r^{3/2}} \sum_{m=o,N}^{\infty} \epsilon_m \sum_{n=1}^{N} f(m,q,n)$$

$$\cdot \left[\int_{r-.05}^{r-.01} + \int_{r+.01}^{r+.05}\right] \frac{Q'_{m-\frac{1}{2}}(z)}{\rho^{3/2}}\, d\rho \tag{56b}$$

where $z = r^2 + \rho^2/2r\rho$.

As shown in Appendix E ,

$$I_4 = \left[\int_{r-.05}^{r-.01} + \int_{r+.01}^{r+.05}\right] \frac{Q_{m-\frac{1}{2}}(z)}{\rho^{5/2}}\, d\rho$$

$$= 0.3111\ldots(F_1 - F_{-1}) + 0.7111\ldots(F_2 - F_{-2}) + 0.1777\ldots(F_3 - F_{-3})$$

$$+ 0.3555\ldots(F_4 - F_{-4}) + 0.06222\ldots(F_5 - F_{-5}) \tag{57}$$

where

$$F_p = 0.01\,p\,\frac{Q_{m-\frac{1}{2}}(z_p)}{(r+0.01p)^{5/2}}$$

$$z_p = \frac{r^2+(r+0.01p)^2}{2r(r+0.01p)}$$

$$p = \pm 1,\ \pm 2,\ \pm 3,\ \pm 4,\ \pm 5$$

and

$$I_5 = \left[\int_{r-.05}^{r-.01} + \int_{r+.01}^{r+.05}\right] \frac{Q'_{m-\frac{1}{2}}(z)}{\rho^{3/2}}\, d\rho$$

$$= 2283.2895\,(f_1-f_{-1}) + 2397.1028\,(f_2-f_{-2}) - 169.02\,(f_3-f_{-3})$$

$$+ 350.9914\,(f_4-f_{-4}) + 5.1197\,(f_5-f_{-5}) \qquad (58)$$

where

$$f_p = \frac{(0.01p)^3}{(r+0.01p)^{3/2}}\, Q'_{m-\frac{1}{2}}(z_p)$$

with z_p as before.

THE CHORDWISE LOADING DISTRIBUTION AND GENERALIZED LIFT OPERATOR

As was stated earlier, a direct solution is impossible because of the complexity of the surface integral equation. A large number of modes given by the Birnbaum distribution (Equation [17]) is assumed for the chordwise loading. The integration over θ_o can then be performed after the trigonometric transformation $\theta_o = \sigma^\rho - \theta_b{}^\rho \cos\theta_\alpha$. The surface integral equation is thus reduced to a line integral equation.

Next, the generalized lift operator (Equation [19b]) of $\bar{m}$ modes is applied to both sides of the integral equation. There are now $\bar{m}$ integral equations which are equal in number to the $\bar{n}$ chordwise modes. These equations are given by Equation (20). The unknown spanwise distribution is then found by the collocation method. After subdividing the blade into i-strips along the span, the $\bar{m}$ integral equations are reduced to the set of algebraic equations given by Equation (21).

In this equation the modified kernels $\bar{K}^{\bar{m},\bar{n}}$ are given by

$$\bar{K}^{(1,1)} = \frac{1}{\pi^2}\int_0^\pi\int_0^\pi (1 - \cos\varphi_\alpha)(1 + \cos\theta_\alpha)\, K\, d\theta_\alpha\, d\varphi_\alpha$$

$$\bar{K}^{(2,1)} = \frac{1}{\pi^2}\int_0^\pi\int_0^\pi (1 + 2\cos\varphi_\alpha)(1 + \cos\theta_\alpha)\, K\, d\theta_\alpha\, d\varphi_\alpha$$

$$\bar{K}^{(\bar{m} > 2,1)} = \frac{1}{\pi^2}\int_0^\pi\int_0^\pi \frac{\cos(\bar{m}-1)\varphi_\alpha}{(\bar{m}-1)}(1 + \cos\theta_\alpha)\, K\, d\theta_\alpha\, d\varphi_\alpha$$

$$\bar{K}^{(1,\bar{n}>1)} = \frac{1}{\pi^2}\int_0^\pi\int_0^\pi (1 - \cos\varphi_\alpha)\frac{\sin(\bar{n}-1)\theta_\alpha}{(\bar{n}-1)}\sin\theta_\alpha\, K\, d\theta_\alpha\, d\varphi_\alpha$$

$$\bar{K}^{(2,\bar{n} > 1)} = \frac{1}{\pi^2}\int_0^\pi\int_0^\pi (1 + 2\cos\varphi_\alpha)\frac{\sin(\bar{n}-1)\theta_\alpha}{(\bar{n}-1)}\sin\theta_\alpha\, K d\theta_\alpha\, d\varphi_\alpha$$

[Cont'd]

$$\bar{K}^{(\bar{m},\bar{n})} = \frac{1}{\pi^2}\int_0^{\pi}\int_0^{\pi}\frac{\cos(\bar{m}-1)\varphi_\alpha}{(\bar{m}-1)}\,\frac{\sin(\bar{n}-1)\theta_\alpha}{(\bar{n}-1)}\sin\theta_\alpha\, K d\theta_\alpha\, d\varphi_\alpha$$

$$\text{for}\quad \bar{m} > 2\ ,\ \bar{n} > 1 \qquad (59)$$

where the kernels K are as given in preceding sections.

The following relations are needed for the θ_α-integrations:

$$\Lambda^{(1)}(x) = \frac{1}{\pi}\int_0^{\pi}(1+\cos\theta_\alpha)\, e^{-ix\cos\theta_\alpha}\, d\theta_\alpha = J_0(x) - iJ_1(x)$$

$$\Lambda^{(\bar{n})}(x) = \frac{1}{\pi}\int_0^{\pi}\frac{\sin(\bar{n}-1)\,\theta_\alpha\sin\theta_\alpha}{(\bar{n}-1)}\, e^{-ix\cos\theta_\alpha}\, d\theta_\alpha$$

$$= \frac{(-i)^{\bar{n}-2}}{2(\bar{n}-1)}\left[J_{\bar{n}-2}(x) + J_{\bar{n}}(x)\right]\ ,\ \bar{n} > 1$$

$$\Lambda_1^{(1)}(x) = \frac{1}{\pi}\int_0^{\pi}(1+\cos\theta_\alpha)\cos\theta_\alpha\, e^{-ix\cos\theta_\alpha}\, d\theta_\alpha$$

$$= \frac{1}{2}\left[J_0(x) - J_2(x)\right] - iJ_1(x)$$

$$\Lambda_1^{(\bar{n})}(x) = \frac{1}{\pi}\int_0^{\pi}\frac{\sin(\bar{n}-1)\,\theta_\alpha\sin\theta_\alpha\cos\theta_\alpha}{(\bar{n}-1)}\, e^{-ix\cos\theta_\alpha}\, d\theta_\alpha$$

$$= \frac{(-i)^{\bar{n}+1}}{4(\bar{n}-1)}\left[J_{\bar{n}-3}(x) - J_{\bar{n}+1}(x)\right]\ ,\ \bar{n} > 1 \qquad (60)$$

The values for (-x) are the complex conjugates of the above expressions for (+x).

For the $\bar{m}$ modes of the lift operator:

$$I^{(1)}(x) = \frac{1}{\pi}\int_0^{\pi} (1 - \cos\varphi_\alpha)\, e^{+ix\cos\varphi_\alpha}\, d\varphi_\alpha = J_o(x) - iJ_1(x)$$

$$I^{(2)}(x) = \frac{1}{\pi}\int_0^{\pi} (1 + 2\cos\varphi_\alpha)\, e^{+ix\cos\varphi_\alpha}\, d\varphi_\alpha = J_o(x) + 2iJ_1(x)$$

$$I^{(\bar{m})}(x) = \frac{1}{\pi}\int_0^{\pi} \frac{\cos(\bar{m}-1)\varphi_\alpha}{(\bar{m}-1)}\, e^{+ix\cos\varphi_\alpha}\, d\varphi_\alpha = \frac{i^{\bar{m}-1}J_{\bar{m}-1}(x)}{(\bar{m}-1)}\ , \quad \bar{m} > 2$$

$$I_1^{(1)}(x) = \frac{1}{\pi}\int_0^{\pi} (1 - \cos\varphi_\alpha)\cos\varphi_\alpha\, e^{+ix\cos\varphi_\alpha}\, d\varphi_\alpha$$

$$= -\frac{1}{2}\,[J_o(x) - J_2(x)] + iJ_1(x)$$

$$I_1^{(2)}(x) = \frac{1}{\pi}\int_0^{\pi} (1 + 2\cos\varphi_\alpha)\cos\varphi_\alpha\, e^{+ix\cos\varphi_\alpha}\, d\varphi_\alpha$$

$$= [J_o(x) - J_2(x)] + iJ_1(x)$$

$$I_1^{(\bar{m})}(x) = \frac{1}{\pi}\int_0^{\pi} \frac{\cos(\bar{m}-1)\,\varphi_\alpha}{(\bar{m}-1)}\cos\varphi_\alpha\, e^{ix\cos\varphi_\alpha}\, d\varphi_\alpha$$

$$= \frac{i^{(\bar{m}-2)}}{2(\bar{m}-1)}\left[- J_{\bar{m}}(x) + J_{\bar{m}-2}(x)\right]\ , \quad \bar{m} > 2 \qquad (61)$$

where again the values for (-x) are the complex conjugates of those for (+x).

The left-hand side of Equation (20) or Equation (21) is, with the introduction of skewness,

$$\frac{V(r)}{U} \, I^{\bar{m}}(q\theta_b{}^r) \, e^{-iq\sigma^r} \tag{62}$$

When $q = 0$,

$$I^{(1)}(q\theta_b{}^r) = I^{(2)}(q\theta_b{}^r) = 1$$

$$I^{(\bar{m} > 2)}(q\theta_b{}^r) = 0$$

The evaluation of $k^{(\bar{m},\bar{n})}(r_i,\rho_j)$ is performed in the following manner:

(1) From Equations (59) and (39), if the definitions of φ_o and θ_o are used,

$$k_2^{(\bar{m},\bar{n})}(r_i,\rho_j) = \int_{\rho_j-\beta}^{\rho_j+\beta} \bar{K}_2^{(\bar{m},\bar{n})} \, d\rho = 2\beta e^{-iq(\sigma^r-\sigma^\rho)}$$

$$\cdot \, I^{(\bar{m})}(q\theta_b{}^r) \;\; \Lambda^{(\bar{n})}(q\theta_b{}^\rho) \cdot F(r,\rho) \tag{63}$$

where $F(r,\rho)$ is the factor of $e^{-iq(\varphi_o-\theta_o)}$ in Equation (38a) or (38b).

(2) For $\rho_j \neq r_i$,

$$k_1^{(\bar{m},\bar{n})}(r_i,\rho_j) = \int_{\rho_j-\beta}^{\rho_j+\beta} \bar{K}_1^{(\bar{m},\bar{n})} \, d\rho$$

$$= \frac{1}{\pi a r^{3/2}\sqrt{1+a^2r^2}} \sum_{m=o,N}^{\infty} \epsilon_m \sum_{n=1}^{N} \bar{f}^{(\bar{m},\bar{n})} \int_{\rho_j-\beta}^{\rho_j+\beta} \frac{m^2 Q_{m-\frac{1}{2}}(z) - a^2 r\rho Q'_{m-\frac{1}{2}}(z)}{\rho^{5/2}} \, d\rho \tag{64a}$$

with derivatives normal to the helicoid, and

$$k_1^{(\bar{m},\bar{n})}(r_i,\rho_j) = -\frac{1}{\pi r^{3/2}} \sum_{m=o,N}^{\infty} \epsilon_m \sum_{n=1}^{N} \bar{f}^{(\bar{m},\bar{n})} \int_{\rho_j-\beta}^{\rho_j+\beta} \frac{Q'_{m-\frac{1}{2}}(z)}{\rho^{3/2}}\, d\rho \qquad (64b)$$

with derivatives in axial direction, where

$$z = \frac{r^2 + \rho^2}{2r\rho}$$

and the ρ-integration is done by Gaussian quadrature for next-to-main-diagonal elements and by tangential rule, which was used for calculation of k_2 , for other off-diagonal elements.

Here, for $m \neq q$, from Equations (43) and (59),

$$\sum_{n=1}^{N} \bar{f}^{(\bar{m},\bar{n})} = \frac{iN}{2} \left\{ e^{-iq(\sigma - \sigma^\rho)}\, I^{(\bar{m})}(q\theta_b{}^r)\, \Lambda^{(\bar{n})}(q\theta_b{}^\rho) \left[\frac{e^{-i(m+q)\bar{\theta}_o/2}}{m+q} - \frac{e^{i(m-q)\bar{\theta}_o/2}}{m-q} \right] \right.$$

$$+ \frac{e^{-im(\sigma^r - \sigma^\rho)}}{m-q}\, I^{(\bar{m})}(m\theta_b{}^r)\, \Lambda^{(\bar{n})}(m\theta_b{}^\rho)$$

$$\left. - \frac{e^{im(\sigma^r - \sigma^\rho)}}{m+q}\, I^{(\bar{m})}(-m\theta_b{}^r)\, \Lambda^{(\bar{n})}(-m\theta_b{}^\rho) \right\}$$

for $m = q \neq 0$,

$$\sum_{n=1}^{N} \bar{f}^{(\bar{m},\bar{n})} = \frac{N}{2} \left\{ e^{-iq(\sigma^r - \sigma^\rho)}\, I^{(\bar{m})}(q\theta_b{}^r)\, \Lambda^{(\bar{n})}(q\theta_b{}^\rho) \left[\frac{\bar{\theta}_o}{2} + \sigma^r - \sigma^\rho + \frac{ie^{-iq\bar{\theta}_o}}{2q} \right] \right.$$

$$- \frac{ie^{+iq(\sigma^r - \sigma^\rho)}}{2q}\, I^{(\bar{m})}(-q\theta_b{}^r)\, \Lambda^{(\bar{n})}(-q\theta_b{}^\rho)$$

$$\left. + e^{-iq(\sigma^r - \sigma^\rho)} \left[-\theta_b{}^r\, I_1^{(\bar{m})}(q\theta_b{}^r)\, \Lambda^{(\bar{n})}(q\theta_b{}^\rho) + \theta_b{}^\rho\, I^{(\bar{m})}(q\theta_b{}^r)\, \Lambda_1^{(\bar{n})}(q\theta_b{}^\rho) \right] \right\}$$

and for $m = q = 0$,

$$\sum_{n=1}^{N} \bar{f}^{(\bar{m},\bar{n})} = N \left\{ \left[\frac{\bar{\theta}_o}{2} + (\sigma^r - \sigma^\rho) \right] I^{(\bar{m})}(o) \, \Lambda^{(\bar{n})}(o) \right.$$

$$\left. - \theta_b{}^r \, I_1{}^{(\bar{m})}(o) \, \Lambda^{(\bar{n})}(o) + \theta_b{}^\rho \, I^{(\bar{m})}(o) \, \Lambda_1{}^{(\bar{n})}(o) \right\} \qquad (65)$$

(3) In the region $r_i - 0.01 < \rho < r_i + 0.01$, with derivatives normal to the helicoid as in Equation (53a),

$$\int_{r_i-.01}^{r_i+.01} \bar{K}_1^{(\bar{m},\bar{n})}(r_i,\rho) \, d\rho \approx \frac{1}{\pi a r^4 \sqrt{1+a^2 r^2}} \sum_{m=o,N}^{\infty} \epsilon_m \sum_{n=1}^{N} \bar{f}^{(\bar{m},\bar{n})} \left[m^2 I_1 - a^2 I_2 \right] \qquad (66a)$$

where I_1 and I_2 are given by Equations (54) and (55); with derivatives normal to the staircase path as in Equation (53b),

$$\int_{r_i-.01}^{r_i+.01} \bar{K}_1^{(\bar{m},\bar{n})}(r_i,\rho) \, d\rho \approx -\frac{1}{\pi r^5} \sum_{m=o,N}^{\infty} \epsilon_m \sum_{n=1}^{N} \bar{f}^{(\bar{m},\bar{n})} \, I_2 \qquad (66b)$$

In Equations (66a) and (66b) it is assumed that for this small region $\sigma^r = \sigma^\rho$ and $\theta_b{}^r = \theta_b{}^\rho$.

(4) In the regions adjacent to the singular region,

$$\left[\int_{r_i-.05}^{r_i-.01} + \int_{r_i+.01}^{r_i+.05} \right] \bar{K}_1^{(\bar{m},\bar{n})} \, d\rho = \frac{1}{\pi a r^{3/2} \sqrt{1+a^2 r^2}} \cdot \sum_{m=o,N}^{\infty} \epsilon_m \sum_{n=1}^{N} \bar{f}^{(\bar{m},\bar{n})} \left[m^2 I_4 - a^2 r \, I_5 \right] \qquad (67a)$$

with derivatives normal to the helicoid; or

$$= - \frac{1}{\pi r^{3/2}} \sum_{m=o,N}^{\infty} \epsilon_m \sum_{n=1}^{N} \bar{f}^{(\bar{m},\bar{n})} \; I_5 \qquad (67b)$$

with derivatives in the axial direction, where I_4 and I_5 are given by Equations (57) and (58). Here, also, it is assumed that $\sigma^r = \sigma^\rho$ and $\theta_b{}^r = \theta_b{}^\rho$.

LOADING DUE TO BLADE CAMBER AND FLOW INCIDENCE ANGLE

Equations (14) through (21) have been written for hull-induced velocities obtained from wake surveys in the propeller plane as

$$V(r)\ e^{-iq\varphi_0}$$

where $V(r)$ are the Fourier coefficients of the wake velocity normal to the propeller blade. However, the various small disturbances imposed on this flow can be treated similarly. The velocities induced by the disturbances are simply added to the wake velocities.

Since the propeller blades do not coincide with the assumed helicoidal surface of pitch 1/a, but are located on a nearby surface, additional flow disturbances arise due to incidence angle and blade camber. The velocities induced by these are independent of time because the blades are considered rigid, so that only the stationary part $(q = o)$ of the loading will be affected.

The loading L_{c+f}, due to camber and flow-angle disturbances V_c and V_f, is obtained from the steady state part of the integral equation with the left-hand side replaced by $(V_c + V_f)/U$.

The flow-angle disturbance depends only on the radial position, not on φ_α, and therefore contributes only when $\bar{\bar{m}} = 1$ and 2.
The velocity due to flow-angle effect is

$$\frac{\bar{V}_f^{(1),(2)}(r)}{U} = -\sqrt{1+a^2 r}\ \left(\tan^{-1}\frac{P(r)}{2\pi r} - \tan^{-1}\frac{1}{ar}\right) \qquad (68)$$

where the incident flow angle is defined by the difference between the geometric pitch angle $\tan^{-1}(P/2\pi r)$ and the hydrodynamic pitch angle $\tan^{-1}(1/ar)$ of the assumed surface.

The velocity due to camber effect is

$$V_c = + U \sqrt{1+a^2 r^2}\, \frac{\partial f(r,s)}{\partial s} \tag{69}$$

where $\partial f(r,s)/\partial s$ is the slope of the camber line $f(r,s)$ given at discrete points measured from the face pitch line. This slope can be expressed in a Fourier series expansion in terms of $s = b(1 - \cos \varphi_\alpha)$ where b is the semichord in feet. On application of the lift operators, Equation (69) becomes

$$\bar{V}_c^{(\bar{m})} = \frac{1}{\pi} \int_0^\pi \begin{Bmatrix} 1 - \cos \varphi_\alpha \\ 1 + 2 \cos \varphi_\alpha \\ \dfrac{\cos (\bar{m}-1)\, \varphi_\alpha}{\bar{m}-1} \end{Bmatrix} V_c \, d\varphi_\alpha \tag{70}$$

Because $\partial f/\partial s$ is predominantly a $\cos \varphi_\alpha$-function, $\bar{V}_c^{(\bar{m})}$ will be negligible for $\bar{m} > 2$. For $\bar{m} = 1$,

$$\frac{\bar{V}_c^{(1)}(r)}{U} = \frac{\sqrt{1+a^2 r^2}}{2b(r)} \left\{ \frac{1}{\pi} \int_0^\pi \frac{\partial f(r,s')}{\partial s'} (1 - \cos \varphi_\alpha)\, d\varphi_\alpha \right\} \tag{71}$$

where $s' = s/2b(r) = (1 - \cos \varphi_\alpha)/2$. If Equation (71) is integrated by parts after changing the variable of integration from φ_α to s', then

$$\frac{\bar{V}_c^{(1)}(r)}{U} = - \sqrt{1+a^2 r^2} \left\{ \frac{1}{2\pi b(r)} \int_0^1 \frac{f(r,s')\, ds'}{(1-s')\sqrt{s'(1-s')}} \right\} \tag{72}$$

The factor in the brace of Equation (72) is the theoretical no-lift angle of Glauert. Ordinates of the camberline $f(r,s')$ are more accurately read than slopes; therefore Equation (72) is to be preferred to Equation (71). Integration is done by the trapezoidal rule from $s' = 0.05$ to 0.90, and the ends are integrated analytically after substitution of a simple function in s' for $f(r,s')$. For example, if the parabola $s'(1 - s') \cdot f(0.05)/0.0475$ is taken for $f(s')$ at the leading edge ($s' = 0$ to 0.05), and the line $(1 - s')\, f(0.95)/0.05$ for $f(s')$ at the trailing edge ($s' = 0.90$ to 1.00), and it is noted that in this case $f(0.90) = 2f(0.95)$, integration will yield the Burrill[15] factors for $f(s')$ at $s' = 0.05$, 0.90 and 0.95.

On application of the second lift operator,

$$\frac{\bar{V}_c^{(2)}(r)}{U} = \frac{\sqrt{1+a^2 r^2}}{2b(r)} \left\{ \frac{1}{\pi} \int_0^{\pi} (1 + 2 \cos \varphi_\alpha) \frac{\partial f(r,s')}{\partial s'}\, d\varphi_\alpha \right\}$$

and it can be shown that

$$\frac{\bar{V}_c^{(2)}(r)}{U} = \frac{\bar{V}_c^{(1)}(r)}{U} - \frac{\sqrt{1+a^2 r^2}}{2b(r)} \left\{ \frac{-3}{2\pi} \int_0^1 \frac{f(r,s')\, ds'}{s'(1-s')\sqrt{s'(1-s')}} \right\} \qquad (73)$$

Here the integration over s' is done by the trapezoidal rule from $s' = 0.10$ to 0.90, and the ends are integrated analytically after substituting the parabola for $f(s')$ at the leading edge and the straight line at the trailing edge.

NUMERICAL RESULTS

Calculations have been performed for seven marine propellers, one 5-blade, one 7-blade, four 3-blade, and one 4-blade. The 5-blade and 7-blade propellers operate in two different wakes; the wake designated by Test No. 1 is associated with portside data and that designated by Test No. 4 with starboard data, in the propeller plane behind the same vessel. The 3-blade propellers operate in a 3-cycle wake generated by a screen in a 24-inch water tunnel. The 4-blade propeller is the one treated in earlier reports as having sector-form blades without skewness, but here its true geometry is taken into account. The pertinent information on these propellers is tabulated below.

TABLE 1

MODEL PARTICULARS

	Propeller Characteristics				
No. of Blades	Diameter, ft	EAR	P/D at 0.7 r_o	Skewness	Wake Generator
5	16	0.597	0.714	0	Model Tests No. 1
7	16	0.584	0.694	22.5°	Model and No. 4
3	1	0.3	1.086	0	Screen
3	1	0.6	1.077	0	Screen
3	1	1.2	1.073	0	Screen
3	1	0.6	1.071	120.0°	Screen
4	21.5	0.36	1.03	6.7°	Model AE21

SPANWISE LOADING DISTRIBUTION

For the 4-blade, 5-blade, and 7-blade propellers, the assumed chordwise mode shapes were first mode (flat plate), first three modes, first four modes, and first five modes. In the case of the 3-blade propellers, the first three, four, and five modes were considered; the flat-plate mode was not treated except for propeller No. 4118 at q = 3. Typical spanwise loading results are presented in Figures 2-7. It is apparent that the spanwise loading distribution, and therefore the steady and time-dependent thrust, converge to a stable value after several chordwise modes. For these calculations the propeller span has been divided into equal strips, 0.1 propeller radius in length.

Calculations have in some instances been made with double the number of strips or control points, considering only the chordwise distribution described by the first three terms of the Birnbaum series. Figures 8 and 9 show the spanwise loading distribution on the 5-blade propeller in Wake No. 4, for q = 0 and q = 5, and compare the results with seven control points (solid lines) and fourteen control points (dash lines). The trends of solid and dash lines are similar. At q = 0 the total loading from fourteen strips is 2-percent less and at q = 5 10-percent less than from seven strips. Similar calculations for the 7-blade propeller in Wake No. 4 show that at q = 0 the total loading from fourteen strips is the same as that from seven strips and that at q = 7 it is 7-percent less.

The ratios of theoretical mean thrust to the mean thrust calculated at DTMB are shown below.

TABLE 2

RATIO OF THEORETICAL TO DTMB — CALCULATED MEAN THRUST

		Wake	
Propeller	No. of Control Pts.	Test No. 1	Test No. 4
5-blade	7	1.15	1.14
	14		1.12
7-blade	7	1.18	1.16
	14		1.16

The theoretical values reported here are those calculated by the consistent mathematical model described in previous sections, with directional derivatives in the axial direction normal to the assumed staircase path. The values of mean thrust obtained by the inconsistent model, a staircase approximation of the helicoidal wake of the blades with derivatives normal to the helicoidal surface, are about 10-percent higher than these, which are already higher than the DTMB calculated thrusts.

Table 3, following, compares values of the ratio of double amplitude of vibratory thrust to mean thrust, as calculated here and by quasi-steady theory at DTMB, with experimental data obtained by DTMB by means of two different testing techniques. The Davidson Laboratory theoretical results are those computed with seven control points.

The results of calculations for the 4-blade propeller, not simplified as in the earlier Davidson Laboratory reports but with actual blade form and skewness, are compared in Table 4 with the experimental data from model tests at DTMB. These calculations also were done with seven control points.

TABLE 3

CORRELATION OF RESULTS OF THEORY AND EXPERIMENTS
Double Amplitude of Vibratory Thrust
in Percent of Mean Thrust

No. of Blades	Characteristics	Theory				DTMB Quasi-steady Calculations	DTMB Experiments
		1 Mode	3 Modes	4 Modes	5 Modes		
5	Test No. 1						
	1st Blade Freq.						
	Unsteady	15.0	13.0	11.8	12.9		10.4 , 13.8
	Quasi-steady	13.3	12.5	12.6	12.4	16.2	
	2nd Blade Freq.						
	Unsteady	1.5	1.46	1.38	1.48		1.76, 1.46
	Quasi-steady	1.3	1.38	1.42	1.30	1.6	
	Test No. 4						
	1st Blade Freq.						
	Unsteady	11.6	10.4	9.4	10.3		8.8 , 13.8
	Quasi-steady	10.5	9.8	9.8	9.8	12.3	
	2nd Blade Freq.						
	Unsteady	1.6	1.47	1.43	1.43		1.42, 1.46
	Quasi-steady	1.3	1.37	1.43	1.34	1.4	
7	Test No. 1						
	1st Blade Freq.						
	Unsteady	2.5	2.61	2.38	2.60		1.64, 3.10
	Quasi-steady	1.5	1.41	1.51	1.41	2.5	
	2nd Blade Freq.						
	Unsteady	1.1	1.07	1.03	1.11		1.0 , 0.53
	Quasi-steady	0.25	0.18	0.25	0.15	0.62	
	Test No. 4						
	1st Blade Freq.						
	Unsteady	1.3	1.43	1.28	1.44		1.4 , 3.10
	Quasi-steady	1.2	1.16	1.19	1.16	1.6	
	2nd Blade Freq.						
	Unsteady	1.3	1.11	1.15	1.18		0.6 , 0.53
	Quasi-steady	0.11	0.13	0.04	0.07	0.14	

TABLE 4

MEAN THRUST $\bar{T}$ AND DOUBLE AMPLITUDE OF VIBRATORY THRUST IN PERCENT OF MEAN THRUST $\Delta T/\bar{T}$ FOR 4-BLADE PROPELLER

	Theory				DTMB Model Data
	1 Mode	3 Modes	4 Modes	5 Modes	
$\bar{T}$, lb	167,300	185,700	182,600	184,700	173,000
$\Delta T/\bar{T}$ (1st blade frequency)					
Unsteady	15.1	12.5	11.5	12.2	26.6*
Quasi-steady	14.1	13.1	13.6	13.2	

*Average of model data; first blade harmonic from full-scale ship trials is 13.8 percent.

For the series of 3-blade propellers, calculations have been performed to evaluate the $\bar{K}_T$ vs. J curve in the open-water condition (i.e., thrust coefficient versus advance ratio) and to evaluate the vibratory $\tilde{K}_T$ coefficient at design J by the unsteady and quasi-steady methods. The results of these calculations are summarized in Tables 5-7, where they are compared with the corresponding DTMB measurements.

These propellers operated in the wake generated by a screen in such manner that the mean (zero harmonic) of the wake velocity, averaged over the blade span, was equal to the free-stream velocity. There is then only negligible contribution of the wake to the steady-state loading on the propellers. This steady-state loading can be said to equal the loading in the open-water condition and arises, in the present theory, from camber and flow-angle effects only.

It is interesting to note that, although the theoretically determined $\bar{K}_T$-curves are higher in magnitude than the experimental data for the three non-skewed propellers, they have approximately the same slope (Fig. 10); and that the smaller the expanded area ratio the closer the results of experiment and linear theory. The 120-degree skewed propeller certainly stretches this theory, but in spite of this the vibratory thrust calculated by the theory shows the proper relation to the other propellers.

TABLE 5

CORRELATION OF THEORETICAL AND EXPERIMENTAL $\bar{K}_T$ VALUES IN THE OPEN-WATER CONDITION FOR 3-BLADE PROPELLERS

		Theory				
EAR	J	3 Modes 8 Contr. Pts.	4 Modes 8 Contr. Pts.	5 Modes 8 Contr. Pts.	3 Modes 16 Contr. Pts.	Experiment
0.3	0.701	0.207	0.204	0.206		0.195
	0.841	0.168	0.168	0.168	0.163	0.150
	1.01	0.110	0.115	0.111		0.090
0.6	0.693	0.227	0.221	0.222		0.208
	0.831	0.180	0.179	0.178		0.150
	0.997	0.109	0.114	0.109		0.080
1.2	0.703	0.275	0.281	0.272		0.225
	0.844	0.216	0.226	0.216	0.206	0.150
	1.013	0.124	0.141	0.129		0.070
0.6 (Skewed)	0.876	0.099	0.102	0.101		0.150

TABLE 6

CORRELATION OF UNSTEADY SINGLE AMPLITUDE $\tilde{K}_T$ VALUES FOR 3-BLADE PROPELLERS AT FIRST BLADE FREQUENCY

EAR	J	No. of Spanwise Control Points	Theory			Experiment
			3 Modes	4 Modes	5 Modes	
0.3	0.841	8	0.060	0.055	0.059	0.053
		16	0.056			
0.6	0.831	8	0.061	0.055	0.060	0.066
1.2	0.844	8	0.041	0.043	0.038	0.032
		16	0.033			
0.6 (Skewed)	0.876	8	0.010	0.009	0.009	0.0078

TABLE 7

QUASI-STEADY SINGLE AMPLITUDE $\tilde{K}_{Tq}$ VALUES FOR 3-BLADE PROPELLERS AT FIRST BLADE FREQUENCY

EAR	J	No. of Spanwise Control Points	Theory		
			3 Modes	4 Modes	5 Modes
0.3	0.841	8	0.069	0.060	0.069
		16	0.066		
0.6	0.831	8	0.065	0.068	0.064
1.2	0.844	8	0.055	0.050	0.038
		16	0.057		
0.6 (Skewed)	0.876	8	0.011	0.010	0.010

Another comparison that has been made concerns the differences between spanwise loading as calculated according to the present three-dimensional theory and by a stripwise application of two-dimensional non-stationary theory. As shown in previous reports[3,4] the two-dimensional solution of the loading is

$$L_o(r,q) = 2\pi\rho_f U^2 \theta_b^r \frac{(1+a^2 r^2)}{a} S(k) \frac{V(r,q)}{U} e^{-iq\sigma^r}$$

where a and r are dimensional
$S(k)$ is the Sears function
$k = q\theta_b{}^r$ is reduced frequency

Table 8 gives the ratios $R_{3/2}$ of spanwise integrated lift by three-dimensional theory to spanwise integrated lift by the stripwise method, for the 3-blade non-skewed propellers. For the reduced frequency $k = q\theta_b^r$ the chordwise measurement at 0.75 radius is chosen to typify the blade. The differences between phases of the loading by the two methods, $(\beta_3 - \beta_2)$, at 0.75 radius are also tabulated.

TABLE 8

LIFT RATIO $R_{3/2}$ FOR 3-BLADE PROPELLERS

EAR	q	$k = q\theta_b^r$ at 0.75 r_o	$R_{3/2}$	$(\beta_3 - \beta_2)$ at 0.75 r_o
0.3	0	0	0.376	0
	3	0.82	0.656	9.8°
0.6	0	0	0.234	0
	3	1.64	0.495	16.4°
1.2	0	0	0.154	0
	3	3.29	0.369	24.0°

As EAR decreases, the three-dimensional lift approaches closer to the two-dimensional value at lower frequencies, whereas, when EAR increases, the coincidence of values is postponed to higher and higher frequencies.

An example of the variation of phases over the span can be seen in Figure 11 for the 3-blade propeller of 0.60 expanded area ratio, at $q = 3$.

The charts exhibit, in addition to β_3 and β_2, the input phases of the wake normal components to the blade with respect to the midchord line. Figure 12 shows the differences between β_3 and the input phases for the three non-skewed 3-blade propellers of different expanded area ratio, and Figure 13 the differences between β_3 and β_2, at $q = 3$. (At $q = 0$, the input phases as well as β_3 and β_2 are all 180°.)

These phase charts show that the effects of three-dimensionality are more pronounced at the hub and the tip than around midspan; and Figure 12 shows that the phase lag after the input wake increases with increasing expanded area ratio.

Similar trends can be shown for the other propellers.

CHORDWISE LOADING DISTRIBUTION

It has been shown that the spanwise loading distribution and hence the thrust converge after a few terms of the Birnbaum distribution are taken. This means that the integrated effect of the loading distribution along the chord is not changed appreciably by adding more chordwise modes. However, the chordwise loading distribution itself has shown no sign of convergence even when, in the case of the 3-blade propeller 4118, ten terms of the Birnbaum series were taken.

It seems that the solution tries to change the magnitude (or mitigate the effect) of the leading-edge singularity through the contribution of higher-frequency terms of the sine series. As is shown in Appendix F, the sine series builds up a term proportional to the cotangent term, which reduces the coefficient $\ell^{(o)}$ of the Birnbaum distribution

$$\ell^{(o)} \cot \frac{\theta}{2} + \sum_{n=1}^{\infty} \ell^{(n)} \sin n\theta$$

At the same time the coefficients $\ell^{(n)}$ of the remaining sine series are also reduced. The solution develops a pressure distribution whose center moves away from the $\frac{1}{4}$-chord line towards the leading edge, but which leaves unchanged the nature of the leading-edge singularity. The latter remains the same as in the two-dimensional case. Although the high-frequency terms do not contribute to the spanwise distribution or the mean and vibratory thrust, their presence is important in the formation of the chordwise distribution and is felt mainly in the neighborhood of the leading edge and, to a smaller extent, toward the trailing edge.

The calculations have shown that the coefficients $\ell^{(n)}$ not only remain of the same order of magnitude but, with increasing number of modes, tend to a constant value c . It appears that the coefficients of the sine series are of the form

$$\ell^{(n)} = a_n + c$$

where $a_n \rightarrow o$ as $n \rightarrow \infty$. The assumed chordwise distribution can then be written as

$$\ell^{(o)} \cot \frac{\theta}{2} + \sum_{n=1}^{\infty} (\ell^{(n)} - c) \sin n\theta + c \sum_{n=1}^{\infty} \sin n\theta$$

the last term of which represents a divergent series, whose value nevertheless exists in the Cesàro sense and is given by

$$c \sum_{n=1}^{\infty} \sin n\theta = \frac{c}{2} \cot \frac{\theta}{2}$$

(see Appendix F).

The chordwise distribution can be modified to the form

$$(\ell^{(o)} + \frac{c}{2}) \cot \frac{\theta}{2} + \sum_{n=1}^{M} (\ell^{(n)} - c) \sin n\theta \tag{74}$$

since

$$\lim_{n\to\infty} (\ell^{(n)} - c) = \lim_{n\to\infty} a_n \to 0$$

Hence the sum will converge and the chordwise distribution will rapidly reach its final form.

This observation brings out two important facts:

(a) The expansion of the chordwise distribution in terms of the Birnbaum series does not satisfy the claim that the expansion functions are linearly independent, since the sine series gives rise to a term proportional to cot $(\theta/2)$.

(b) The chordwise distribution is established after employment of the Cesàro summability which is a useful approach in obtaining the limit of slowly convergent or even divergent series. This method suppresses the contribution of the higher-frequency constituents and puts emphasis on the lower ones.

Application of Cesàro sums to the sine series of the chordwise distribution given by

$$S_n = \ell^{(o)} \cot\frac{\theta}{2} + \sum_{n=1}^{M} \ell^{(n)} \sin n\theta$$

will yield

$$\sigma_n = \ell^{(o)} \cot\frac{\theta}{2} + \sum_{n=1}^{M} \left(\frac{M-n+1}{M}\right) \ell^{(n)} \sin n\theta \tag{75}$$

It is shown in Appendix F that, as $M \to \infty$, (74) and (75) are identical. Therefore the approach of subtracting a constant term from the sine coefficients, and adding half its value to the cotangent coefficient, and the approach of applying Cesàro summability to the partial sine series are equivalent. In spite of the lower rate of convergence of the sine series in the latter approach, this approach has the advantage that the constant term is never required explicitly. Calculations have shown that both approaches yield approximately the same results.

The results of calculations of the unsteady chordwise loading distribution at 0.75 radius of the 3-blade propeller 4118 (EAR = 0.6) are exhibited in Figures 14-16 for a series of modes M = 1 to 10. Figures 14a and 14b present the real parts, Figures 15a and 15b the imaginary parts, and Figures 16a and 16b the magnitudes of the unsteady loading for q = 3. It appears that, except for the neighborhood of the leading and trailing edges, the distribution is being established after M = 6.

In an attempt to minimize the effect of truncation of the chordwise distribution series, use has also been made of the least-squares method. This method has been used in the field of aerodynamics to improve the solution of the unsteady lifting-surface integral equation by the collocation method.[17,18] It was introduced there in an attempt to minimize errors between the self-induced velocity and the downwash distribution at various points other than the collocation points, and to distribute the errors uniformly over the entire planform. In the present case it is utilized to minimize errors between self-induced velocity and downwash distribution due to truncating the assumed chordwise series. However, the results of the least-squares method have been very close to the direct solution of the integral equation, indicating that the latter is the best possible solution with the presently available means. It can be concluded that the truncation of the series is not the hindrance to rapid convergence of the chordwise distribution, but that the basic trouble is the assumed chordwise modes.

Another facet of the present study is the capability of the program to judge how well a given propeller is designed, either for open-water or prescribed wake conditions. Figures 17a and 17b present the normal sum and Cesàro summability of the chordwise loading distribution in the steady-state case, q = o , for the 3-blade propeller designed for operation in open water at J = 0.831. These show that the distribution converges after three or four modes are taken, and is of the expected form. Figures 18a and 18b present similar calculations for the off-design advance ratio J = 0.700. The contrast is vivid. The presence of the singularity at the leading edge is more pronounced than in the design case.

Figures 19a and 19b show the steady-state chordwise distribution for the wake-adapted 5-blade propeller, when normal and Cesāro sums are taken. When the effects of wake are separated from the flow angle and camber effects (see Figures 20 and 21), the chordwise distribution is not established after five modes are taken, even with the Cesāro summability method. When their effects are combined, as in Figures 19a and 19b, the chordwise distribution as obtained either by normal summation or by Cesāro summability is similar to that of the 3-blade propeller which was designed for open-water conditions.

CONCLUSION

A theory has been developed for the evaluation of the steady and time-dependent loading distributions on the blades of a marine propeller operating in spatially non-uniform flow. The resulting surface integral equation has been solved by means of the collocation method in conjunction with the generalized lift operator for a prescribed set of chordwise modes which reproduce the proper leading-edge singularity and fulfill the Kutta condition at the trailing edge.

General computer programs have been developed to accomodate any geometry of propeller operating in a specified non-uniform inflow condition for a large but finite number of chordwise modes. The calculations indicate that the spanwise loading distribution and hence the steady and vibratory thrust are approximated by a rapidly convergent series of chordwise modes. After the first three terms, adding chordwise modes does not appreciably change the integrated effect along the blade chord.

A comparison of theoretical and experimental results for the vibratory thrust shows good agreement for the most part. There are still discrepancies. Hence questions inevitably arise as to limitation of the linearized theory and failure of the Kutta-Joukowski hypothesis. However, the validity of the experimental results should not be excluded from question.

It is believed that, in the case of propellers operating behind a model, a major cause of discrepancies between measured and calculated vibratory thrust arises from the lack of precise knowledge of wake harmonics. The wake harmonics are derived from wake surveys made in the absence of the propeller and hence any effects due to the action of the mean flow induced by the propeller on the hull boundary layer are not included. Indeed, recently reported experiments at the Ordnance Research Laboratory of Pennsylvania State University have revealed considerable reduction of certain harmonic constituents of the wake behind a body of revolution with appendages, when wakes measured without and with propeller running were compared. It is conjectured that the mean pressure reduction generated by the propeller on the near-afterbody surface reduces the adverse pressure gradient and so alters the shape of the wake shed into the propeller disc. Measurements to verify this statement should be made on ship models.

Although the spanwise loading distribution and the steady and vibratory thrust converge to a stable value after three to five chordwise modes, the loading distribution along the chord does not converge even when ten terms of the Birnbaum series are taken. With the introduction of the Cesāro summability, which is a proper method for summing diverging or slowly converging series, the distribution is, after six modes, established over the major portion of the chord, but not in the neighborhood of the leading and trailing edges.

The cause of the slow rate of convergence of the chordwise distribution is attributed to the type of assumed chordwise modes (the Birnbaum series). The terms of this series are not linearly independent, since part of the sine series produces a cotangent term, which when combined with the flat-plate mode reduces the value of the coefficient of this first mode. At the same time the coefficients of the sine series are also reduced in such a way that the combined effect on the pressure distribution is to move the center of pressure away from the $\frac{1}{4}$-chord line toward the leading edge.

The fact that application of the least-squares method yields results very close to the normal solution of the integral equation indicates that the present solution is the best possible with the presently available means.

The capability of the present program to pass judgment on whether or not a given propeller is well designed under open-water or wake conditions should be considered of very practical interest.

As for the conclusion of earlier reports, that the two-dimensional unsteady aerodynamic theory applied in stripwise manner is invalid for the marine propeller, this still holds true. With propellers of aspect ratio 1 to 2 and reduced frequency 1 to 2.5, neither the airfoil theory nor the low-aspect-ratio wing theory can be utilized.

ACKNOWLEDGEMENT

The authors wish to acknowledge their indebtedness to Dr. John P. Breslin and Dr. Charles J. Henry for their valuable discussions, which clarified certain aspects of the present study.

REFERENCES

1. SHIOIRI, J. and TSAKONAS, S., "Three-Dimensional Approach to the Gust Problem for a Screw Propeller," DL-Report 940, Stevens Institute of Technology, March 1963; J. Ship Research, Vol. 7, No. 4, April 1964, pp. 29-53.

2. TSAKONAS, S., ENG, K., and JACOBS, W. R., Confidential DL Report 987, Stevens Institute of Technology, 1963.

3. TSAKONAS, S. and JACOBS, W. R., "Unsteady Lifting Surface Theory for a Marine Propeller of Low Pitch Angle with Chordwise Loading Distribution," DL Report 994, Stevens Institute of Technology, January 1964; J. Ship Research, Vol. 9, No. 2, September 1965, pp. 79-101.

4. TSAKONAS, S., CHEN, C. Y., and JACOBS, W. R., Confidential DL Report 1055, Stevens Institute of Technology, February 1965.

5. TSAKONAS, S., CHEN, C. Y., and JACOBS, W. R., "Exact Treatment of the Helicoidal Wake in the Propeller Lifting-Surface Theory," DL Report 1117, Stevens Institute of Technology, August 1966.

6. SPARENBERG, J. A., "Application of Lifting-Surface Theory to Ship Screws," Koninkl. Ned. Akad. Wetenschap. Proc. (Amsterdam) Series B, Vol. 62, 1959, p. 286.

7. HANAOKA, T., "Introduction to the Nonuniform Hydrodynamics Concerning a Screw Propeller," J. Society of Naval Architects of Japan, No. 109, p. 1; and "On the Integral Equation Concerning an Oscillating Screw Propeller by Lifting Line Theory," ibid., No. 110, p. 185.

8. YAMAZAKI, R., "On the Theory of Screw Propellers," Memoirs of the Faculty of Engineering, Kyushu University, Japan, Vol. 23, No. 2, 1963; and "On the Theory of Screw Propellers in Nonuniform Flows," ibid., Vol. 25, No. 2, 1966.

9. BROWN, N. A., "Periodic Propeller Forces in Nonuniform Flow," Report 64-7, Massachusetts Institute of Technology, 1964.

10. GREENBERG, M. D., "The Unsteady Loading on a Marine Propeller in a Nonuniform Flow," J. Ship Research, Vol. 8, No. 3, December 1964, pp. 27-38.

11. WATKINS, C. E., WOOLSTON, D. S., and CUNNINGHAM, H. J., "A Systematic Kernel Function Procedure for Determining Aerodynamic Forces on Oscillating or Steady Finite Wings at Subsonic Speeds," NASA Technical Report R-48, 1959.

12. LAWRENCE, H. R., "The Lift Distribution on Low Aspect Ratio Wings at Subsonic Speeds." Presented at the Supersonic Aerodynamics Session, 19th Annual Meeting IAS, New York, 29 January - 1 February 1951.

13. MIKHLIN, S. G., Integral Equations. Pergamon Press, New York-London, 1957.

14. SLUYTER, M. M., "A Computational Program and Extended Tabulation of Legendre Functions of Second Kind and Half Order," THERM Report TAR-TR601, 1960.

15. BURRILL, L. C., "Calculation of Marine Propeller Performance Characteristics," North-East Coast Inst. of Engineers and Shipbuilders, March 1944, p. 264 ff.

16. WIDDER, D. V., Advanced Calculus, 2nd ed., Prentice-Hall, Inc., Englewood Cliffs, N. J., 1961, Chap. 9.

17. FROMME, J. A., "Least-Squares Approach to Unsteady Kernel Function Aerodynamics," AIAA Journal, Vol. 2, No. 7, July 1964.

18. REVELL, J. D. and RODDEN, W. P., "Remarks on Numerical Solutions of the Unsteady Lifting Surface Problem," AIAA Journal, Vol. 4, No. 1, January 1966.

BLANK PAGE

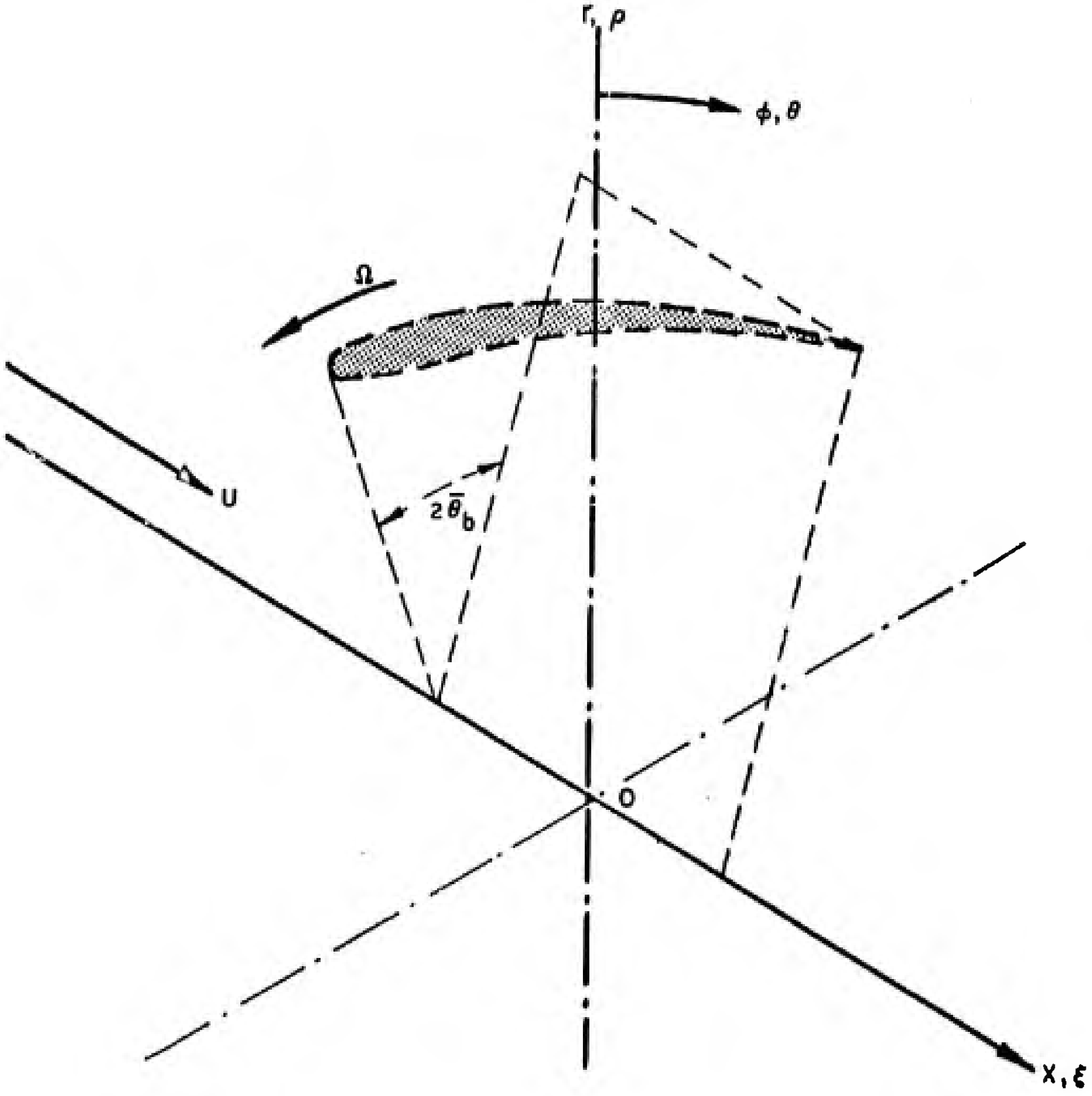
r, ρ
φ, θ
Ω
U
$2\bar{\theta}_b$
O
x, ξ

FIGURE I. COORDINATE SYSTEM AND NOTATIONS

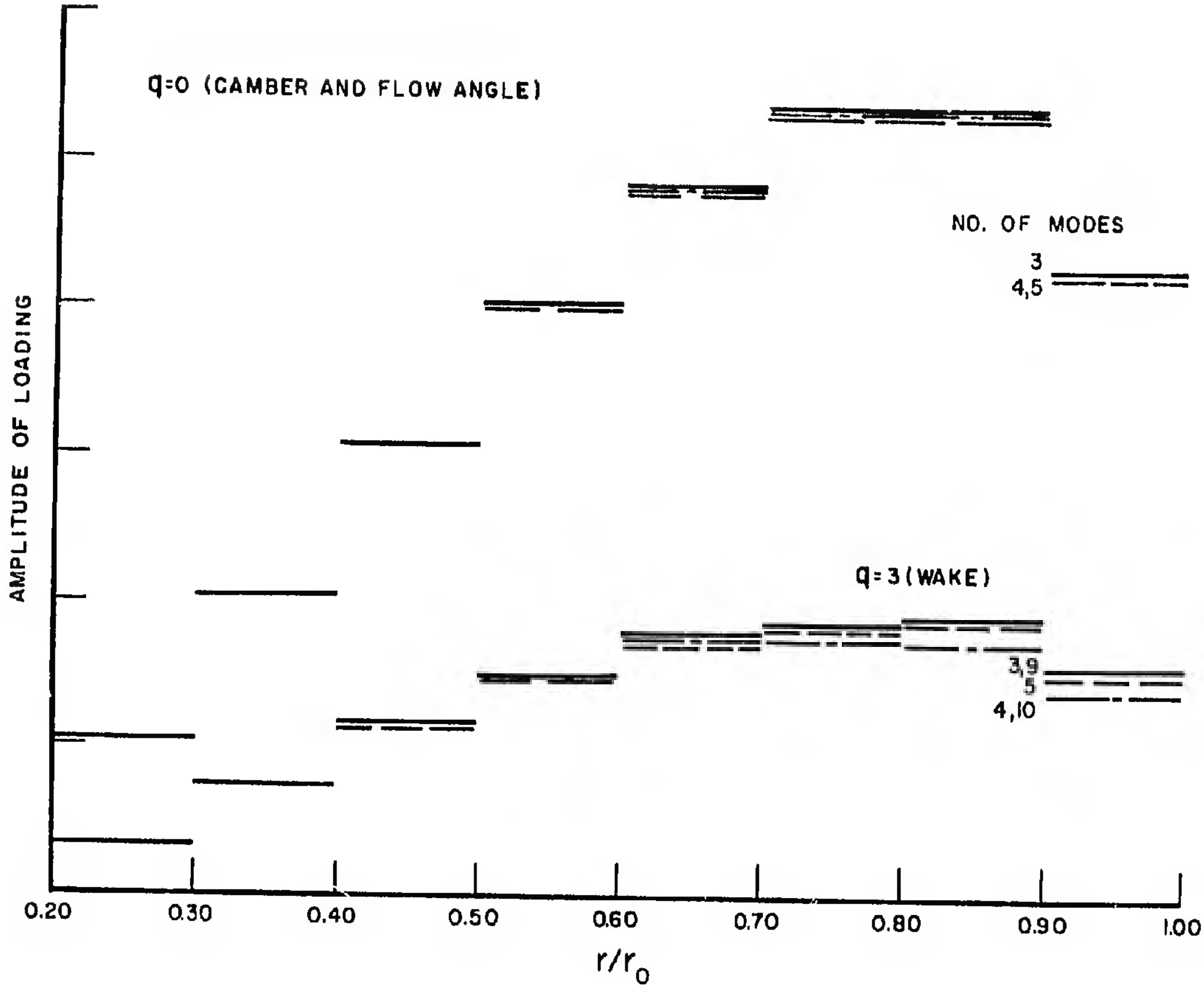

FIGURE 2. SPANWISE LOADING ON 3-BLADED PROPELLER (EAR=0.6) IN SCREEN-GENERATED WAKE

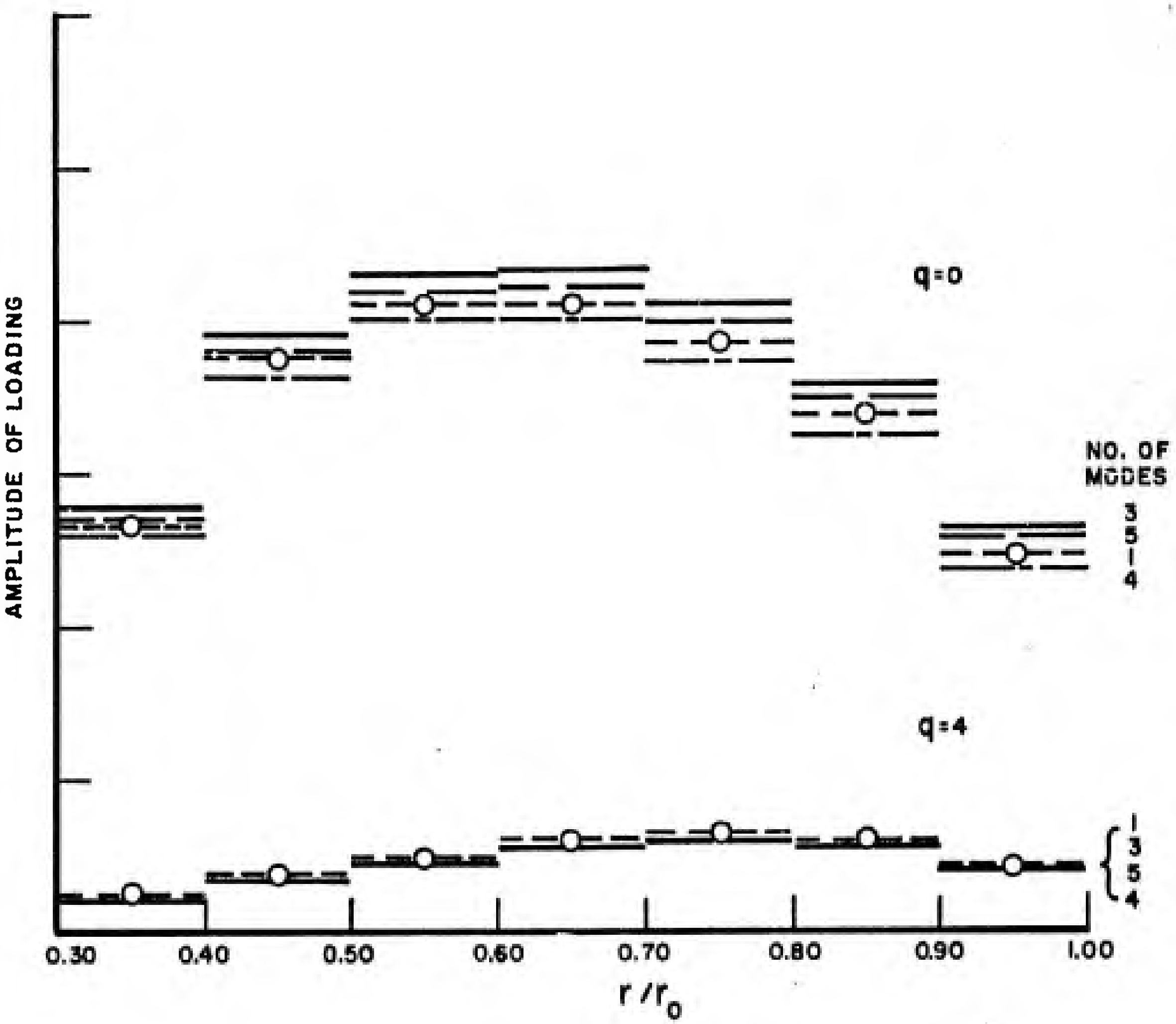

FIGURE 3. SPANWISE LOADING DUE TO SHIP WAKE ONLY ON 4-BLADED PROPELLER

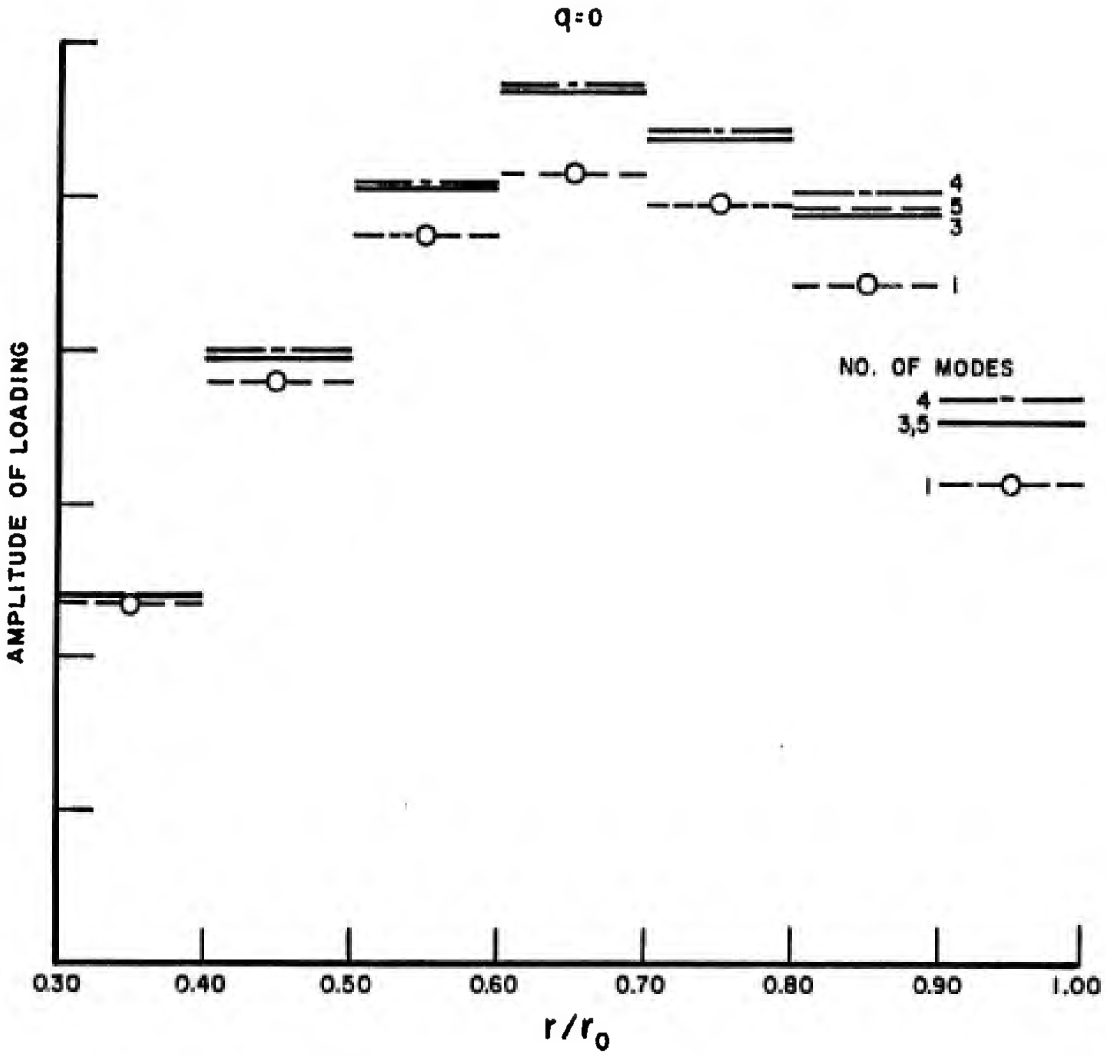

FIGURE 4. STEADY SPANWISE LOADING DUE TO WAKE, CAMBER AND FLOW ANGLE ON 5-BLADED PROPELLER IN WAKE NO. 1

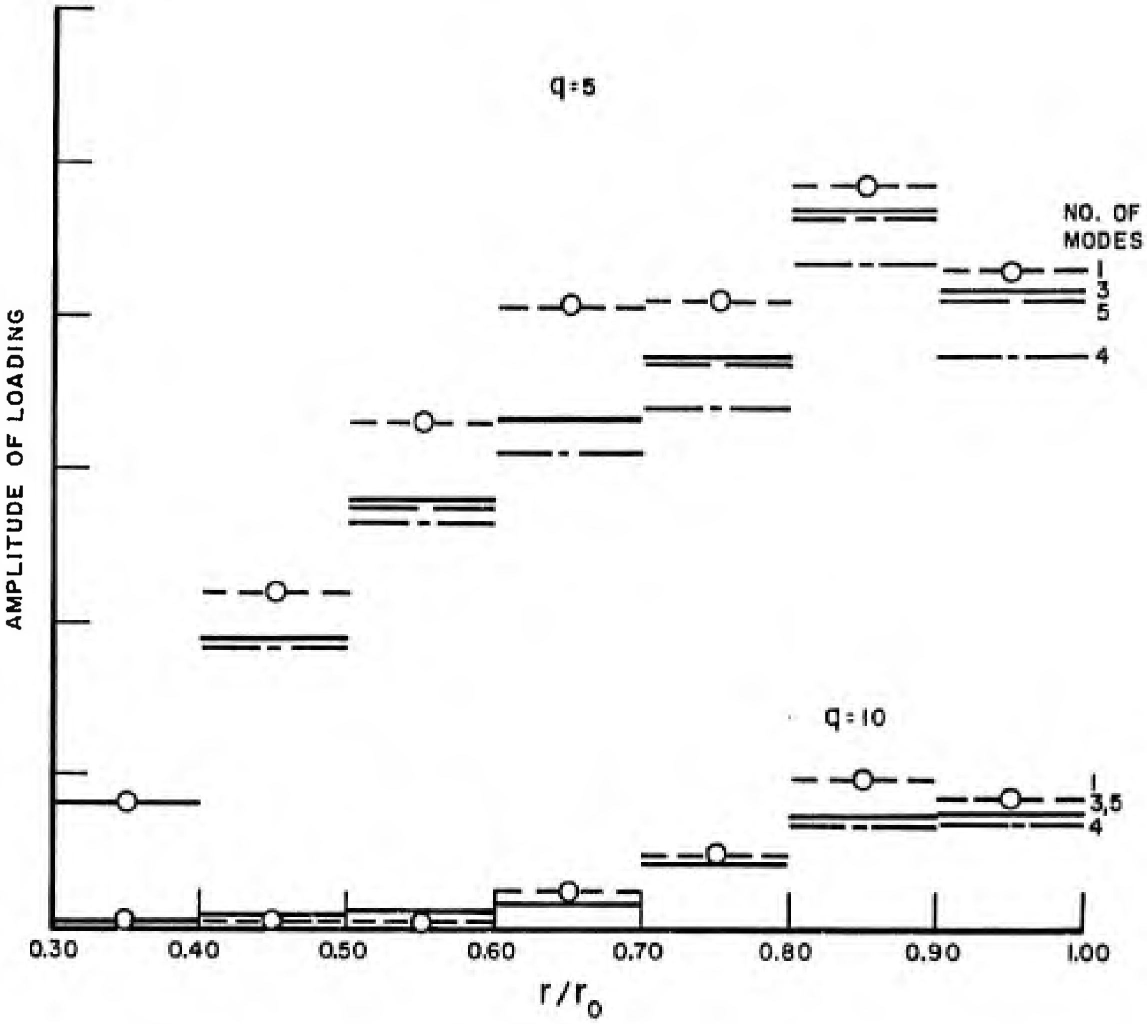

FIGURE 5. UNSTEADY SPANWISE LOADING DUE TO WAKE NO.1 ON 5-BLADED PROPELLER

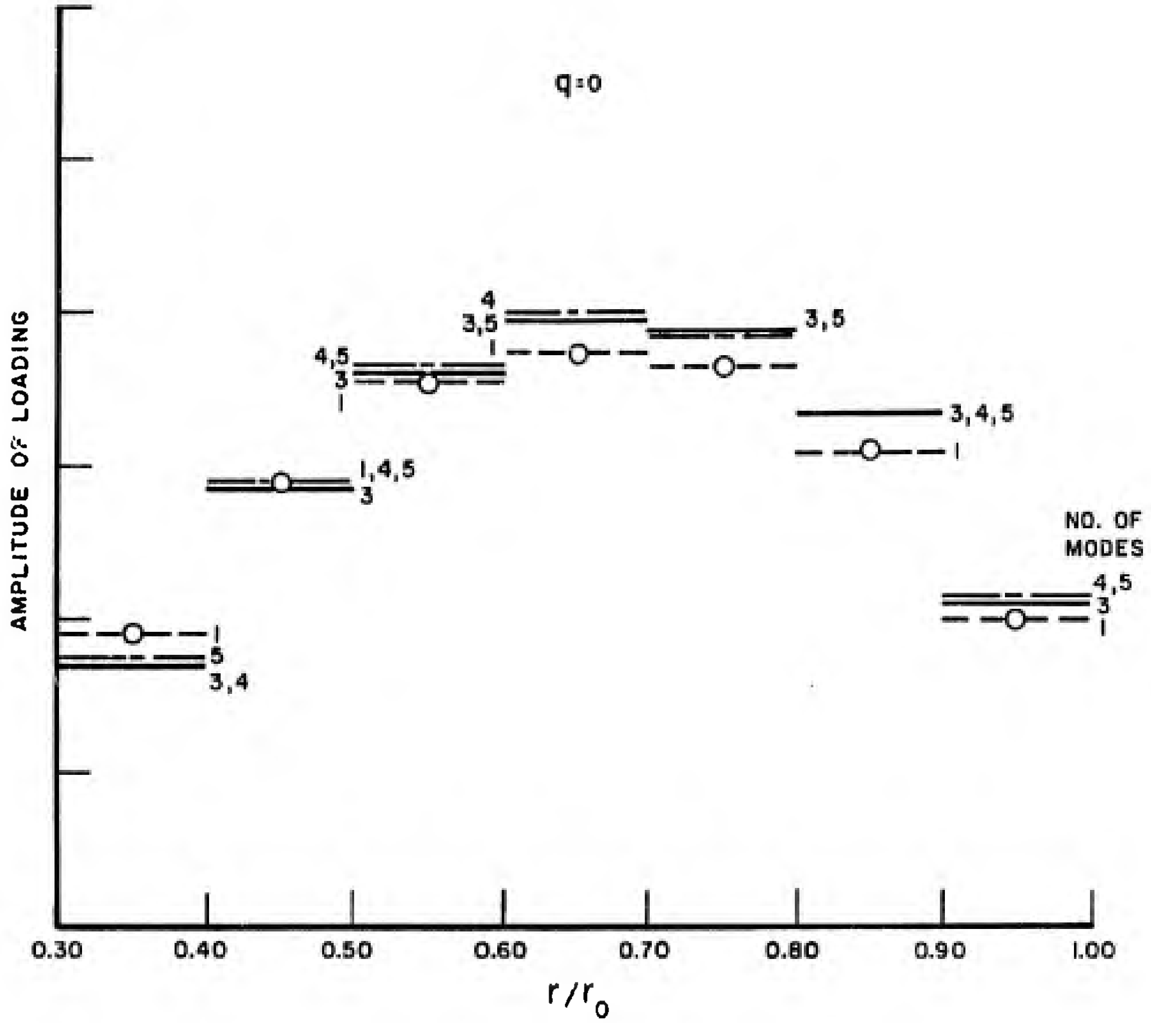

FIGURE 6. STEADY SPANWISE LOADING DUE TO WAKE, CAMBER, AND FLOW ANGLE ON 7-BLADED PROPELLER IN WAKE NO. 1

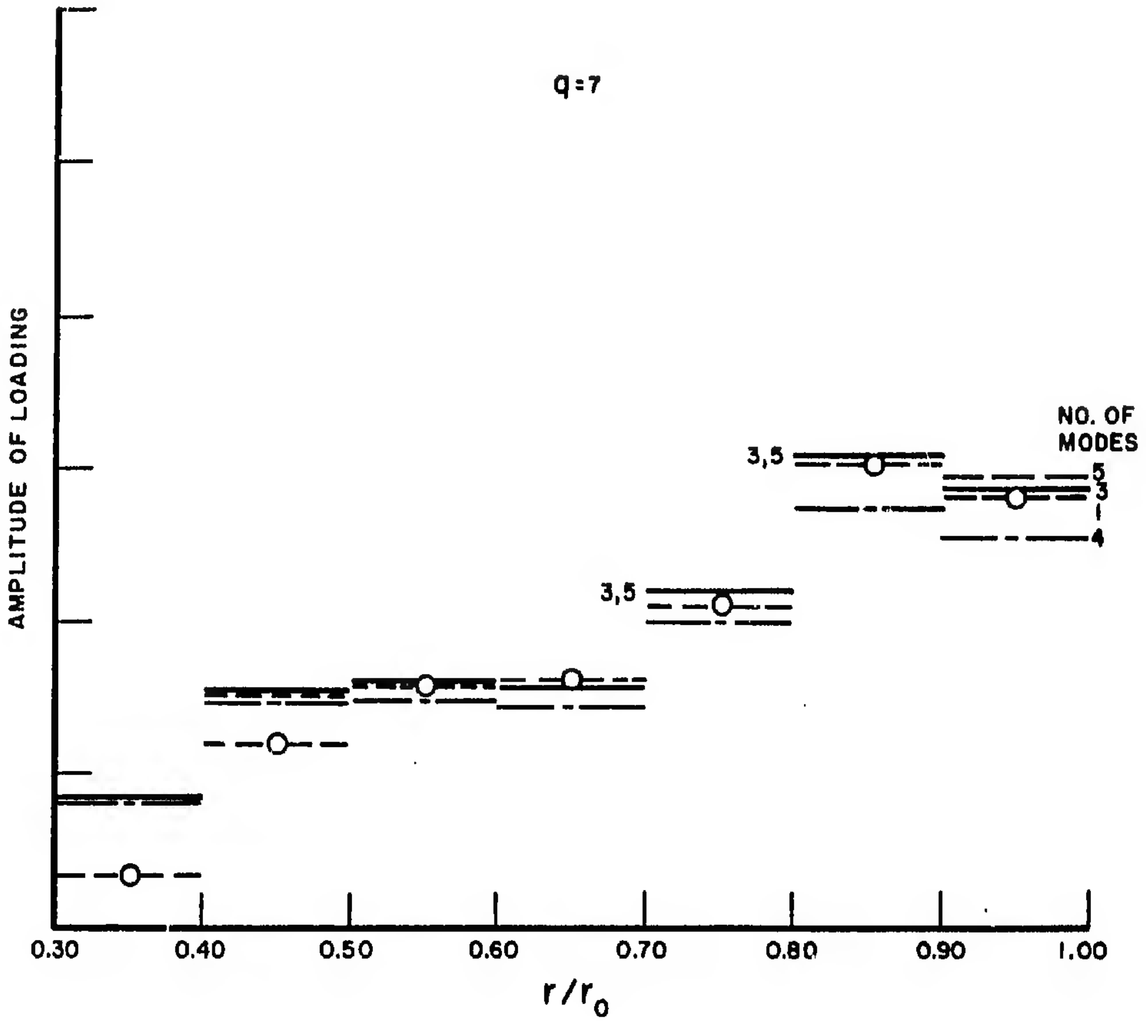

FIGURE 7. UNSTEADY SPANWISE LOADING DUE TO WAKE NO.1 ON 7-BLADED PROPELLER

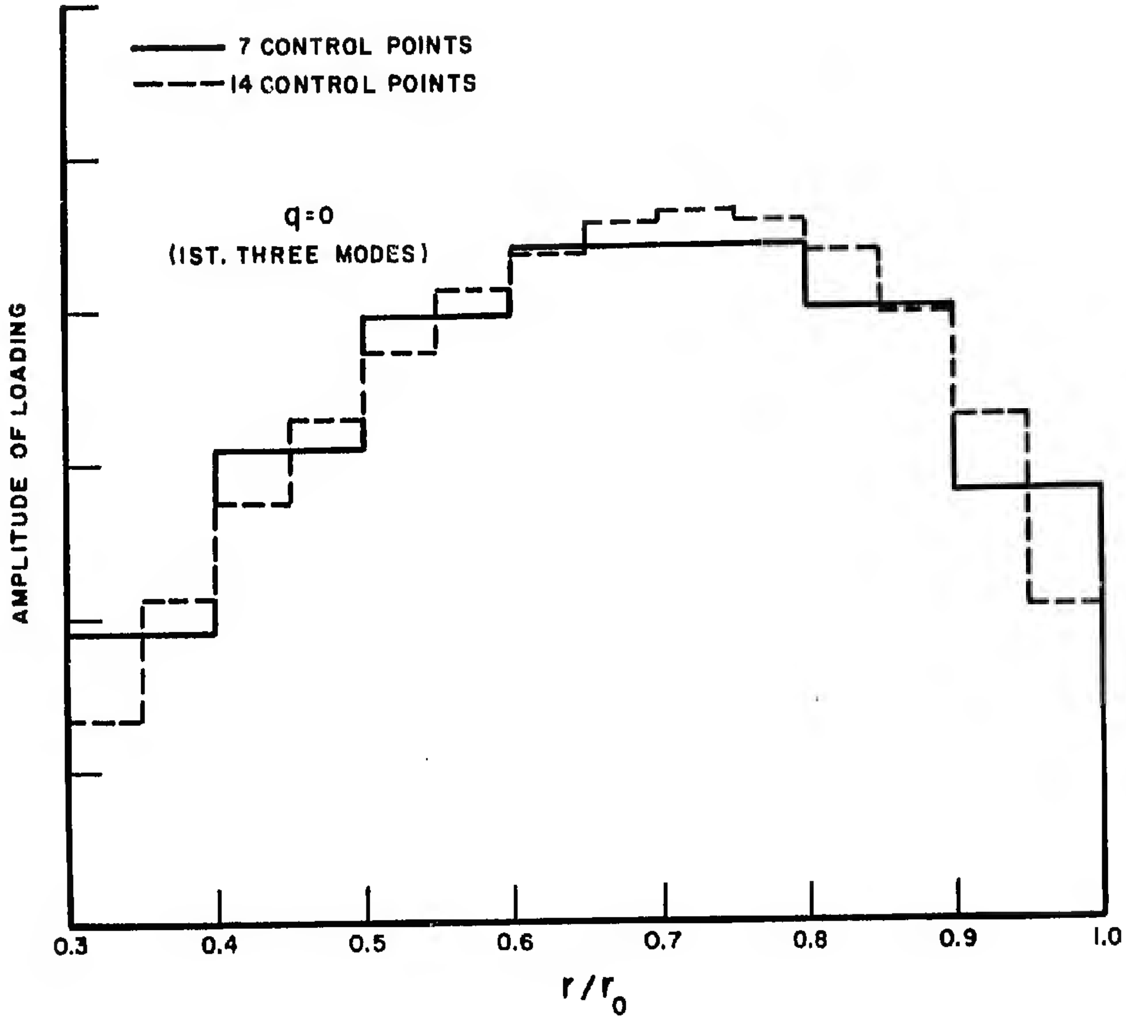

FIGURE 8. STEADY SPANWISE LOADING DUE TO WAKE NO. 4, CAMBER, AND FLOW ANGLE ON 5-BLADED PROPELLER

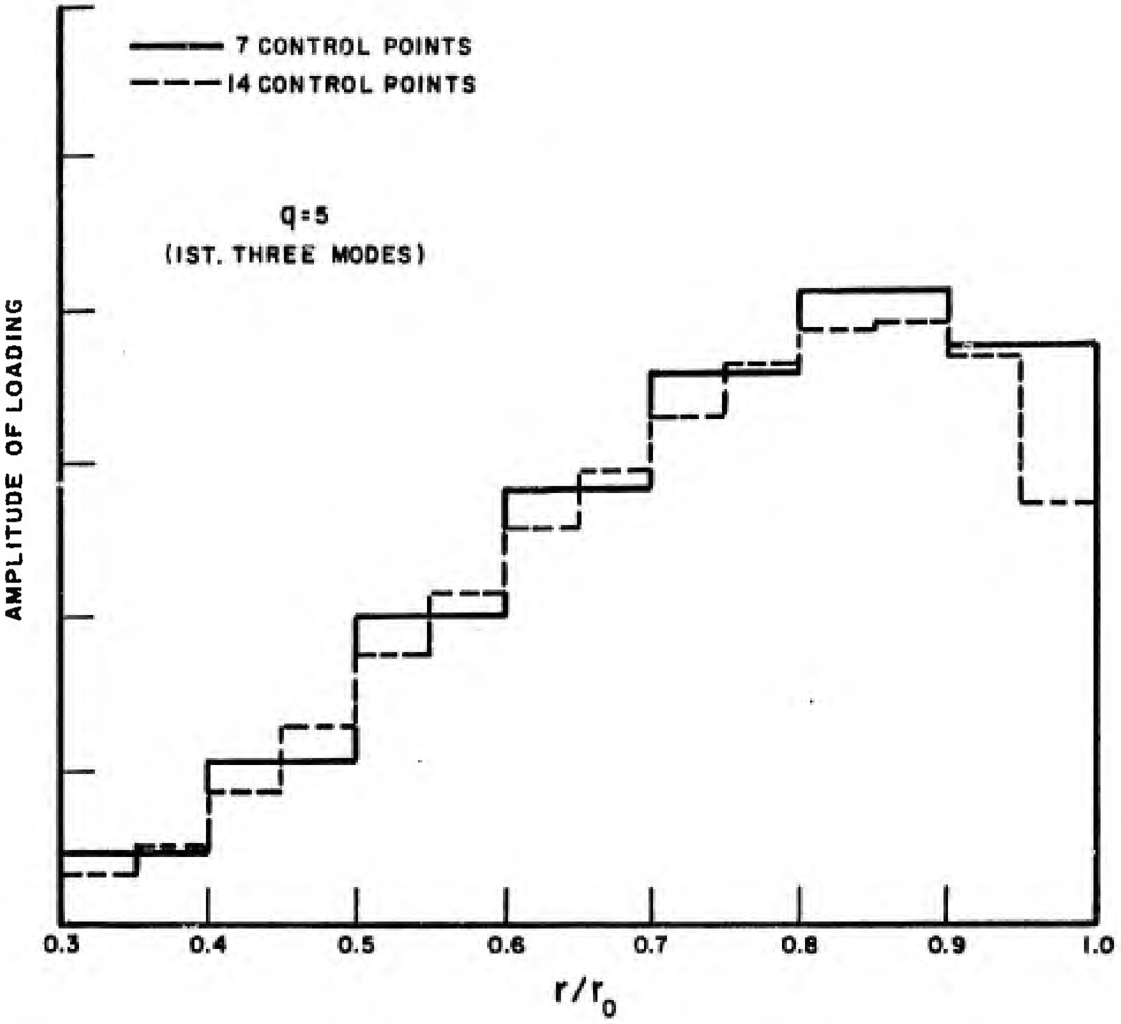

FIGURE 9. UNSTEADY SPANWISE LOADING DUE TO WAKE NO.4 ON 5-BLADED PROPELLER

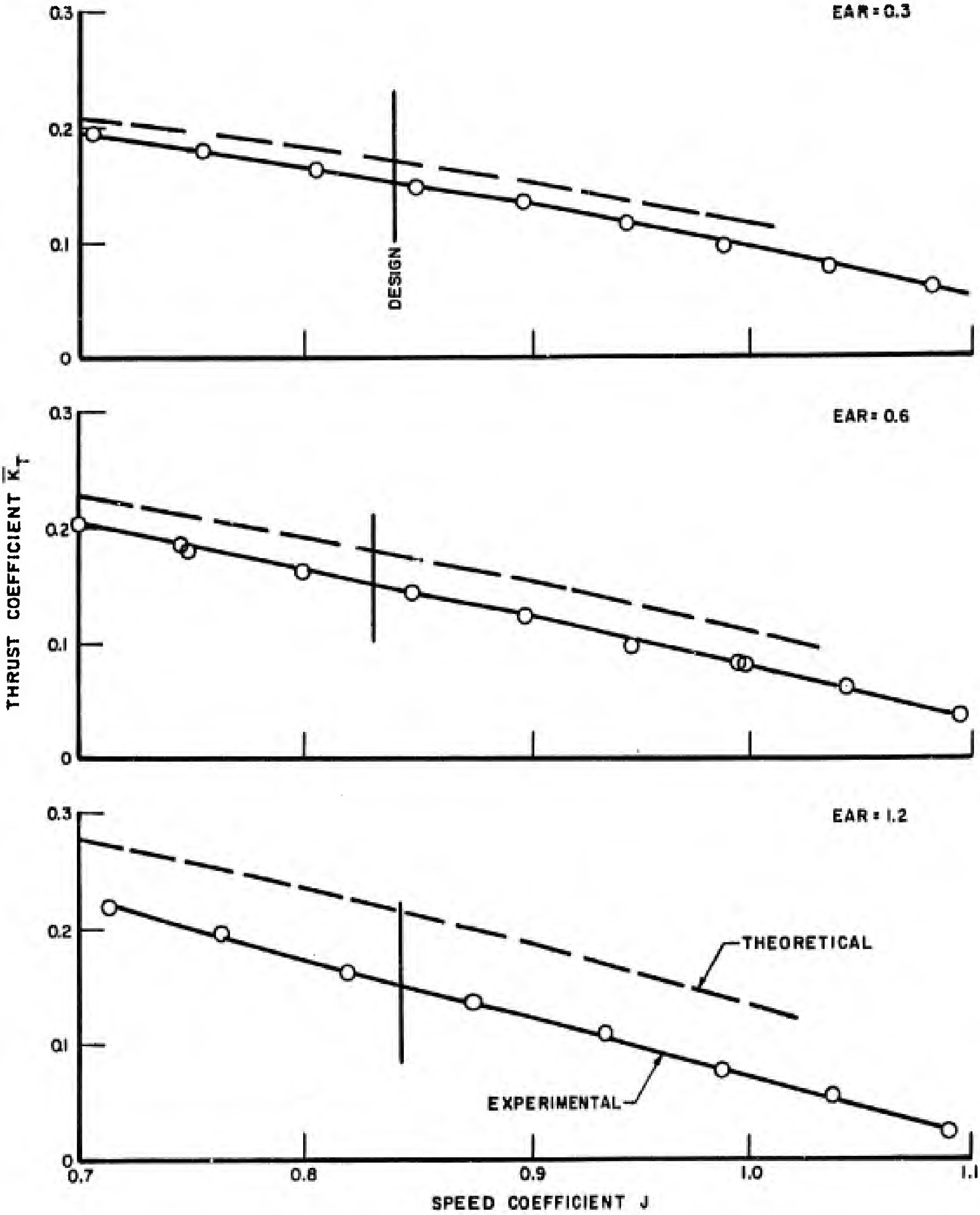

FIGURE 10. THEORETICAL AND EXPERIMENTAL $\bar{K}_T$ VERSUS J IN THE OPEN-WATER CONDITION FOR 3-BLADED PROPELLERS

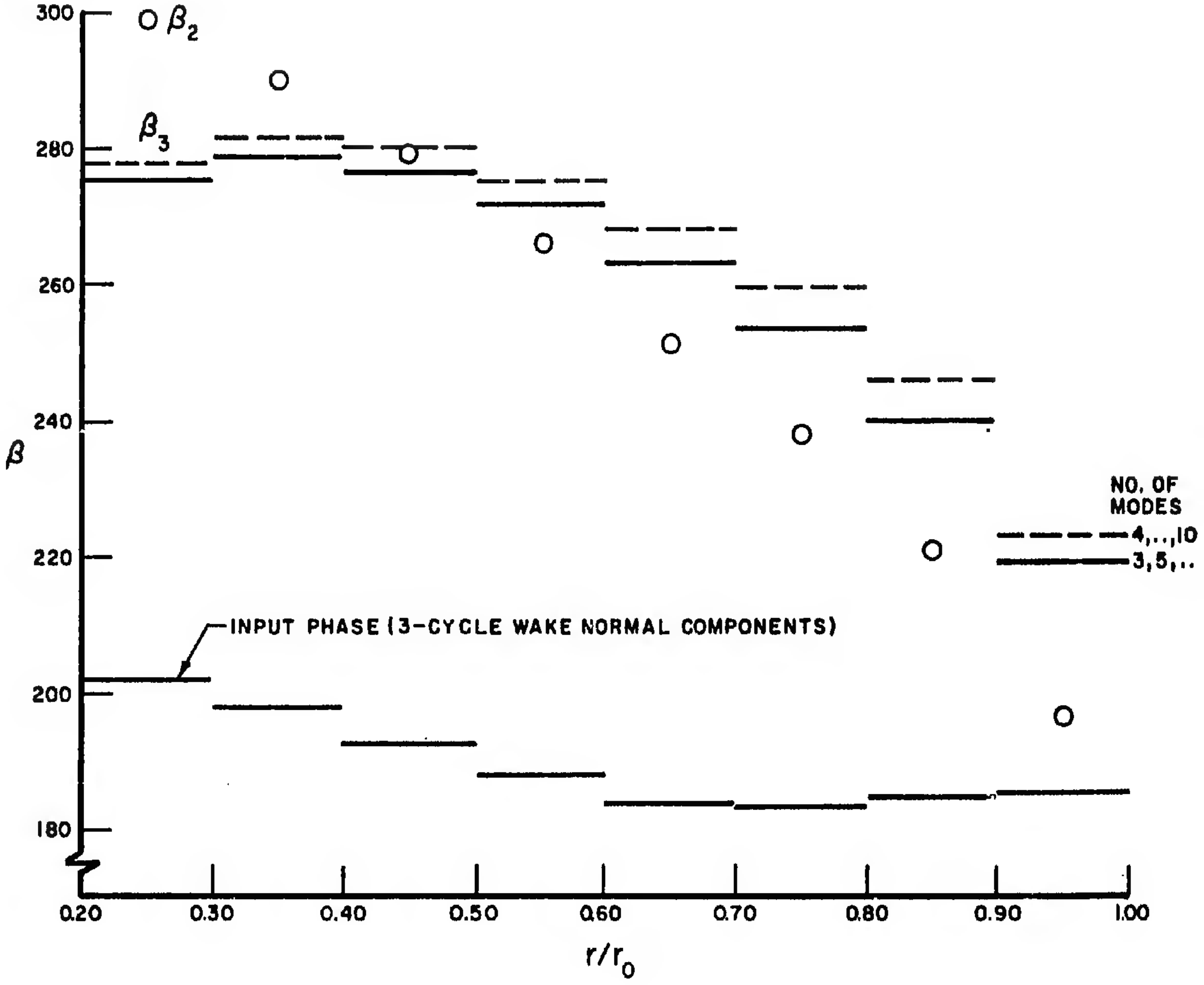

FIGURE 11. PHASES, β_3 AND β_2, OF UNSTEADY BLADE-FREQUENCY LOADING L_w FOR 3-BLADE PROPELLER NO. 4118 (EAR=0.60), BY 3-DIMENSIONAL AND 2-DIMENSIONAL UNSTEADY THEORIES

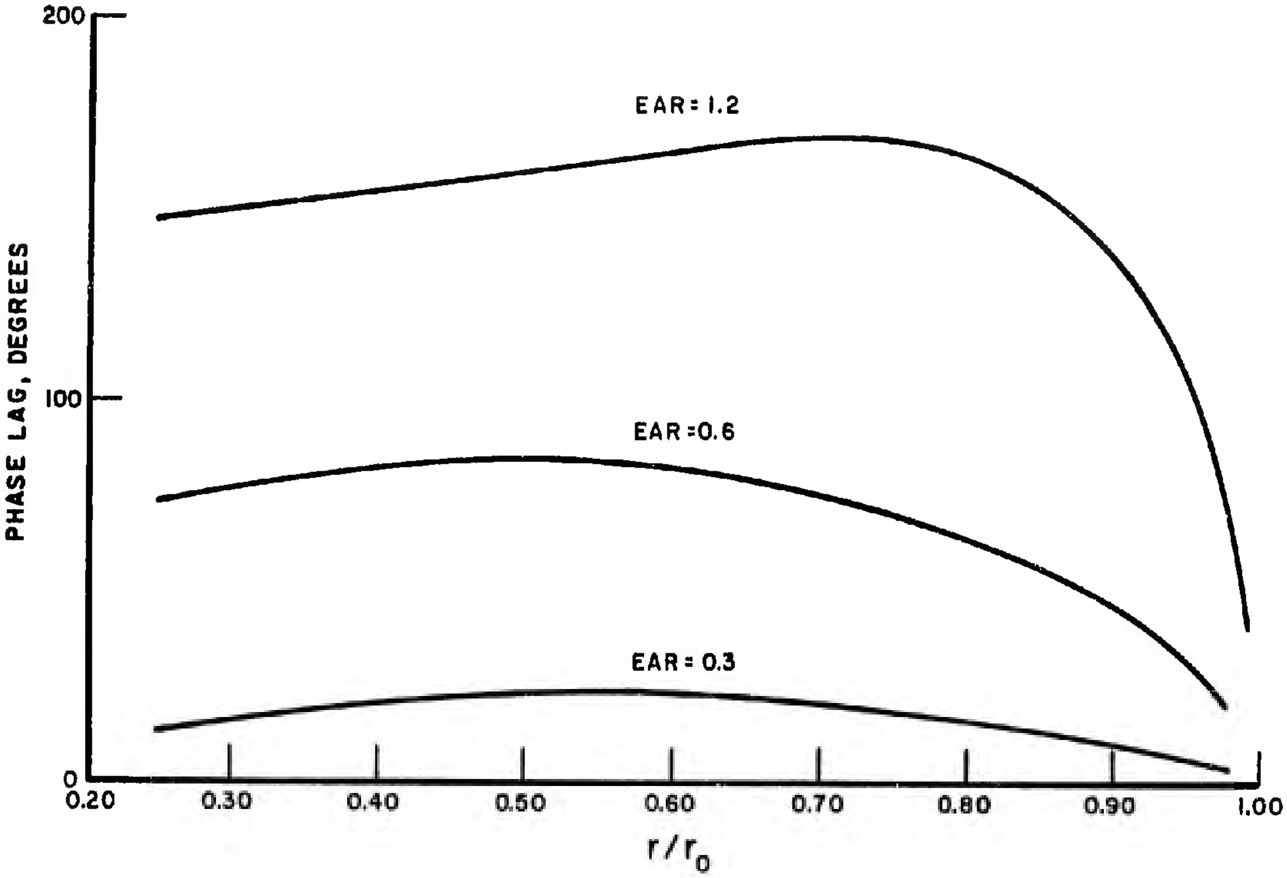

FIGURE 12. PHASES, β_3, OF UNSTEADY BLADE-FREQUENCY LOADING L_W MEASURED FROM THOSE OF INPUT WAKE FOR 3-BLADE PROPELLERS (3 CHORDWISE MODES)

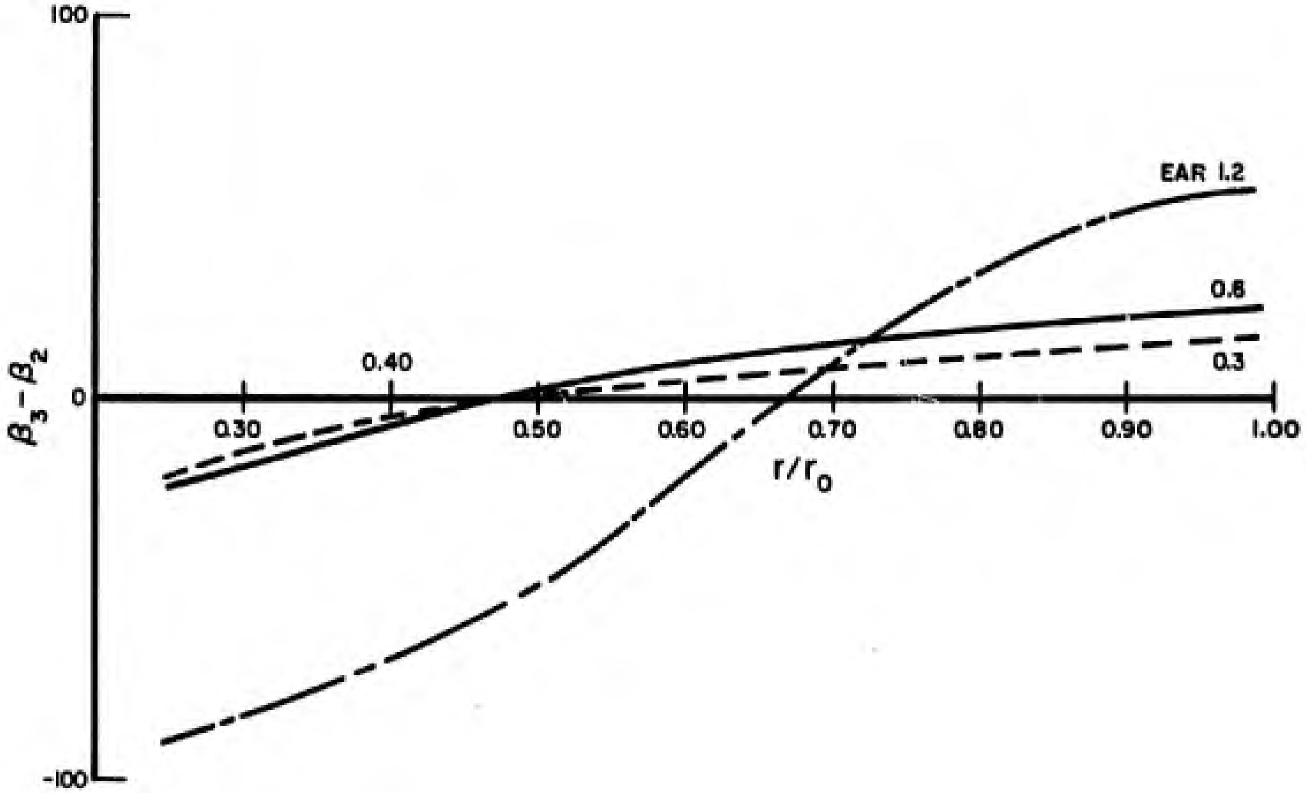

FIGURE 13. PHASE DIFFERENCES ($\beta_3-\beta_2$) FOR 3-BLADE PROPELLERS AT BLADE-FREQUENCY

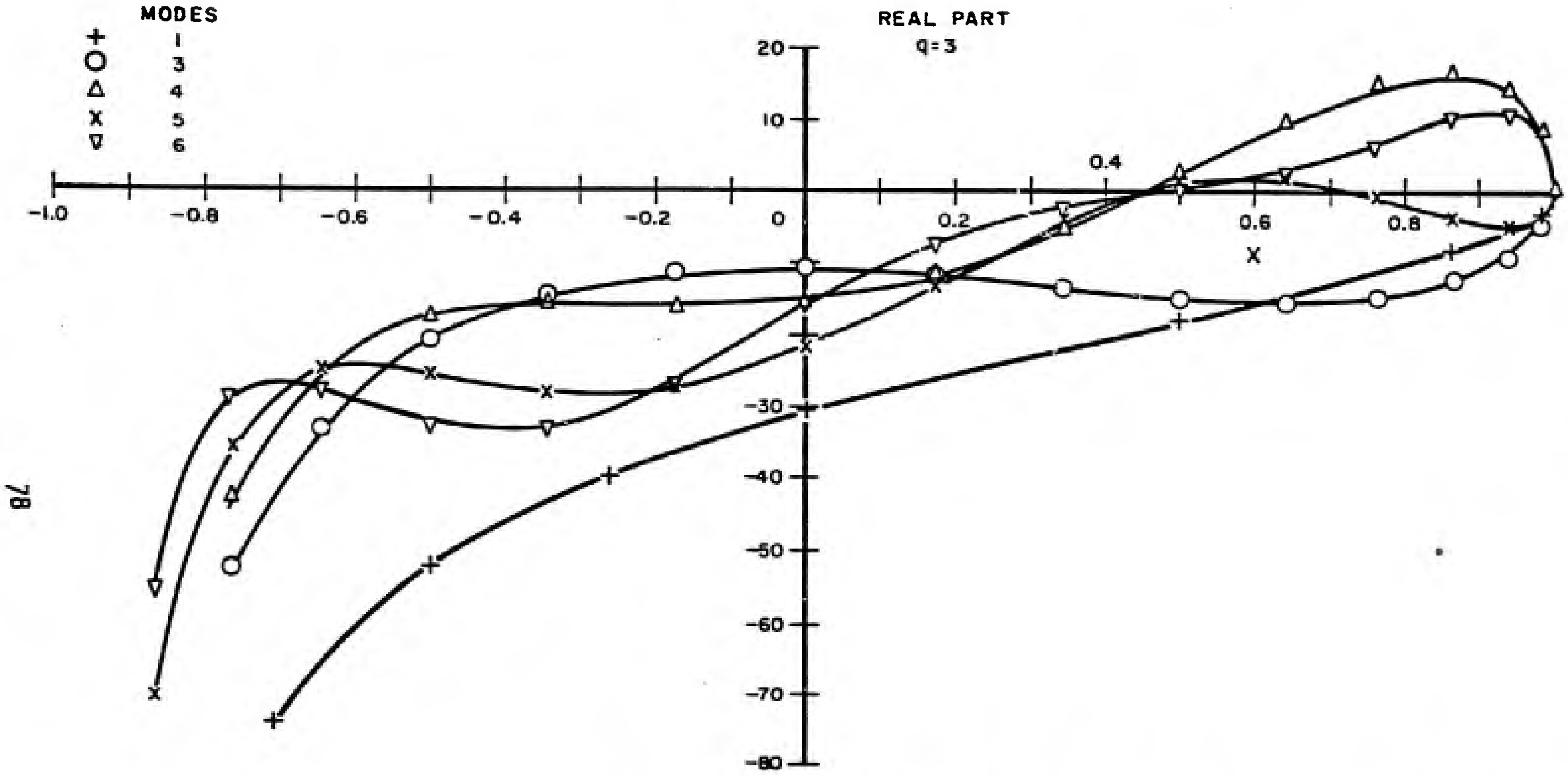

FIGURE 14a. UNSTEADY CHORDWISE LOADING DISTRIBUTION AT 0.75 r_0 FOR PROPELLER 4118 (EAR=0.6) AT DESIGN J=0.831 (CESÀRO-SUMMABILITY OF SINE TERMS)

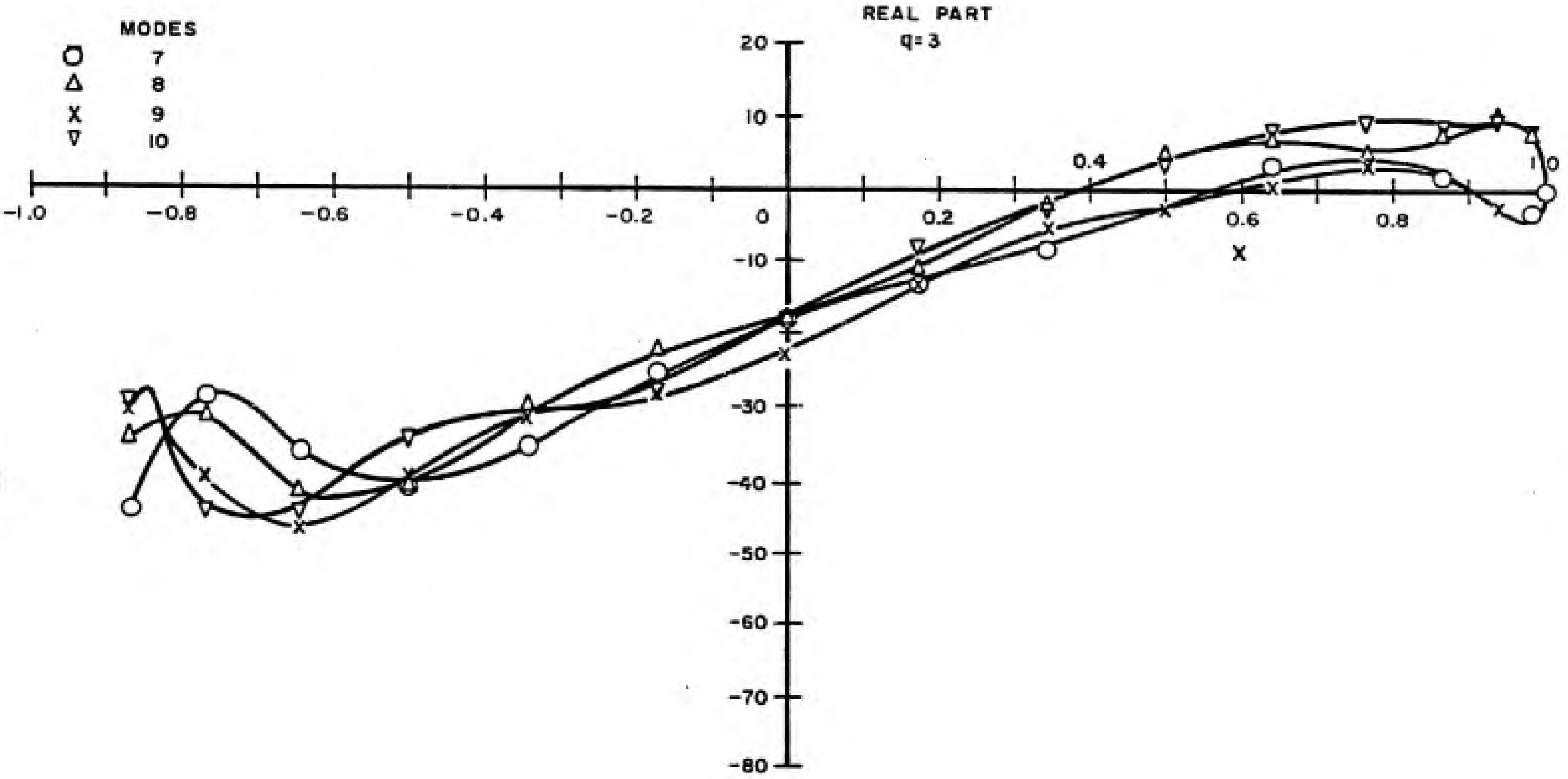

FIGURE 14b. UNSTEADY CHORDWISE LOADING DISTRIBUTION AT 0.75r_0 FOR PROPELLER 4118 (EAR=0.6) AT DESIGN J=0.831 (CESÀRO-SUMMABILITY OF SINE TERMS)

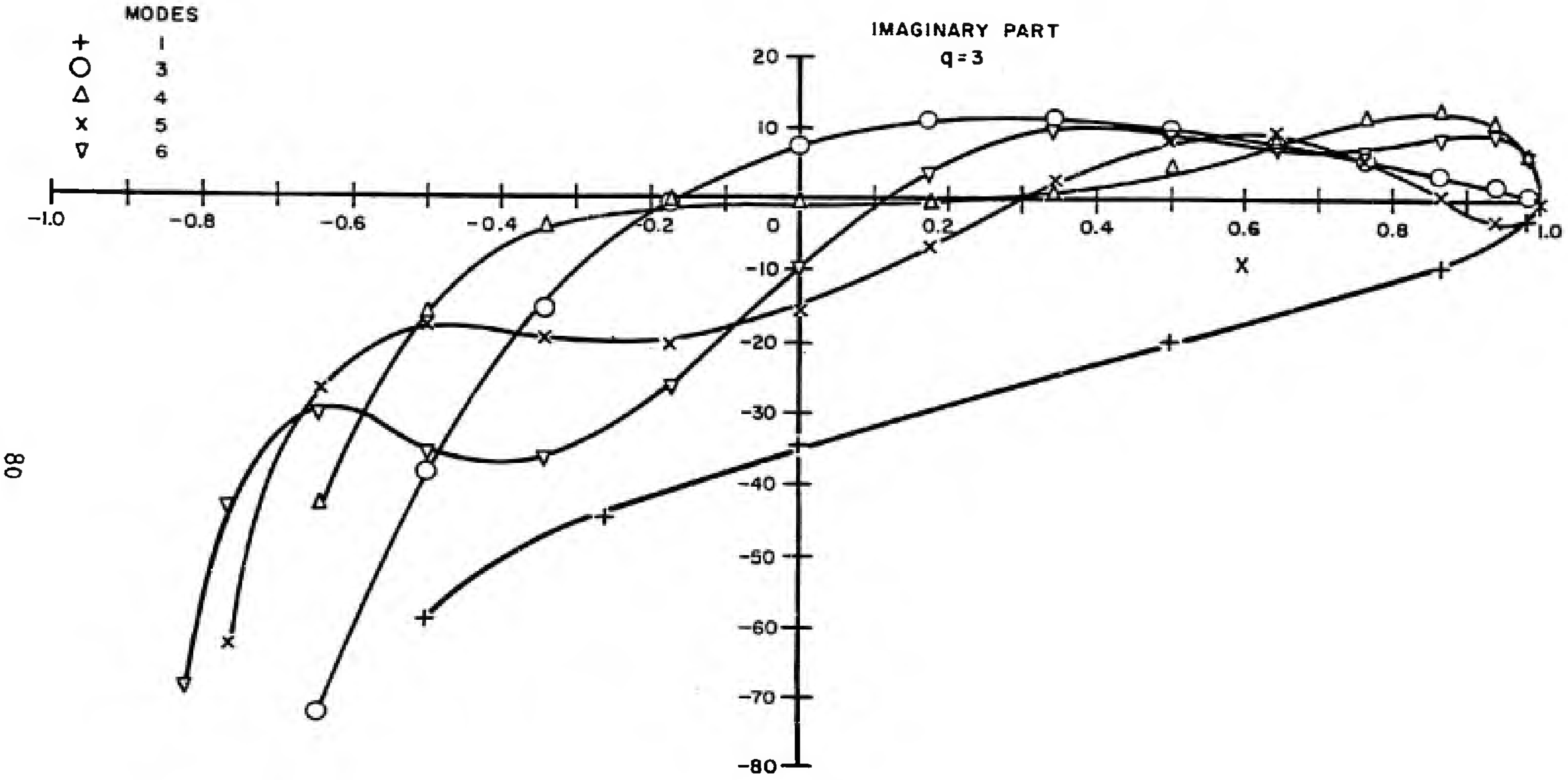

FIGURE 15a. UNSTEADY CHORDWISE LOADING DISTRIBUTION AT 0.75r_0 FOR PROPELLER 4118 (EAR=0.6) AT DESIGN J=0.831 (CESÀRO-SUMMABILITY OF SINE TERMS)

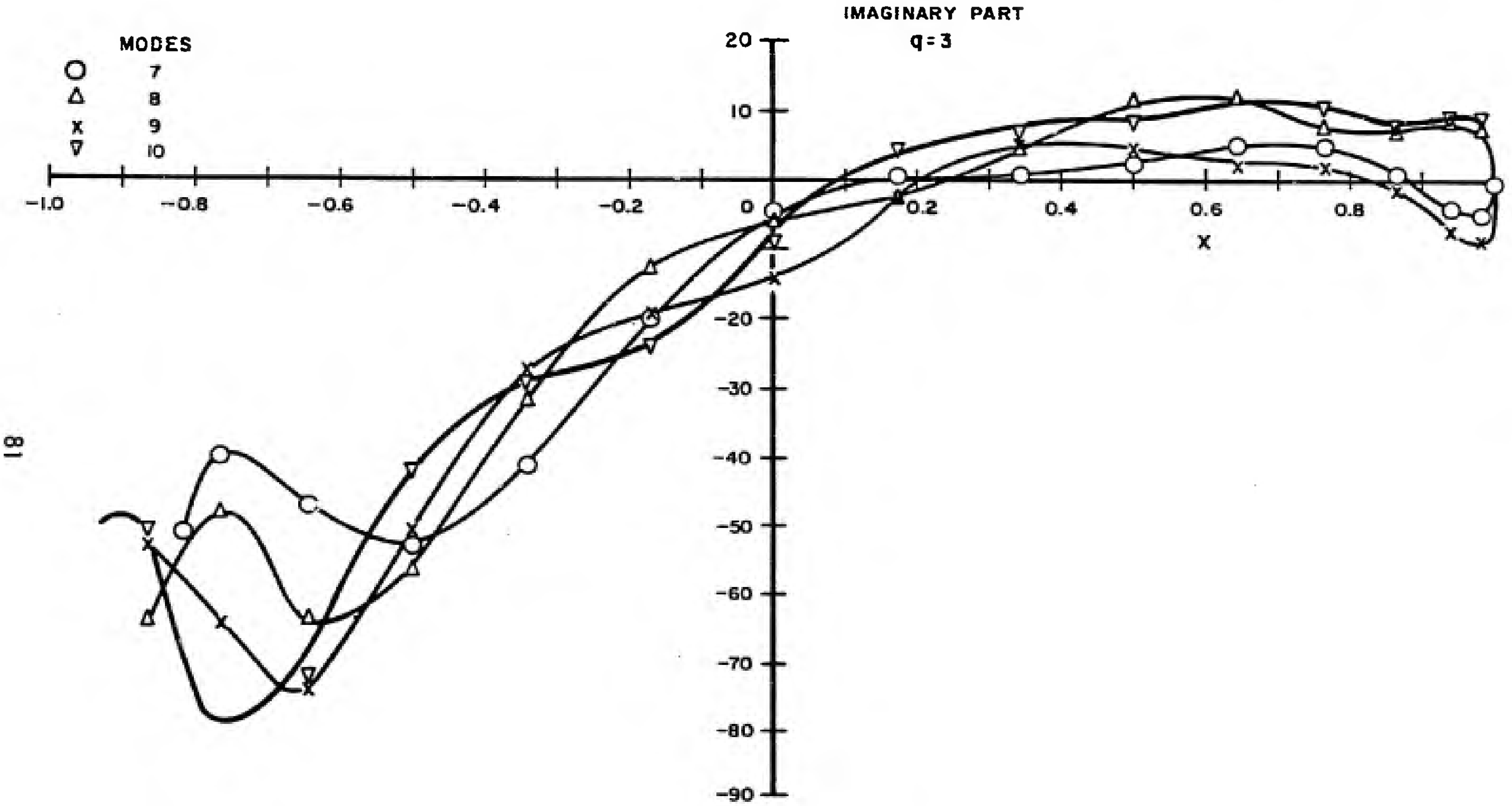

FIGURE 15b. UNSTEADY CHORDWISE LOADING DISTRIBUTION AT 0.75r_0 FOR PROPELLER 4118 (EAR=0.6) AT DESIGN J=0.831 (CESARO–SUMMABILITY OF SINE TERMS)

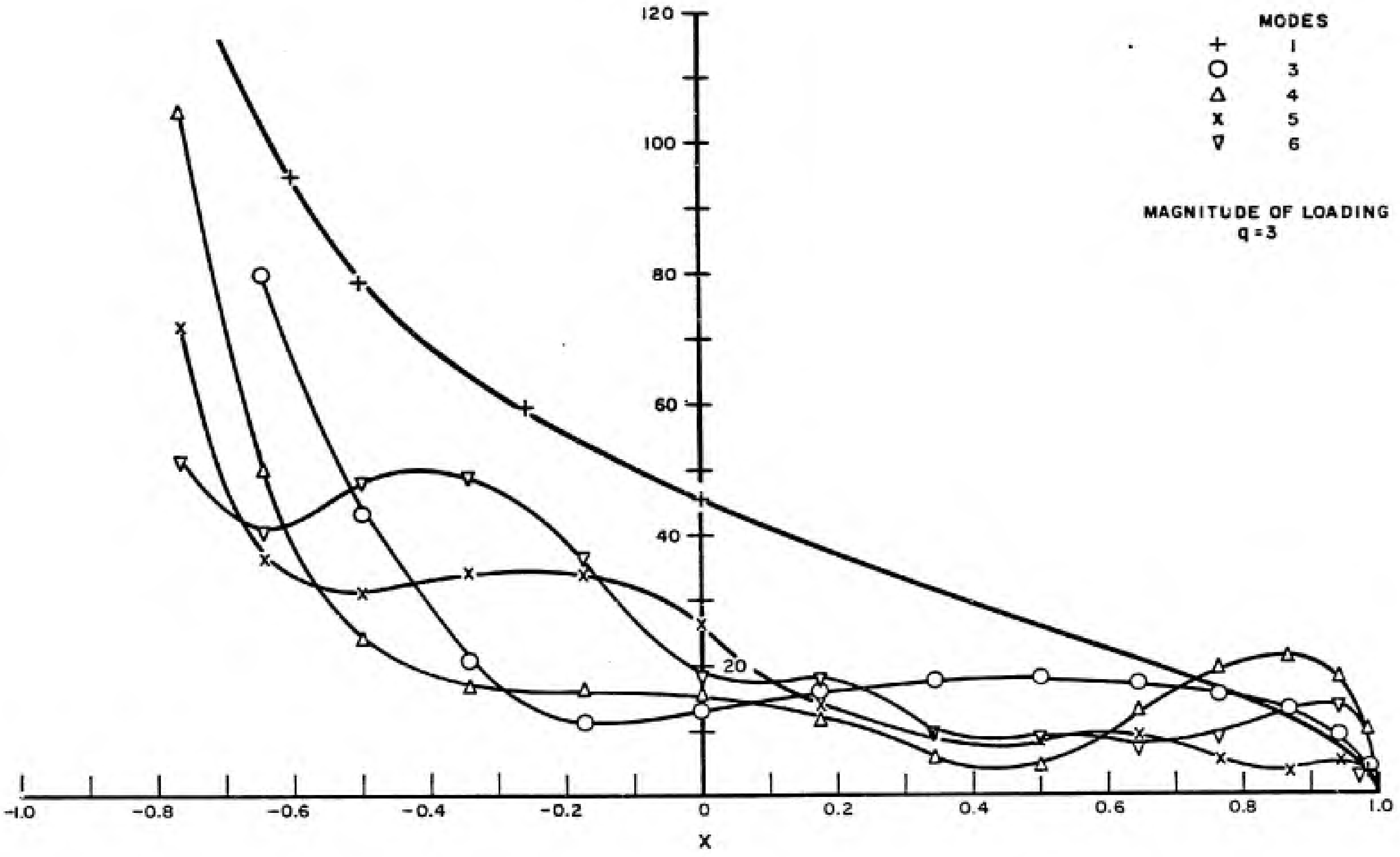

FIGURE 16a. UNSTEADY CHORDWISE LOADING DISTRIBUTION AT $0.75r_o$ FOR PROPELLER 4118 (EAR=0.6) AT DESIGN J=0.831 (CESÃRO–SUMMABILITY OF SINE TERMS)

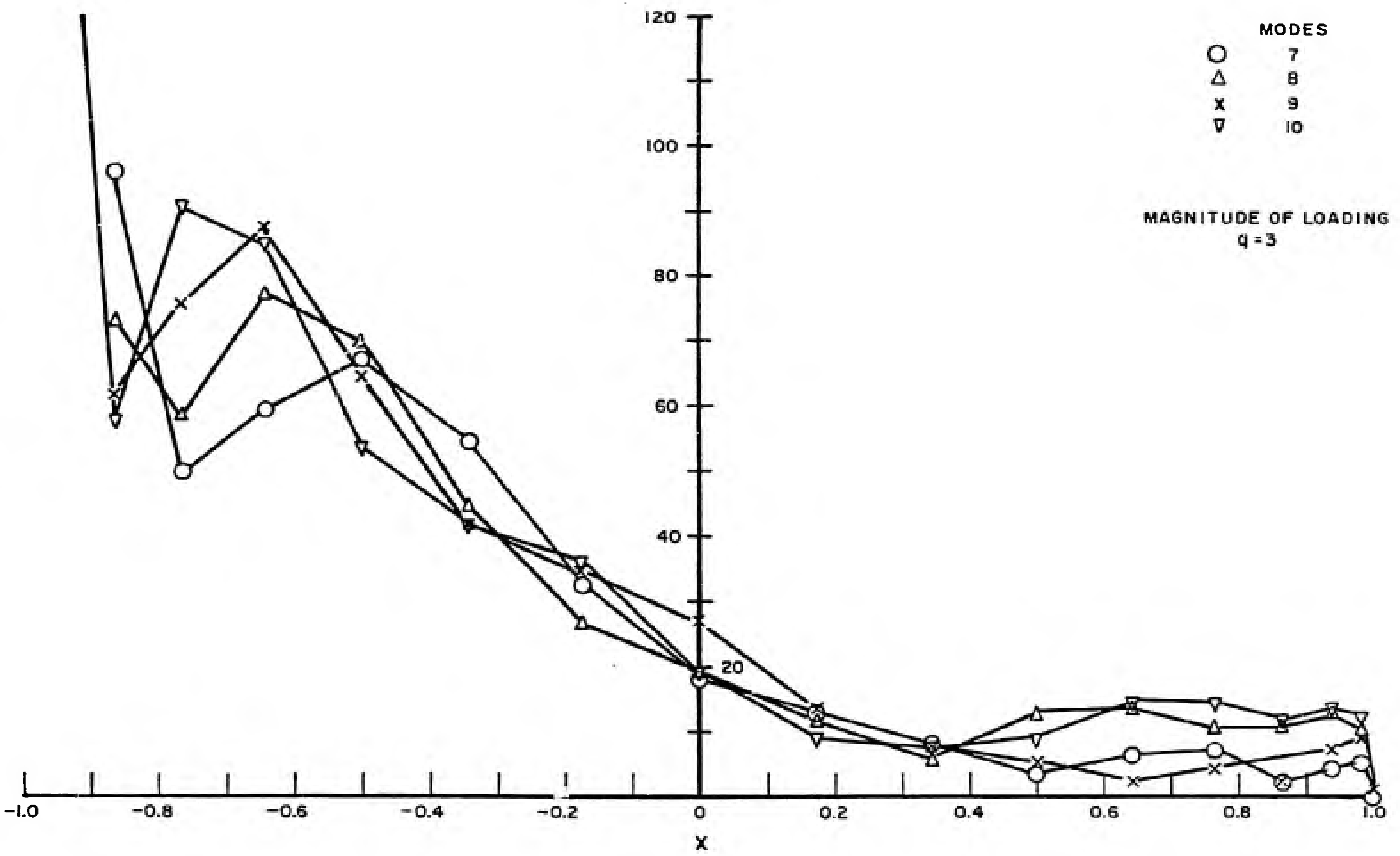

FIGURE 16b. UNSTEADY CHORDWISE LOADING DISTRIBUTION AT $0.75r_0$ FOR PROPELLER 4118 (EAR=0.6) AT DESIGN J=0.831 (CESÀRO-SUMMABILITY OF SINE TERMS)

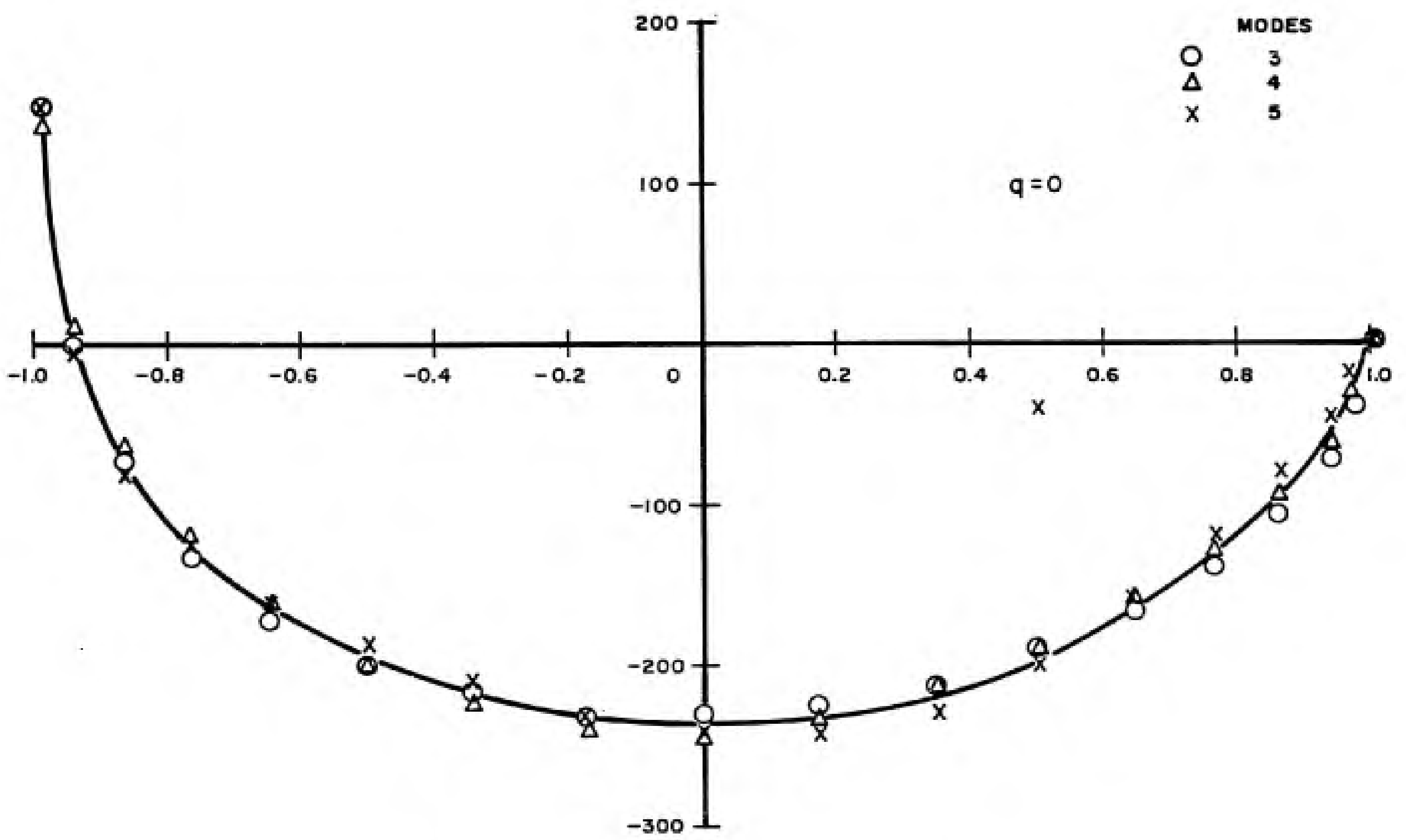

FIGURE 17a. STEADY CHORDWISE LOADING DISTRIBUTION AT 0.75 r_o FOR PROPELLER 4118 (EAR=0.6) AT DESIGN J = 0.831 (NORMAL SUM)

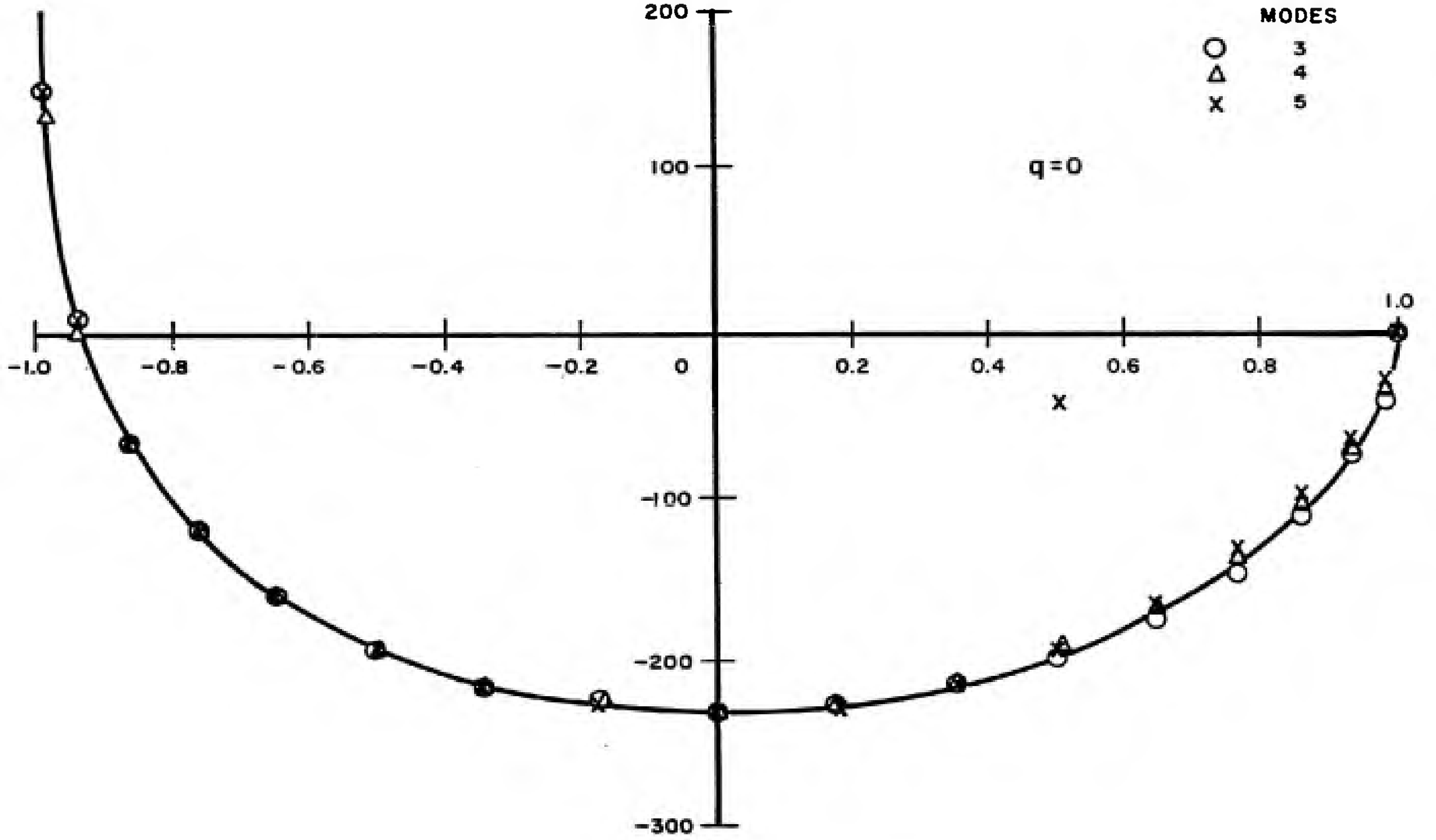

FIGURE 17b. STEADY CHORDWISE LOADING DISTRIBUTION AT 0.75 r_o FOR PROPELLER 4118 (EAR=0.6) AT DESIGN J=0.831 (CESÃRO-SUMMABILITY OF SINE TERMS)

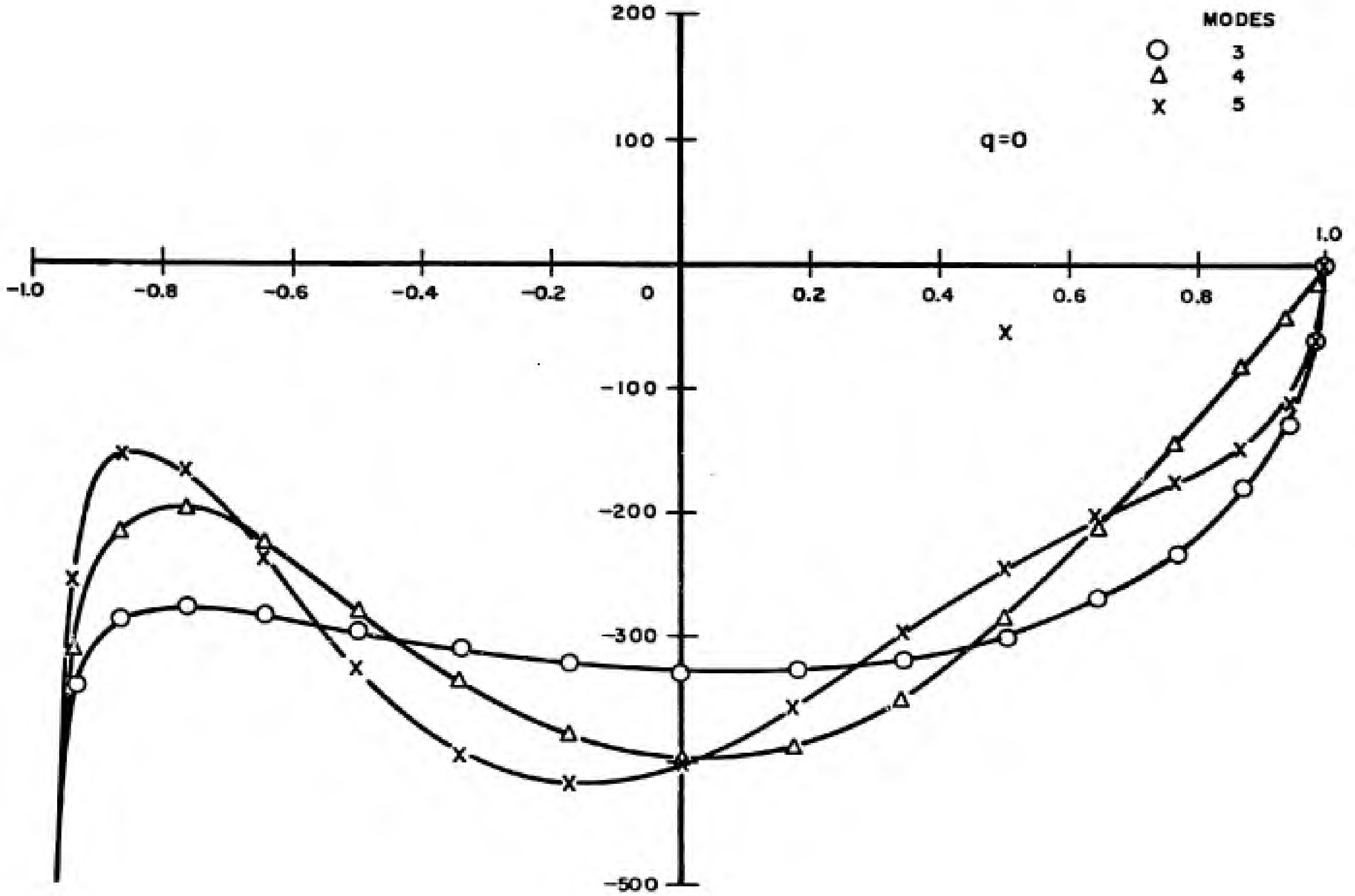

FIGURE 18a. STEADY CHORDWISE LOADING DISTRIBUTION AT 0.75 r_o FOR PROPELLER 4118 (EAR=0.6) AT J=0.7 (NORMAL SUM)

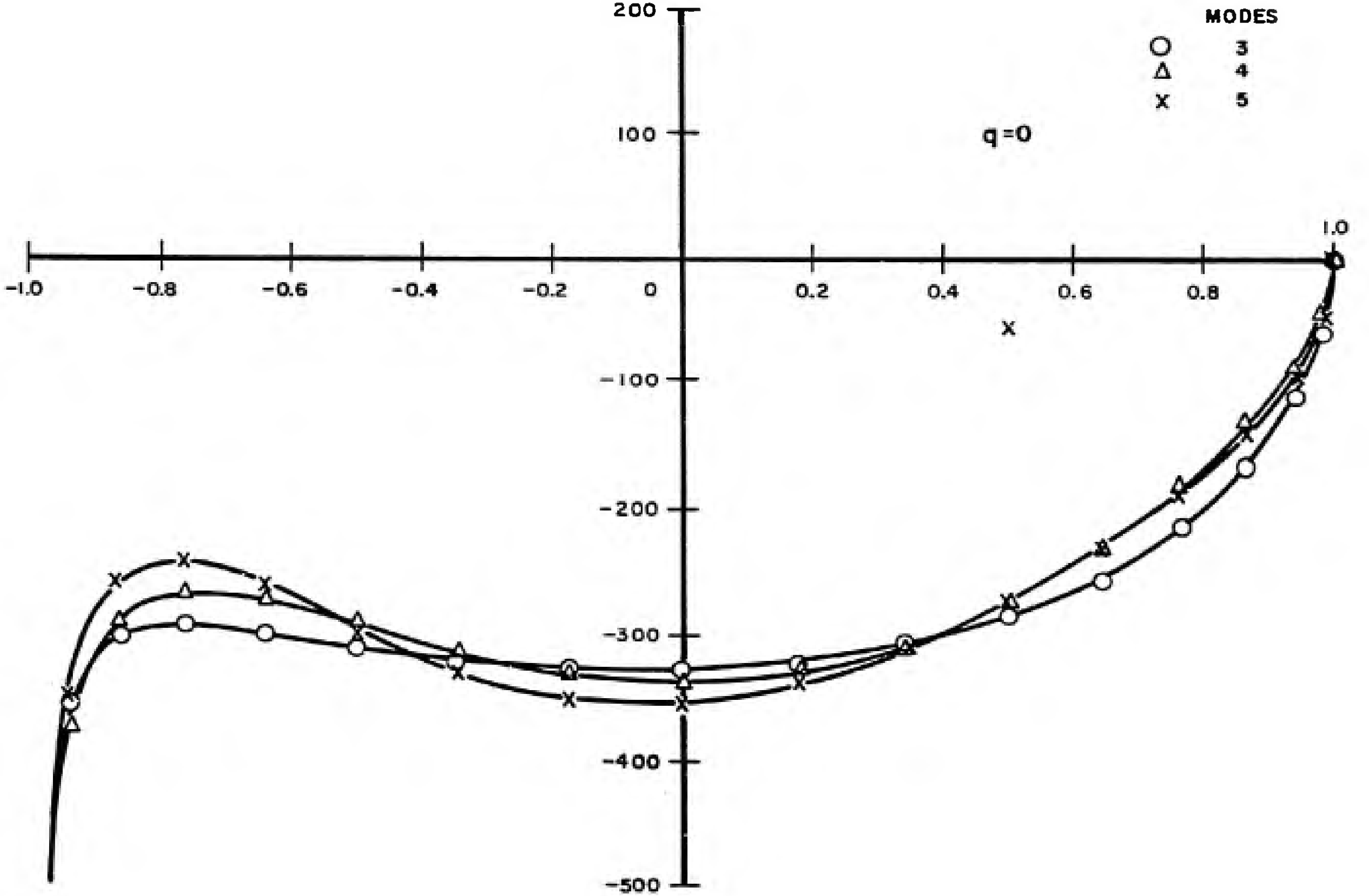

FIGURE 18b. STEADY CHORDWISE LOADING DISTRIBUTION AT 0.75 r_0 FOR PROPELLER 4118 (EAR=0.6) AT J=0.7 (CESÀRO–SUMMABILITY OF SINE TERMS)

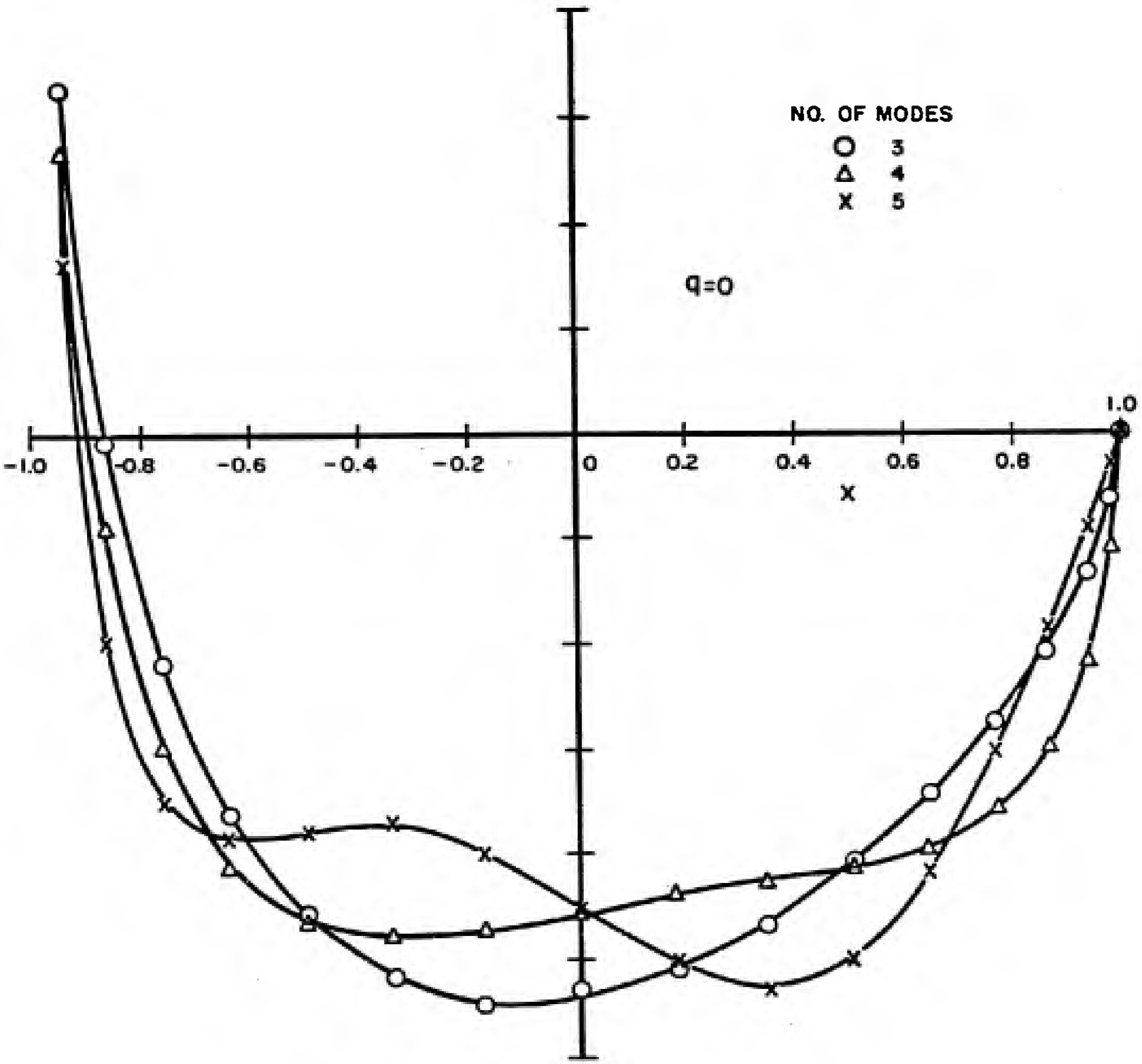

FIGURE 19a. STEADY CHORDWISE LOADING DISTRIBUTION AT $0.75r_0$, DUE TO WAKE NO. 1, CAMBER AND FLOW ANGLE FOR 5-BLADE PROPELLER AT J=0.762 (NORMAL SUM)

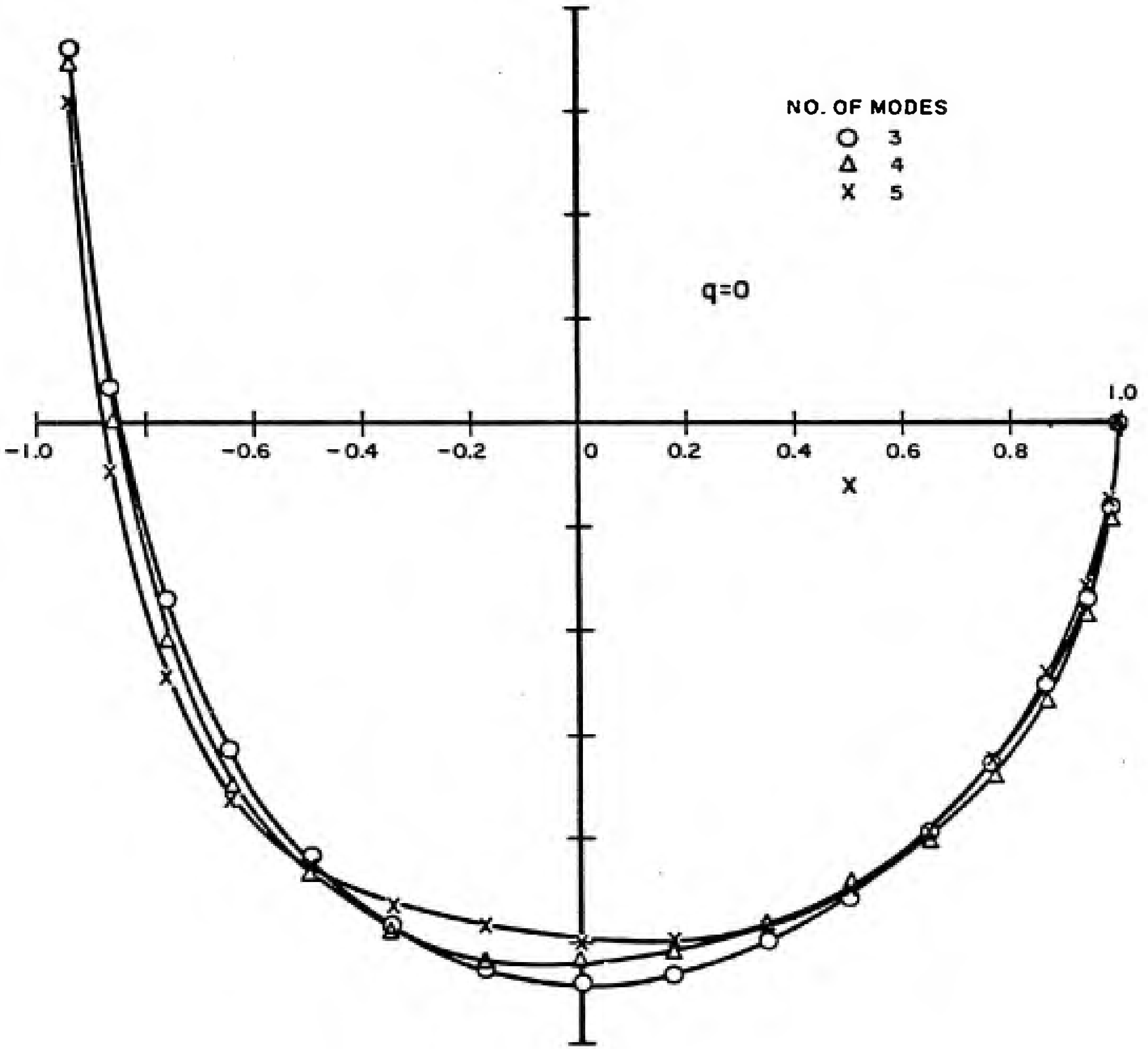

FIGURE 19b. STEADY CHORDWISE LOADING DISTRIBUTION AT 0.75r_0 DUE TO WAKE NO.1, CAMBER AND FLOW ANGLE FOR 5-BLADE PROPELLER AT J=0.762 (CESÀRO-SUMMABILITY OF SINE TERMS)

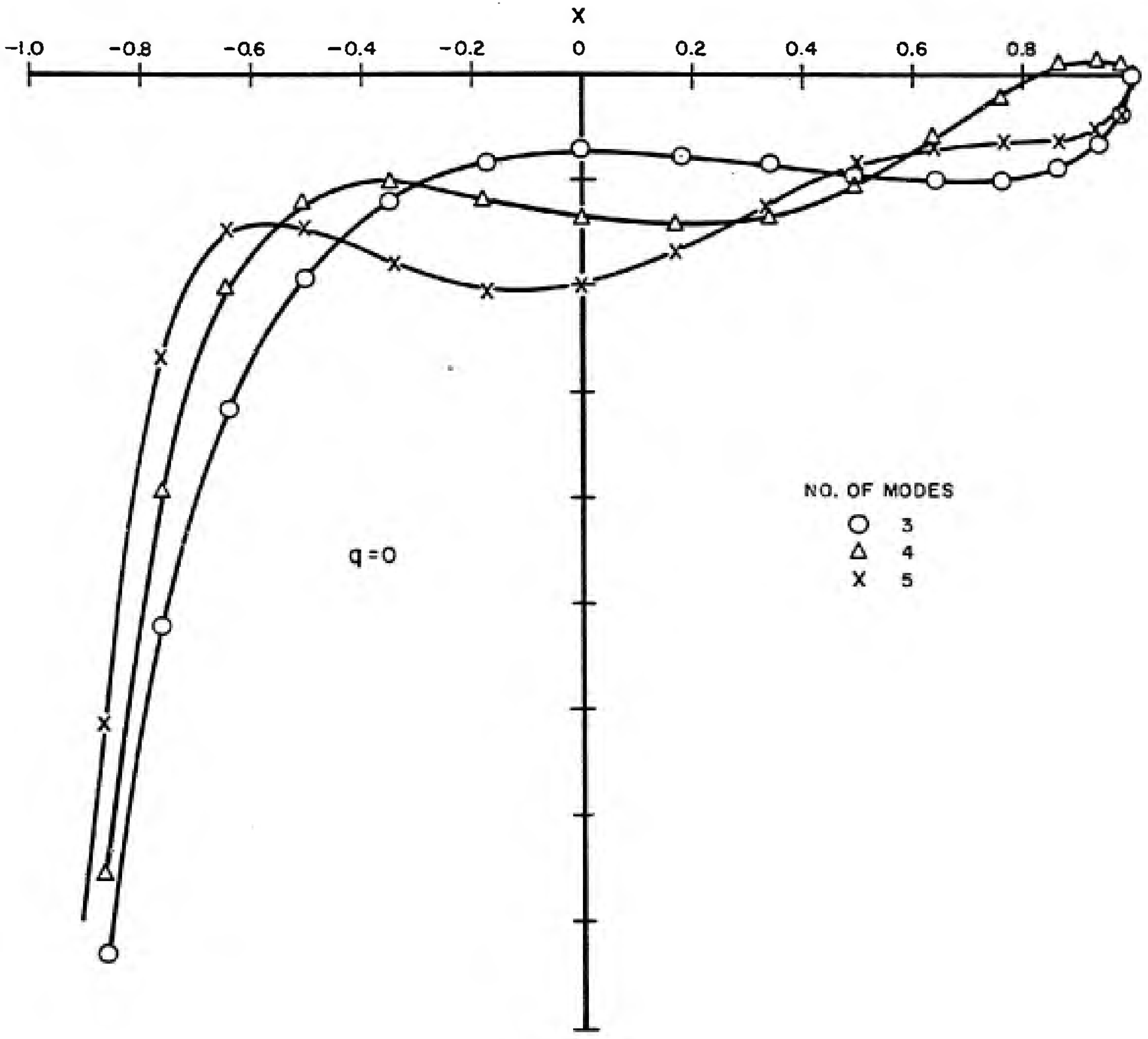

FIGURE 20. STEADY CHORDWISE LOADING DISTRIBUTION AT $0.75r_0$ DUE TO WAKE NO.1 FOR 5-BLADE PROPELLER AT J=0.762 (CESÀRO-SUMMABILITY OF SINE TERMS)

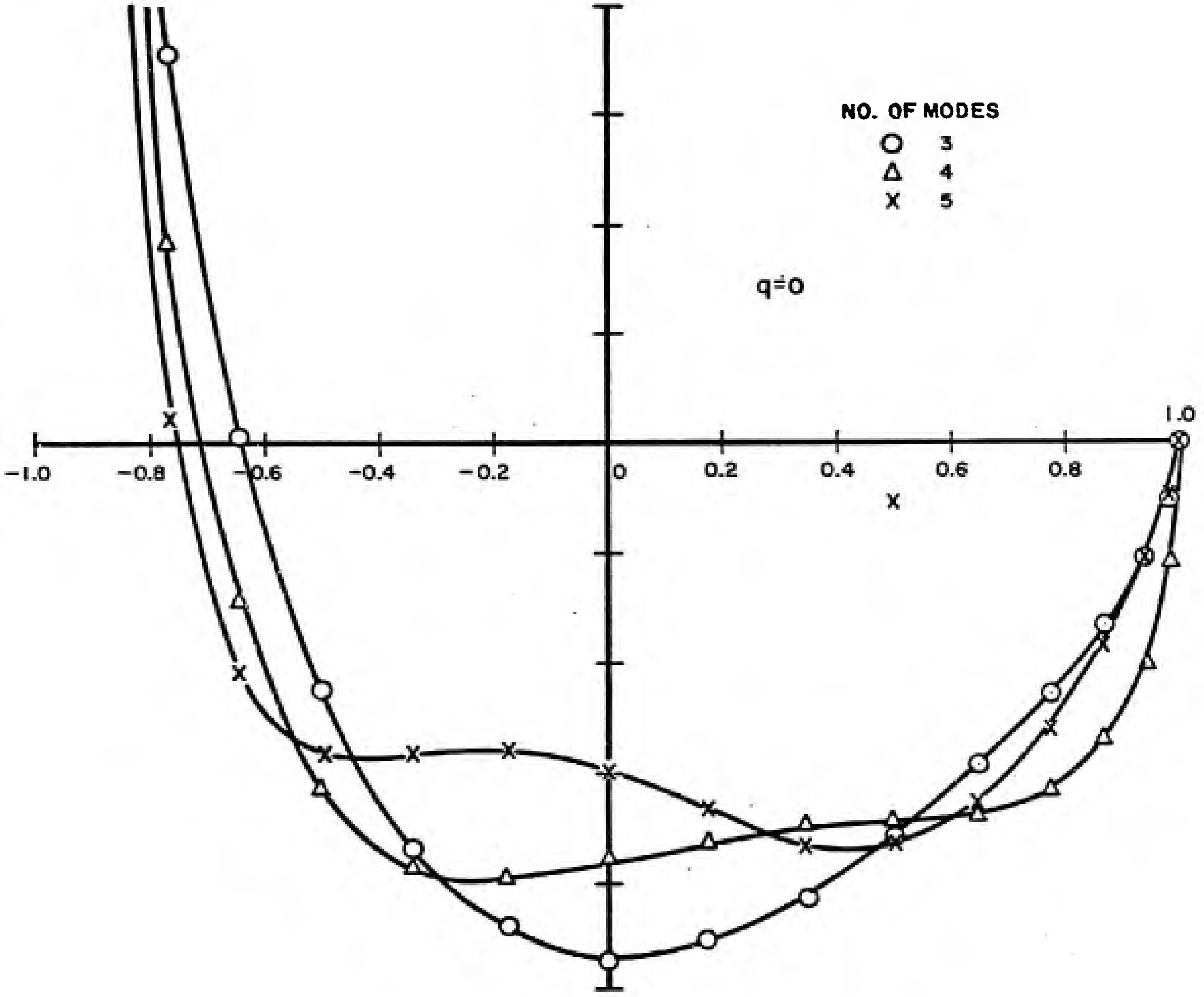

FIGURE 21. STEADY CHORDWISE LOADING DISTRIBUTION AT 0.75r_0 DUE TO CAMBER AND FLOW ANGLE EFFECTS FOR 5-BLADE PROPELLER AT J=0.762 (CESÃRO-SUMMABILITY OF SINE TERMS)

BLANK PAGE

APPENDIX A

PROOF OF THE EQUIVALENCE OF EQUATIONS (28) AND (29)

The derivatives with respect to X and Θ indicated in Equation (29) are, with the help of Equation (29b),

$$\frac{\partial}{\partial X}\left(\frac{1}{R}\right) = -\frac{i}{\pi}\sum_{m=-\infty}^{\infty} e^{im\Theta}\int_{-\infty}^{\infty} k I_m(k\rho)\, K_m(kr)\, e^{-iXk}\, dk$$

$$\frac{\partial^2}{\partial X^2}\left(\frac{1}{R}\right) = -\frac{1}{\pi}\sum_{m=-\infty}^{\infty} e^{im\Theta}\int_{-\infty}^{\infty} k^2 I_m(k\rho)\, K_m(kr)\, e^{-iXk}\, dk$$

$$\frac{\partial^2}{\partial\Theta\partial X}\left(\frac{1}{R}\right) = \frac{1}{\pi}\sum_{m=-\infty}^{\infty} m\, e^{im\Theta}\int_{-\infty}^{\infty} k I_m(k\rho)\, K_m(kr)\, e^{-iXk}\, dk$$

$$\frac{\partial^2}{\partial\Theta^2}\left(\frac{1}{R}\right) = -\frac{1}{\pi}\sum_{m=-\infty}^{\infty} m^2 e^{im\Theta}\int_{-\infty}^{\infty} I_m(k\rho)\, K_m(kr)\, e^{-iXk}\, dk \tag{A-1}$$

After substituting

$$X = \frac{\Theta - \bar{\theta}_n + \varphi_o - \theta_o}{a} - (x-\xi)$$

the Θ integral becomes

$$\frac{r}{\pi a\sqrt{1+a^2r^2}} \int_{\bar{\theta}_n+\theta_o-\varphi_o}^{\infty} e^{-iq(\Theta+\varphi_o-\theta_o)} \sum_{m=-\infty}^{\infty} e^{im\Theta}$$

$$\cdot \int_{-\infty}^{\infty} \left[a^2k^2 + a\left(\frac{1}{r^2}+\frac{1}{\rho^2}\right) mk + \frac{m^2}{r^2\rho^2}\right] I_m(k\rho)\, K_m(kr)$$

$$\cdot\, e^{-i\frac{k}{a}(\Theta-\bar{\theta}_n)}\, e^{-i\frac{k}{a}(\varphi_o-\theta_o) + ik(x-\xi)}\, dk\, d\Theta$$

$$(A\text{-}2)$$

The Θ integration involves

$$\int_{\bar{\theta}_n+\theta_o-\varphi_o}^{\infty} e^{i(m-q)\Theta}\, e^{-i\frac{k}{a}\Theta}\, d\Theta = \pi a\,\delta\,[a(m-q)-k] - \frac{iae^{i(m-q)(\bar{\theta}_n+\theta_o-\varphi_o)-i\frac{k}{a}(\bar{\theta}_n+\theta_o-\varphi_o)}}{k-a\,(m-q)}$$

$$(A\text{-}3)$$

It can be easily shown that Equations (28) and (29) are equivalent, by substituting (A-3) into (A-2) and making use of the following relation for the Dirac delta function, $\delta(\ )$,

$$\int_{-\infty}^{\infty} f(k)\ \delta[a(m-q)-k]\ dk = f[a(m-q)] \qquad (A\text{-}4)$$

APPENDIX B

APPROXIMATION OF THE INFINITE p-SERIES OF K_2

Equation (37a), with $z = (X^2 + r^2 + \rho^2)/2r\rho$, can be written as

$$K_2 = \sum_{p=1}^{\infty} \frac{2e^{-iq(\varphi_o - \theta_o)}}{\sqrt{1+a^2 r^2}\, a\rho} \Bigg\{ - a^2 \sqrt{r\rho} \, \frac{\partial^2}{\partial X^2} Q_{q-\frac{1}{2}}(z) + \frac{q^2}{(r\rho)^{3/2}} Q_{q-\frac{1}{2}}(z) + \frac{ia(r^2+\rho^2)q}{(r\rho)^{3/2}} \frac{\partial}{\partial X} Q_{q-\frac{1}{2}}(z) \Bigg\} \qquad \text{(B-1)}$$

where $X = p\,\bar{\theta}_o/a$

If use is made of the relations

$$Q_{q-\frac{1}{2}}(z) = \pi\sqrt{r\rho} \int_0^{\infty} J_q(kr)\, J_q(k\rho)\, e^{-Xk}\, dk \qquad \text{(B-2)}$$

$$\frac{\partial}{\partial X} Q_{q-\frac{1}{2}}(z) = -\pi\sqrt{r\rho} \int_0^{\infty} k\, J_q(kr)\, J_q(k\rho)\, e^{-Xk}\, dk \qquad \text{(B-3)}$$

$$\frac{\partial^2}{\partial X^2} Q_{q-\frac{1}{2}}(z) = \pi\sqrt{r\rho} \int_0^{\infty} k^2 J_q(kr)\, J_q(k\rho)\, e^{-Xk}\, dk \qquad \text{(B-4)}$$

then

$$K_2 = \sum_{p=1}^{\infty} \frac{2e^{-iq(\varphi_o-\theta_o)}}{\sqrt{1+a^2r^2}\ ap} \Bigg\{ - a^2\sqrt{r\rho}\left[\pi\sqrt{r\rho}\int_o^{\infty} k^2 J_q(kr)\ J_q(k\rho)\ e^{-p\bar{\theta}_o k/a}\ dk\right]$$

$$- \frac{ia(r^2+\rho^2)q}{(r\rho)^{3/2}}\left[\pi\sqrt{r\rho}\int_o^{\infty} kJ_q(kr)\ J_q(k\rho)\ e^{-p\bar{\theta}_o k/a}\ dk\right]$$

$$+ \frac{q^2}{(r\rho)^{3/2}}\left[\pi\sqrt{r\rho}\int_o^{\infty} J_q(kr)\ J_q(k\rho)\ e^{-p\bar{\theta}_o k/a}\ dk\right]\Bigg\} \qquad \text{(B-5)}$$

But

$$\sum_{p=1}^{\infty} e^{-p\bar{\theta}_o k/a} = \frac{e^{-\bar{\theta}_o k/a}}{1-e^{-\bar{\theta}_o k/a}} \qquad \text{(B-6)*}$$

It is seen from Figure (B-1) that a good approximation of

$$\left\{\frac{\bar{\theta}_o{}^2k^2}{a^2}\ \frac{e^{-\bar{\theta}_o k/a}}{1-e^{-\bar{\theta}_o k/a}}\right\} \quad \text{is} \quad \left\{5.94\ e^{-0.678\ \bar{\theta}_o k/a} - 19.53\ e^{-1.16\ \bar{\theta}_o k/a} + 13.59\ e^{-1.30\ \bar{\theta}_o k/a}\right\} \qquad \text{(B-7)}$$

---

*See L. B. W. Jolley, Summation of Series, Dover Publications, Inc., New York, 1961.

of

$$\left\{\frac{\bar{\theta}_o k}{a}\,\frac{e^{-\bar{\theta}_o k/a}}{1-e^{-\bar{\theta}_o k/a}}\right\} \quad \text{is} \quad \left\{e^{-0.67\,\bar{\theta}_o k/a} + e^{-0.60\,\bar{\theta}_o k/a} - e^{-0.75\,\bar{\theta}_o k/a}\right\} \tag{B-8}$$

A satisfactory approximation for

$$\left\{\frac{e^{-\bar{\theta}_o k/a}}{1-e^{-\bar{\theta}_o k/a}}\right\} \quad \text{is} \quad \left\{e^{-\bar{\theta}_o k/a} + e^{-2\,\bar{\theta}_o k/a} + e^{-3\,\bar{\theta}_o k/a} + 6.7\,e^{-5.3\,\bar{\theta}_o k/a}\right\} \tag{B-9}$$

With substitutions (B-7,8,9) and (B-2), Equation (37a) becomes

$$\begin{aligned} K_2 \approx \frac{2e^{-iq(\varphi_o-\theta_o)}}{\sqrt{1+a^2r^2}\;a\rho} \Bigg\{ & \frac{-a^4\sqrt{r\rho}}{\bar{\theta}_o^{\,2}}\Big[5.94\,Q_{q-\frac{1}{2}}(z_1) - 19.53\,Q_{q-\frac{1}{2}}(z_2) \\ & \qquad + 13.59\,Q_{q-\frac{1}{2}}(z_3)\Big] \\ & - \frac{ia^2(r^2+\rho^2)q}{\bar{\theta}_o(r\rho)^{3/2}}\Big[Q_{q-\frac{1}{2}}(z_4) + Q_{q-\frac{1}{2}}(z_5) - Q_{q-\frac{1}{2}}(z_6)\Big] \\ & + \frac{q^2}{(r\rho)^{3/2}}\Big[Q_{q-\frac{1}{2}}(z_7) + Q_{q-\frac{1}{2}}(z_8) + Q_{q-\frac{1}{2}}(z_9) + 6.7\,Q_{q-\frac{1}{2}}(z_{10})\Big]\Bigg\} \end{aligned} \tag{B-10}$$

where

$$z_1 = \left[\left(\frac{0.678\,\bar{\theta}_o}{a}\right)^2 + r^2 + \rho^2\right]/2r\rho$$

$$z_2 = \left[\left(\frac{1.16\,\bar{\theta}_o}{a}\right)^2 + r^2 + \rho^2\right]/2r\rho$$

$$z_3 = \left[\left(\frac{1.30\ \bar{\theta}_o}{a}\right)^2 + r^2 + \rho^2\right]/2r\rho$$

$$z_4 = \left[\left(\frac{0.67\ \bar{\theta}_o}{a}\right)^2 + r^2 + \rho^2\right]/2r\rho$$

$$z_5 = \left[\left(\frac{0.60\ \bar{\theta}_o}{a}\right)^2 + r^2 + \rho^2\right]/2r\rho$$

$$z_6 = \left[\left(\frac{0.75\ \bar{\theta}_o}{a}\right)^2 + r^2 + \rho^2\right]/2r\rho$$

$$z_7 = \left[\left(\frac{\bar{\theta}_o}{a}\right)^2 + r^2 + \rho^2\right]/2r\rho$$

$$z_8 = \left[\left(\frac{2\bar{\theta}_o}{a}\right)^2 + r^2 + \rho^2\right]/2r\rho$$

$$z_9 = \left[\left(\frac{3\bar{\theta}_o}{a}\right)^2 + r^2 + \rho^2\right]/2r\rho$$

$$z_{10} = \left[\left(\frac{5.3\ \bar{\theta}_o}{a}\right)^2 + r^2 + \rho^2\right]/2r\rho \qquad \text{(B-11)}$$

Similarly, Equation (37b) can be approximated by

$$K_2 \approx -\frac{-2e^{-iq(\varphi_o-\theta_o)}}{(r\rho)^{1/2}}\ \frac{a^2}{\bar{\theta}_o^{\,2}}\left[5.94\ Q_{q-\frac{1}{2}}(z_1) - 19.53\ Q_{q-\frac{1}{2}}(z_2) + 13.59\ Q_{q-\frac{1}{2}}(z_3)\right] \qquad \text{(B-12)}$$

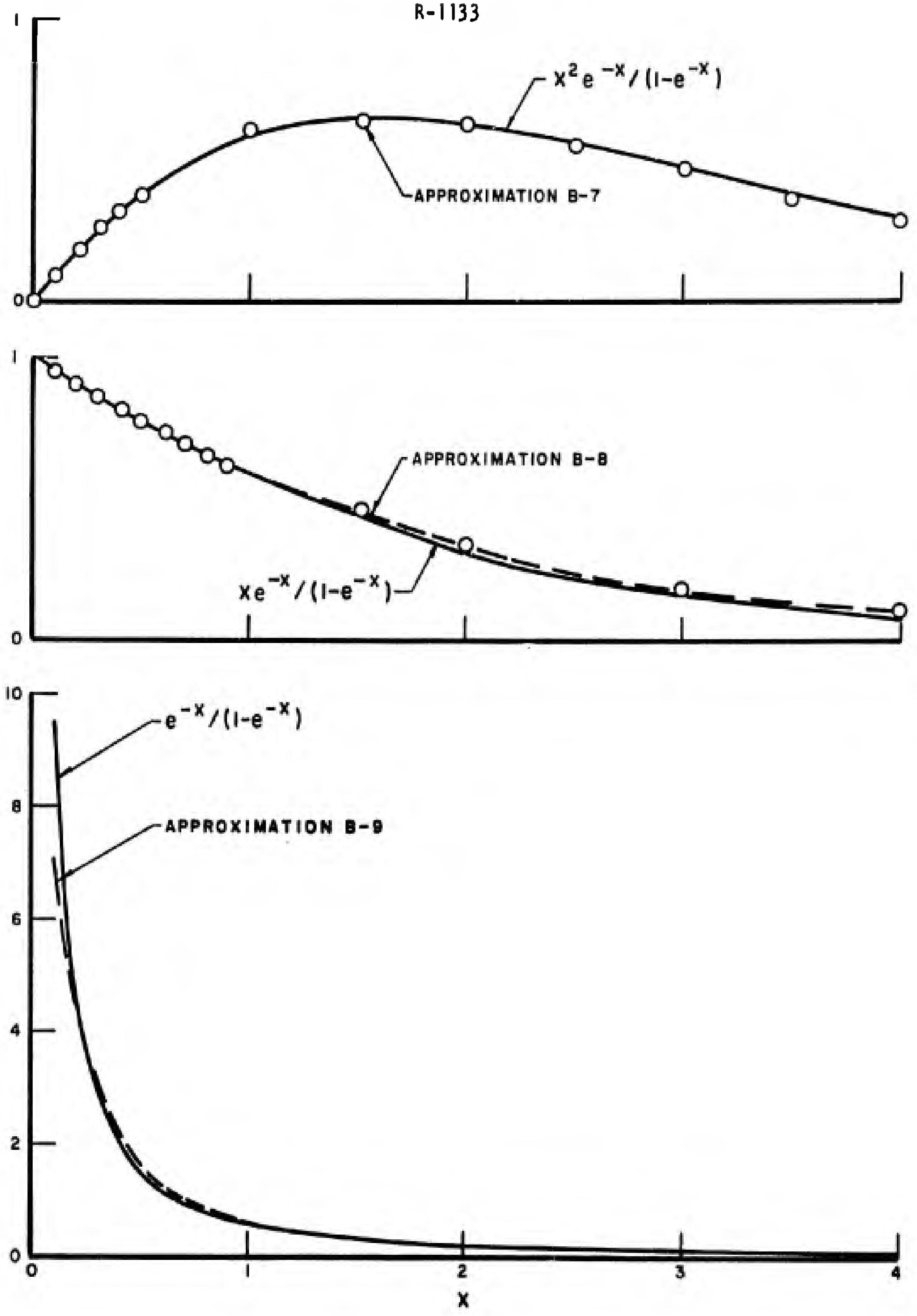

FIGURE B-1. APPROXIMATIONS OF THE INFINITE p-SERIES

BLANK PAGE

APPENDIX C

EVALUATION OF f(m, q, n)

The Θ-integration (in Equation [41]) results in

$$\int_{\bar{\theta}_n-(\varphi_o-\theta_o)}^{\bar{\theta}_n+\bar{\theta}_o/2} e^{-iq\Theta}\cos m\Theta\, d\Theta$$

$$= -\frac{i}{2}\left[\frac{e^{i(m-q)\Theta}}{m-q} - \frac{e^{-i(m+q)\Theta}}{m+q}\right]_{\bar{\theta}_n-\varphi_o+\theta_o}^{\bar{\theta}_n+\bar{\theta}_o/2} \qquad \text{for } m \neq q$$

$$= \left[\frac{\Theta}{2} + \frac{ie^{-i2q\Theta}}{4q}\right]_{\bar{\theta}_n-\varphi_o+\theta_o}^{\bar{\theta}_n+\bar{\theta}_o/2} \qquad \text{for } m = q \neq 0$$

$$= \Theta\Big|_{\theta_n-\varphi_o+\theta_o}^{\bar{\theta}_n+\bar{\theta}_o/2} \qquad \text{for } m = q = 0 \tag{C-1}$$

Then for $m \neq q$,

$$f(m,q,n) = -\frac{ie^{i(m-q)\,\bar{\theta}_n}}{2(m-q)}\left[e^{i(m-q)\,\bar{\theta}_o/2}\; e^{-iq(\varphi_o-\theta_o)} - e^{-im(\varphi_o-\theta_o)}\right]$$

$$+ \frac{ie^{-i(m+q)\,\bar{\theta}_n}}{2(m+q)}\left[e^{-i(m+q)\,\bar{\theta}_o/2}\; e^{-iq(\varphi_o-\theta_o)} - e^{im(\varphi_o-\theta_o)}\right] \tag{C-2}$$

for $m = q \neq 0$,

$$f(m,q,n) = e^{-iq(\varphi_o-\theta_o)}\left[\frac{\bar{\theta}_o}{4} + \frac{\varphi_o-\theta_o}{2} + \frac{ie^{-i2q\bar{\theta}_n}}{4q}\, e^{-iq\bar{\theta}_o}\right] - e^{iq(\varphi_o-\theta_o)}\left(\frac{ie^{-i2q\bar{\theta}_n}}{4q}\right) \tag{C-3}$$

and for $m = q = 0$

$$f(m,\ q,\ n) = \frac{\bar{\theta}_o}{2} + \varphi_o - \theta_o \tag{C-4}$$

Since $\bar{\theta}_n = \frac{2\pi}{N}(n-1)$

$$\sum_{n=1}^{N} e^{\mp i(m\pm q)\bar{\theta}_n} = \begin{cases} N & \text{for } m \pm q = \lambda N\ ,\ \lambda = 0,1,2,3\ \ldots \\ 0 & \text{for all other values} \end{cases}$$

and

$$\sum_{n=1}^{N} e^{-i2q\bar{\theta}_n} = N$$ since q is always an integer multiple of N . Utilizing the above results of Equations (C-2,-3,-4) yields the expressions given by Equation (43) in the text.

APPENDIX D

EVALUATION OF INTEGRALS I_1, I_2, AND I_3

(1)
$$I_3 = \lim_{X\to 0} \int_{r-\beta}^{r+\beta} \frac{X(r^2+\rho^2)}{(r\rho)^{5/2}} \rho \; Q'_{m-\frac{1}{2}}(z)\, d\rho$$

With Equation (50), this becomes

$$I_3 = \lim_{X\to 0} \int_{r-\beta}^{r+\beta} \frac{X(r^2+\rho^2)}{(r\rho)^{5/2}} \rho \left[\sum_{s=0}^{\infty} a_{ms}\; s(z-1)^{s-1} + \frac{b_{mo}}{z-1} + \sum_{s=1}^{\infty} b_{ms}(z-1)^{s-1} \right.$$
$$\left. + \, b_{m1} \ln(z-1) + \ln(z-1) \sum_{s=2}^{\infty} b_{ms}\; s(z-1)^{s-1} \right] d\rho$$

$$= \lim_{\substack{X\to 0 \\ \text{and} \\ z\to 1}} \int_{r-\beta}^{r+\beta} \frac{X(r^2+\rho^2)}{(r\rho)^{5/2}} \rho \left[\frac{b_{mo}}{(z-1)} + b_{m1} \ln (z-1) \right] d\rho \qquad \text{(D-1)}$$

where
$$(z-1) = \frac{X^2 + (r-\rho)^2}{2r\rho}$$

Since β is small, ρ can be approximated by r outside the factor $[X^2+(r-\rho)^2]$.

Then

$$I_3 \approx \lim_{X\to 0} \left\{ \frac{4b_{mo}}{r^2} X \int_{r-\beta}^{r+\beta} \frac{d\rho}{[X^2+(r-\rho)^2]} + \frac{2b_{m1} X}{r^4} \int_{r-\beta}^{r+\beta} \ln\, [X^2+(r-\rho)^2]\, d\rho \right\}$$
(D-2)

Let $(r-\rho) = Y$.

$$I_2 \approx \lim_{X\to 0} \left\{ \frac{4\, b_{mo}}{r^2}\; X \int_{-\beta}^{\beta} \frac{dY}{X^2+Y^2} + \frac{2\, b_{m1}}{r^4}\; X \int_{-\beta}^{\beta} \ln\,(X^2+Y^2)\, dY \right\} \tag{D-3}$$

But

$$\lim_{X\to 0} X \int_{-\beta}^{\beta} \frac{dY}{X^2+Y^2} = \lim_{X\to 0} \left[\tan^{-1} \frac{Y}{X} \right]_{-\beta}^{\beta} = 0$$

and

$$\lim_{X\to 0} X \int_{-\beta}^{\beta} \ln\,(X^2+Y^2)\, dY = 0$$

Therefore

$$I_2 \to 0 \tag{D-4}$$

(2)

$$I_1 = \lim_{\substack{X\to 0\\ z\to 1}} \int_{r-\beta}^{r+\beta} Q_{m-\frac{1}{2}}(z)\, d\rho$$

With Equation (49), this becomes

$$I_1 = \lim_{\substack{X\to 0\\ z\to 1}} \int_{r-\beta}^{r+\beta} \left[\sum_{s=o}^{\infty} a_{ms}\, (z-1)^s + \ln\,(z-1) \sum_{s=o}^{\infty} b_{ms}\, (z-1)^s \right] d\rho$$

$$\approx \int_{r-\beta}^{r+\beta} \sum_{s=o}^{\infty} \left[a_{ms} + b_{ms} \ln \frac{(r-\rho)^2}{2r^2} \right] \left[\frac{(r-\rho)^2}{2r^2} \right]^s d\rho \tag{D-5}$$

Let $u = \frac{\rho - r}{\beta}$, $du = \frac{d\rho}{\beta}$, $d\rho = \beta du$.

$$I_1 \approx \beta \int_{-1}^{1} \sum_{s=0}^{\infty} \left[a_{ms} + b_{ms} \ln \left(\frac{\beta^2}{2r^2} \right) \right] \left(\frac{\beta^2}{2r^2} \right)^s u^{2s} \, du$$

$$+ 2\beta \int_{-1}^{1} \sum_{s=0}^{\infty} b_{ms} \left(\frac{\beta^2}{2r^2} \right)^s (\ln u) \, u^{2s} \, du$$

$$\approx 2\beta \sum_{s=0}^{\infty} \left[a_{ms} + b_{ms} \ln \left(\frac{\beta^2}{2r^2} \right) \right] \left(\frac{\beta^2}{2r^2} \right)^s \frac{1}{(2s+1)}$$

$$- 4\beta \sum_{s=0}^{\infty} b_{ms} \left(\frac{\beta^2}{2r^2} \right)^s \frac{1}{(2s+1)^2}$$

$$\approx 2\beta \sum_{s=0}^{\infty} \left(\frac{\beta^2}{2r^2} \right)^s \frac{1}{(2s+1)} \left\{ a_{ms} + b_{ms} \ln \left(\frac{\beta^2}{2r^2} \right) - 2 \, b_{ms} \frac{1}{(2s+1)} \right\} \tag{D-6}$$

(3) $$I_2 = \lim_{X \to 0} \int_{r-\beta}^{r+\beta} \left[r\rho \, Q'_{m-\frac{1}{2}}(z) + X^2 \, Q''_{m-\frac{1}{2}}(z) \right] d\rho$$

Using the expansions about $z = 1$ (Equations [50] and [51]) gives

$$\left[r\rho \, Q'_{m-\frac{1}{2}}(z) + X^2 \, Q''_{m-\frac{1}{2}}(z) \right] = \frac{r\rho \, b_{mo}}{(z-1)} + r\rho \sum_{s=1}^{\infty} (a_{ms} s + b_{ms}) \, (z-1)^{s-1}$$

$$+ r\rho \ln (z-1) \sum_{s=1}^{\infty} b_{ms} \, s (z-1)^{s-1} - \frac{X^2 \, b_{mo}}{(z-1)^2} + \frac{X^2 \, b_{m1}}{(z-1)}$$

[Cont'd]

$$+ X^2 \text{ (integrable terms)}$$

$$= b_{mo} \frac{[r\rho(z-1)-X^2]}{(z-1)^2} + b_{m1} \frac{X^2}{(z-1)}$$

$$+ r\rho \sum_{s=1}^{\infty} \left\{ a_{ms}\, s + b_{ms} \left[1 + s \ln (z-1) \right] \right\} (z-1)^{s-1}$$

$$+ X^2 \text{ (integrable terms)} \qquad \text{(D-7)}$$

Therefore

$$I_2 = \lim_{X \to 0} \int_{r-\beta}^{r+\beta} \left\{ b_{mo} \frac{[r\rho(z-1)-X^2]}{(z-1)^2} + b_{m1} \frac{X^2}{(z-1)} \right.$$

$$\left. + r\rho \sum_{s=1}^{\infty} \left\{ a_{ms}\, s + b_{ms} \left[1 + s \ln (z-1) \right] \right\} (z-1)^{s-1} \right\} d\rho \qquad \text{(D-8)}$$

(a)

$$\frac{r\rho(z-1)-X^2}{(z-1)^2} = \frac{2r^2\rho^2[(r-\rho)^2-X^2]}{[X^2+(r-\rho)^2]^2} = 2r^2\rho^2 \frac{d}{d\rho}\left[\frac{r-\rho}{X^2+(\rho-r)^2}\right]$$

$$\approx 2r^4 \frac{d}{d\rho}\left[\frac{r-\rho}{X^2+(\rho-r)^2}\right]$$

Hence

$$\lim_{X \to 0} \int_{r-\beta}^{r+\beta} b_{mo} \frac{[r\rho(z-1)-X^2]}{(z-1)^2}\, d\rho \approx 2r^4\, b_{mo} \left[\frac{r-\rho}{(\rho-r)^2}\right]_{r-\beta}^{r+\beta} \approx -\frac{4r^4\, b_{mo}}{\beta} \qquad \text{(D-9)}$$

(b)

$$\lim_{X\to 0}\int_{r-\beta}^{r+\beta}\frac{X^2}{z-1}\,d\rho \;\approx\; 2r^2\lim_{X\to 0}\int_{r-\beta}^{r+\beta}\frac{X^2}{X^2+(r-\rho)^2}\,d\rho \;\approx\; 2r^2\lim_{X\to 0}\int_{-\beta}^{\beta}\frac{X^2}{X^2+Y^2}\,dY$$

$$\approx\; 2r^2\lim_{X\to 0} X\left[\tan^{-1}\frac{Y}{X}\right]_{-\beta}^{\beta} \;=\; 0 \qquad \text{(D-10)}$$

(c)

$$\lim_{X\to 0}\int_{r-\beta}^{r+\beta} r\rho\sum_{s=1}^{\infty}\left\{a_{ms}\,s + b_{ms}\left[1 + s\,\ln\,(z-1)\right]\right\}(z-1)^{s-1}\,d\rho \,,$$

$$\approx\; r^2\int_{r-\beta}^{r+\beta}\sum_{s=1}^{\infty}\left\{a_{ms}\,s + b_{ms}\left[1 + s\,\ln\frac{(r-\rho)^2}{2r^2}\right]\right\}\left[\frac{(r-\rho)^2}{2r^2}\right]^{s-1}d\rho$$

and with $u = \frac{\rho - r}{\beta}$, $du = \frac{d\rho}{\beta}$, and $d\rho = \beta du$,

$$\approx\; \beta r^2\int_{-1}^{1}\sum_{s=1}^{\infty}\left\{a_{ms}\,s + b_{ms}\left[1 + s\,\ln\left(\frac{\beta^2}{2r^2}\right)\right]\right\}\left(\frac{\beta^2}{2r^2}\right)^{s-1}u^{2s-2}\,du$$

$$+\; 2\beta r^2\int_{-1}^{1}\sum_{s=1}^{\infty} b_{ms}\,s\,\ln u\left(\frac{\beta^2}{2r^2}\right)^{s-1}u^{2s-2}\,du$$

$$\approx\; \beta r^2\sum_{s=1}^{\infty}\left\{a_{ms}\,s + b_{ms}\left[1 + s\,\ln\left(\frac{\beta^2}{2r^2}\right)\right]\right\}\left(\frac{\beta^2}{2r^2}\right)^{s-1}\frac{2}{2s-1}$$

$$+\; 2\beta r^2\sum_{s=1}^{\infty} b_{ms}\,s\left(\frac{\beta^2}{2r^2}\right)^{s-1}\left[\frac{-2}{(2s-1)^2}\right] \qquad \text{(D-11)}$$

The sum of (a), (b), and (c) yields

$$I_2 \approx -\frac{4r^4\, b_{mo}}{\beta} + 2\beta r^2 \sum_{s=1}^{\infty} \left(\frac{\beta^2}{2r^2}\right)^{s-1} \left\{\left(\frac{s}{2s-1}\right)\left[a_{ms} + b_{ms} \ln\left(\frac{\beta^2}{2r^2}\right)\right] - b_{ms}\frac{1}{(2s-1)^2}\right\} \tag{D-12}$$

APPENDIX E

EVALUATION OF THE INTEGRALS IN EQUATIONS (56a) AND (56b), FOR THE REGIONS ADJACENT TO THE SINGULARITY STRIP, BY THE LAGRANGE INTERPOLATION METHOD

The integrals to be evaluated are

$$I_4 = \left[\int_{r-0.05}^{r-0.01} + \int_{r+0.01}^{r+0.05}\right] \frac{Q_{m-\frac{1}{2}}\left(\frac{r^2+\rho^2}{2r\rho}\right)d\rho}{\rho^{5/2}}$$

$$I_5 = \left[\int_{r-0.05}^{r-0.01} + \int_{r+0.01}^{r+0.05}\right] \frac{Q'_{m-\frac{1}{2}}\left(\frac{r^2+\rho^2}{2r\rho}\right)d\rho}{\rho^{3/2}}$$

(1) $\underline{I_4}$

As ρ approaches r , $Q_{m-\frac{1}{2}}(z)$ behaves like $\ln (\rho-r)^2$ (see Equation [49] of the text). If I_4 is taken as

$$I_4 = \int \frac{F(\rho)}{\rho-r}\, d\rho$$

where (E-1)

$$F(\rho) = \frac{(\rho-r)\ Q_{m-\frac{1}{2}}(z)}{\rho^{5/2}}$$

the function $F(\rho)$ can be expanded easily about the singularity $\rho = r$ by the Lagrange interpolation formula*

$$F(\rho) = \sum_{i=o}^{n} \frac{\Pi_n(\rho)\, F_i}{(\rho-\rho_i)\, \Pi_n'(\rho_i)} \quad , \; i = 0,\ 1,\ \ldots\ n$$

where

$$\Pi_n(\rho) = (\rho-\rho_o)\ (\rho-\rho_1)\ \ldots\ (\rho-\rho_n)$$

$$\Pi_n'(\rho_i) = \frac{d}{d\rho}\,\Pi_n(\rho) \quad \text{evaluated at } \rho = \rho_i$$

$$F_i = F(\rho_i)$$

In the strip from r to $r + 0.05$, with $n = 5$, $\delta = 0.01$, $\rho_o = r$, $\rho_1 = r + \delta$, ... $\rho_5 = r + 5\delta$.

Then

$$\Pi_n'(\rho_o) = (-\delta)\ (-2\delta)\ (-3\delta)\ (-4\delta)\ (-5\delta) = (-1)^5\ \delta^5\ 5!$$

$$\Pi_n'(\rho_1) = (\delta)\ (-\delta)\ (-2\delta)\ (-3\delta)\ (-4\delta) = (-1)^4\ \delta^5\ 4!\ 1\,!$$

etc.

and

$$F(\rho) = \frac{1}{\delta^5} \sum_{i=o}^{5} \frac{(-1)^{5-i}}{i!(5-i)!}\ \frac{(\rho-r)(\rho-r-\delta)\ldots(\rho-r-5\delta)}{(\rho-r-i\delta)}\ F_i \qquad \text{(E-2)}$$

---

*See J. B. Scarborough, Numerical Mathematical Analysis, The Johns Hopkins Press, Baltimore, Md., and Oxford University Press, London; 1958.

Since $F_o = F(r) = 0$, It can be shown that

$$F(\rho) = \frac{1}{\delta^5}\left\{ g_o(\rho-r)^5 + g_1\delta\,(\rho-r)^4 + g_2\delta^2\,(\rho-r)^3 + g_3\delta^3\,(\rho-r)^2 + g_4\delta^4\,(\rho-r)\right\} \tag{E-3}$$

and

$$\int_{r+0.01}^{r+0.05} \frac{F(\rho)\,d\rho}{\rho-r} = \frac{1}{\delta^5}\left\{ g_o\frac{(\rho-r)^5}{5} + g_1\delta\,\frac{(\rho-r)^4}{4} + g_2\,\frac{\delta^2(\rho-r)^3}{3} + g_3\,\frac{\delta^3(\rho-r)^2}{2} + g_4\delta^4\rho \right\}\Bigg|_{r+0.01}^{r+0.05} \tag{E-4}$$

$$= 624.8\,g_o + 156\,g_1 + 41.333\,g_2 + 12\,g_3 + 4g_4$$

where

$$g_o = \frac{F_1}{4!1!} - \frac{F_2}{3!2!} + \frac{F_3}{2!3!} - \frac{F_4}{1!4!} + \frac{F_5}{5!}$$

$$g_1 = -14\frac{F_1}{4!1!} + 13\frac{F_2}{3!2!} - 12\frac{F_3}{2!3!} + 11\frac{F_4}{1!4!} - 10\frac{F_5}{5!}$$

$$g_2 = 71\frac{F_1}{4!1!} - 59\frac{F_2}{3!2!} + 49\frac{F_3}{2!3!} - 41\frac{F_4}{1!4!} + 35\frac{F_5}{5!}$$

$$g_3 = -154\frac{F_1}{4!1!} + 107\frac{F_2}{3!2!} - 78\frac{F_3}{2!3!} + 61\frac{F_4}{1!4!} - 50\frac{F_5}{5!}$$

$$g_4 = 120\frac{F_1}{4!1!} - 60\frac{F_2}{3!2!} + 40\frac{F_3}{2!3!} - 30\frac{F_4}{1!4!} + 24\frac{F_5}{5!}$$

It can be shown that

$$\int_{r-0.05}^{r-0.01} \frac{F(\rho)}{\rho-r}\,d\rho = -\left\{ 624.8\,g_o + 156\,g_1 + 41.333\,g_2 + 12\,g_3 + 4\,g_4 \right\} \tag{E-5}$$

where the F_i which make up the g_j are now opposite in sign as well as different in composition, since in this case $\rho_i = r - i\delta$ instead of $r + i\delta$.

The sum of (E-4) and (E-5) can be expressed in terms of F_i as

$$\left[\int_{r+0.01}^{r+0.05} + \int_{r-0.05}^{r-0.01}\right] \frac{F(\rho)\,d\rho}{(\rho-r)}$$

$$= 0.3111.(F_1-F_{-1}) + 0.7111.(F_2-F_{-2}) + 0.1777.(F_3-F_{-3})$$

$$+ 0.3555.(F_4-F_{-4}) + 0.0622.(F_5-F_{-5}) \tag{E-6}$$

where

$$F_p = 0.01p\,\frac{Q_{m-\frac{1}{2}}(z_p)}{(r+0.01p)^{5/2}}$$

and

$$z_p = \frac{r^2 + (r+0.01p)^2}{2r\,(r+0.01p)}$$

$$p = \pm 1, \pm 2, \pm 3, \pm 4, \pm 5$$

(2) I_5

As ρ approaches r , $Q'_{m-\frac{1}{2}}(z)$ behaves like $\frac{1}{z-1}$ or $\frac{1}{(\rho-r)^2}$. Let

$$I_5 = \int \frac{f(\rho)\, d\rho}{(\rho-r)^3} \qquad \text{(E-7)}$$

where

$$f(\rho) = \frac{(\rho-r)^3\, Q'_{m-\frac{1}{2}}\left(\frac{r^2+\rho^2}{2r\rho}\right)}{\rho^{3/2}}$$

Then the function $f(\rho)$ can be expanded readily about $\rho = r$, since $f(r)$ is zero. Use of Equations (E-2) and (E-3) yields

$$\int_{r+0.01}^{r+0.05} \frac{f(\rho)}{(\rho-r)^3}\, d\rho = \frac{1}{\delta^5}\left\{ g_0 \frac{(\rho-r)^3}{3} + g_1 \frac{\delta(\rho-r)^2}{2} + g_2\, \delta^2 \rho + g_3\, \delta^3 \ln(\rho-r) - g_4\, \delta^4 \frac{1}{(\rho-r)} \right\}_{r+0.01}^{r+0.05}$$

$$= 413{,}333.33.\ g_0 + 120{,}000\ g_1 + 40{,}000\ g_2 + (10{,}000 \ln 5)\ g_3 + 8{,}000\ g_4 \qquad \text{(E-8)}$$

Finally,

$$\left[\int_{r+0.01}^{r+0.05} + \int_{r-0.05}^{r-0.01}\right] \frac{f(\rho)}{(\rho-r)^3}\, d\rho$$

$$= 2283.2895\ (f_1-f_{-1}) + 2397.1028\ (f_2-f_{-2}) - 169.02\ (f_3-f_{-3}) + 350.9914\ (f_4-f_{-4}) + 5.1197\ (f_5-f_{-5}) \qquad \text{(E-9)}$$

where

$$f_p = (0.01p)^3 \frac{Q'_{m-\frac{1}{2}}(z_p)}{(r + 0.01p)^{3/2}}$$

and z_p as before .

APPENDIX F

CHORDWISE PRESSURE DISTRIBUTION

This Appendix is concerned with the problem of the chordwise pressure distribution on the propeller blades. It is divided into the following parts:

(1) Cesàro summability of $\sum_{k=1}^{\infty} \sin k\theta$

(2) Equivalence of the Cesàro summability method and that of subtracting a constant from the coefficients of the sine series

(3) Rationalization for the assumption $\ell^{(n)} = a_n + c$

All are considered fundamental to the evaluation of the chordwise pressure distribution.

(1) Cesàro sum of $\sum_{k=1}^{\infty} \sin k\theta$

Let C_n be the nth partial Cesàro sum of $\sum \sin k\theta$.

Then

$$C_n = \sum_{k=1}^{n} \frac{n-k+1}{n} \sin k\theta$$

$$= \frac{n+1}{n} \sum_{k=1}^{n} \sin k\theta - \frac{1}{n} \sum_{k=1}^{n} k \sin k\theta$$

$$= \frac{(n+1)}{n} \left[\frac{\sin \frac{1}{2}(n+1)\,\theta \sin \frac{1}{2} n\theta}{\sin \frac{\theta}{2}} \right] - \frac{1}{n} \left[\frac{\sin (n+1)\,\theta}{4 \sin^2 \frac{\theta}{2}} \right]$$

$$+ \frac{n+1}{n} \left[\frac{\cos \left(\frac{2n+1}{2}\right) \theta}{2 \sin \frac{\theta}{2}} \right]$$

[Cont'd]